Laboratory and field trials evaluation of Transmit Delay Diversity applied to DVB-T/H Networks

A thesis submitted for the degree of
Doctor of Philosophy

School of Engineering and Design
Brunel University,
Uxbridge, UK

July 2009

Raffaele Di Bari

Abstract

The requirements for future DVB-T/H networks demand that broadcasters design and deploy networks that provide ubiquitous reception in challenging indoors and other obstructed situations. It is essential that such networks are designed cost-effectively and with minimized environmental impact. The use of transmit diversity techniques with multiple antennas have long been proposed to improve the performance and capacity of wireless systems. Transmit diversity exploits the scattering effect inherent in the channel by means of transmitting multiple signals in a controlled manner from spatially separated antennas, allowing independently faded signals to arrive at the receiver and improves the chances of decoding a signal of acceptable quality. Transmit diversity can complement receive diversity by adding an additional diversity gain and in situations where receiver diversity is not practical, transmit diversity alone delivers a comparable amount of diversity gain. Transmit Delay Diversity (DD) can be applied to systems employing the DVB standard without receiver equipment modifications. Although transmit DD can provide a gain in NLOS situations, it can introduce degradation in LOS situation. The aim of this thesis is to investigate the effectiveness in real-word applications of novel diversity techniques for broadcast transmitter networks. Tests involved laboratory experiments using a wireless MIMO channel emulator and the deployment of a field measurement campaign dedicated to driving, indoor and rooftop reception. The relationship between the diversity gain, the propagation environment and several parameters such as the transmit antenna separation, the receiver speed and the Forward Error Correction Codes (FEC) configuration are investigated. Results includes the effect of real-word parameter usually not modeled in the software simulation analysis, such as antenna radiation patterns and mutual coupling, scattering vegetation impact, non-Gaussian noise sources and receiver implementation. Moreover, a practical analysis of the effectiveness of experimental techniques to mitigate the loss due to transmit DD loss in rooftop reception is presented. The results of this thesis confirmed, completed and extended the existing predictions with real word measurement results.

List of Contents

List of Figures

List if Tables

Acknowledgement

There are lots of people I would like to thank. First of all, I would like to gratefully acknowledge the enthusiastic supervision of Dr. Raj Nilavalan and Prof. John Cosmas. I would like to thank as well Mr. Maurice Bard for his great support for planning and performing the laboratory tests and field trials. I could not have imagined having better advisors and mentors for my PhD, and without their common sense, knowledge and perceptiveness I would never have finished.

I would like to acknowledge also the contribution of Dr. Amaia Arrinda by helping performing the DVB-H driving tests, the Horseden Hill measurement campaign, the remote controlled measurement campaign and the receiver calibration. Also, I would like to acknowledge the contribution Mr. Paolo Ditto for help to process the DVB-H driving test data and to perform the Horseden Hill tests. I would like to thank Dr. Yue Zhang and Dr. Karim Nassr for their invaluable comments, Dr. K.K. Loo, H. Shirazi and Dr. Krishnapillai for their help in performing the driving tests. A special thank to Mrs. Laura Barsacchi for her support during the “tough time” of this thesis.

Author's declaration

I certify that all material in this thesis which is not my own work has been identified and that no material has previously been submitted and approved for the award of a degree by this or any other University.

Signature …….....

Definitions

ACI	Adjacent Channel Interference
ACS	Add-Compare-Select-Unit
ADC	Analogue Digital Converter
AGC	Automatic Gain Control
AWGN	Additive White Gaussian Noise
BER	Bit Error Rate
BMU	Branch-Metric-Unit
BU	Bad Urban
C/N (CNR)	Carrier to Noise ratio
CDD	Cyclic Delay Diversity
CDMA	Code Division Multiple Access
CIC	filter Cascaded Integrator-Comb filter
CIR	Channel Impulse Response
CMPA	Control, Monitor and Process Applications
COFDM	Coded OFDM
CPE	Common Phase Error
CSI	Channel State Information
DAB	Digital Audio Broadcasting
DAC	Digital Analogue Converter
DB	Decibels
DC	Down Converter
DD	Delay Diversity
DDC	Digital Down Converter
DDoD	Discontinuous Doppler Diversity
DDS	Direct Digital Synthesized
DFT	Discrete Fourier Transform
DANL	Displayed Averaged Noise Level
DSP	Digital Signal Processor
DTV	Digital Television
DUC	Digital Up-Converter
DVB	Digital Video Broadcasting
DVB-C	Digital Video Broadcasting Cable
DVB-H	Digital Video Broadcasting Handheld
DVB-S	Digital Video Broadcasting Satellite
DVB-T	Digital Video Broadcasting Terrestrial
EIRP	Effective Isotropic Radiated Power
ESR	Errored Second Ratio
HT	Hilly Terrain
FER	Frame Error Rate
FEC	Forward Error Correction
FFT	Fast Fourier Transform
FILO	First-In-Last-Out
FIR	Finite Impulse Response
GPS	Global Position System
GSM	Global System for Mobile Telecommunications
ICI	Inter-carrier interference

IF	Intermediate Frequency
IFFT	Inverse Fast Fourier Transform
IR	Impulse Response
ISI	Inter-Symbol Interference
ITU	International Telecommunication Union
LPT	Low Power Transmitter
LAN	Local Area Network
LOS	Line of Sight
LS	least-squares
MER	Modulation Error Rate
MFER	MPE-FEC Frame Error Rate
MIMO	Multiple-Input Multiple-Output
MISO	Multiple-Input Single-Output
MFN	Multi-Frequency Network
MMSE	minimum mean–square error
MPE-FEC	Multi-Protocol Encapsulation Forward Error Correction
MPEG	Moving Picture Experts Group
MRC	Maximum Ratio Combining
MUX	Multiplexer
NCO	Numerical Control Oscillator
NIM	Network Interface Module
NLOS	Non-Line of Sight
OFDM	Orthogonal Frequency Division Multiplexing
OSI	Open Systems Interconnection
PAPR	Peak–to-Average Power Ratio
PD	Phase Diversity
PDP	Power Delay Profile
PID	Packet Identification Number
PLL	Phase locked loop
PLUTO	Physical Layer DVB Transmission Optimization
PRBS	Pseudo Random Binary Sequence
QAM	Quadrature Amplitude Modulation
QEF	Quasi Error Free
RMS	Root Mean Square
RSSI	Received Signal Strength Indication
RA	Rural Area
RBW	Resolution Bandwidth
RF	Radio Frequency
RS	Reed-Solomon
SAW	surface acoustic wave
SISO	Single-Input Single-Output
SIMO	Single-Input Multiple-Output
SFN	Single Frequency Network
SNR (S/N)	Signal Noise Ratio
STB	Set Top Box receiver
STBC	Space-Time Block Coding
STTC	Space-Time Trellis Coding

T-DMB	Terrestrial Digital Multimedia Broadcasting
TBU	Traceback Unit
ToV	Threshold of Visibility
TPS	Transmission Parameter Signalling
TS	Transport Stream
TU	Typical Urban
UHF	Ultra High Frequency
UMTS	Universal Mobile Telecommunications System
VHF	Very High Frequency
WLAN	Wireless Local Area Network
WSSUS	Wide-Sense-Stationary-Uncorrelated-Scattering

1. Introduction

1.1 Development of DTV

Broadcasting has brought entertainment and information to mass audiences around the world for over half a century. However, in the last two decades, the demand for multimedia service consumption anywhere anytime has increased greatly. The spectrum resource limitations required the design of new spectrum–efficient broadcasting technologies [1]. Terrestrial Digital TV (DTV) technology offers a number of benefits in comparison to terrestrial analogue broadcasting and in particular a more efficient use of frequency resources. In fact, more information can be transmitted using less radio spectrum. DTV also provides clearer, sharper pictures than analogue TV. Moreover, the implementation of the digital system, allows transmission to be more robust to interference and to fixed reception problems like ghosting, which affects some analogue viewers in built-up or hilly areas. The Digital Video Broadcasting - Terrestrial (DVB-T) [2] is a standard of the European consortium DVB based on the transmission of audio/video MPEG-2 streaming using Coded Orthogonal Frequency Division Multiplexing (OFDM) system. Analogue TV has only one program per channel, while DVB-T allows multi-program broadcasting. The total capacity in a single 8 MHz channel (from 4.98 to 31.67 Mbit/s) can be allocated for 2 to 4 Standard Definition TV programs (SDTV, requiring about 6 Mbit/s per program) transmitted in time division multiplex or for 2 High Definition Television programs (HDTV, requiring about 12 Mbit/s per program). The spectrum saved by deploying digital television can be used for additional services such as electronic program guides (EPG) and additional languages, spoken or subtitled. Complementary transmission systems based on the same DVB family are the DVB-S for satellite transmission, DVB-C for cable transmission. The final switch off of all analogue broadcasting transmissions is planned in the EU by the end of 2012, although the member countries have may have different deadlines. The switch-off of the analogue services gives the possibility to obtain some “freed” spectrum, which is referred to as the “digital dividend”.

1.2 Portable and Indoor Reception DTV

Digital broadcast networks are generally being designed by broadcast companies whose previous experience is in providing networks for analogue services. These companies are designing their networks based on experience learnt from analogue networks, which requires to maximize power, minimize interference and avoid multipath since this causes ghosting on analogue receivers. These companies are pre-occupied with the logistical challenges of evolving from analogue to digital networks and do not have the effort to invest in technology research. Digital networks such as DVB-T have been designed assuming that receive antennas are fixed at roof height and the opportunity has not been taken to exploit the ability of OFDM to decode main and multipath signals. However, next generation digital TV service providers for mobile and fixed reception are finding that coverage indoors and in areas of non Line Of Sight (LOS) is a fundamental requirement. Moreover, it is essential that such networks are designed cost-effectively and with minimized environmental impact. In this direction, a feasibility study of using DVB-T for mobile networks was analyzed, and in 2000 it was found that mobile reception of DVB-T is possible provided there are dedicated broadcast networks to service the needs of the mobile devices [3]. The study helped to understand differences in the reception of DVB-T in fixed and mobile terminals. As a result, an additional level of error correction to improve the C/N and Doppler performance in mobile channels required to elaborate a separate standard. Thus, the Digital Video Broadcasting–Handhelds (DVB-H) was published by European Telecommunications Standards Institute (ETSI) in 2004 [4] which supports high speed multimedia for new generation handheld devices. DVB-H supports both digital video and Internet Protocol (IP) standards, allowing the transmission of data packets exploitable by the receiver device. Novel technique known as “time slicing” improves the energy efficiency of the handle devices. In February 2007, the DVB consortium published the Digital Video Broadcasting - Satellite services to Handhelds (DVB-SH) standard. DVB-SH is a physical layer standard for delivering IP based media content and data to handheld terminals such as mobile phones or palmtop computers, based on a hybrid satellite/terrestrial downlink. The DVB-SH system was designed for frequencies below 3 GHz, supporting UHF band, L Band or S-band [5].

1.3 MIMO-OFDM for future DTV

A European project PLUTO [6], which started in January 2006, is committed to improve existing network technology and architecture allowing affordable broadband broadcast services to be delivered to European users and particularly in less developed regions. The main idea explores the use of DVB-T/H standard compliant diversity technologies to enhance reception and improve coverage for challenging indoor and mobile situations. The use of Multiple Input-Multiple Output (MIMO) technology in wireless communication systems is a well-documented technique that enables high-rate data transfers and improved the link quality through the use of multiple antennas at both transmitter and receiver. Figure 1-1 shows the schematic diagram of a typical MIMO system deploying N transmit and M receiver antennas. Each pair of transmit and receive antennas provides a different signal path h_{ij} from the i^{th} transmitter to the j^{th} receiver. By sending signals that carry the same information through these different paths, multiple independently faded replicas of the data symbol can be obtained at the receive end. Chapter 3 provides a detailed description of several MIMO systems and related works.

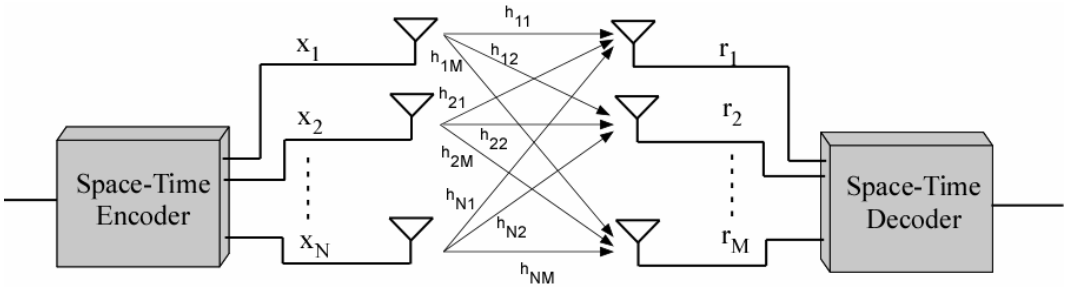

Figure 1-1: A schematics of a MIMO channel

1.4 Transmit Delay Diversity and Cyclic Delay Diversity

Transmit diversity exploits the scattering effect inherent in the channel by means of transmitting multiple signals in a controlled manner from spatially separated antennas. This allows independently faded signals to arrive at the receiver and improves the chances of decoding a signal of acceptable quality. Transmit diversity can complement receive

diversity by adding an additional diversity gain; in situations where receiver diversity is not practical (e.g. for handheld receivers), transmit diversity alone can deliver a comparable amount of diversity gain. Although transmit diversity is a commonly used technique for most wireless communication systems such as mobile telephony and WLAN, (e.g. GSM, UMTS, IEEE 802.11/a,b,g,n), it has not been applied to the area of Digital Broadcast services. Spatial transmit diversity can be implemented by transmitting coded signals from different transmit antennas, which are spatially separated from each other. This spatial separation of transmit antennas is required to achieve a sufficient de-correlation of the channels. Modelling predicts that a minimum separation of approximately 10 times the carrier frequency wavelength is required for a typical urban transmitter. In LOS or near LOS conditions, the respective signal paths between spatially separated antennas and the mobile receiver are likely to be correlated to a certain degree because of insufficient multipath in the channel. In transmit Delay Diversity (DD), the same information is transmitted from both antennas simultaneously but with a delay of several OFDM symbol intervals T, to overcome the effects of flat fading. The main advantage of transmit DD over other diversity coding is that it can be applied to standards based systems such as DVB-T/H, DAB/T-DMB without modifications. A diversity receiver can also be combined with these techniques achieving optimal performance if a Maximal Ratio Combining (MRC) coding is adopted. Figure 1-2 shows the block diagram of N-transmit antennas applied to an OFDM system with DD. The OFDM modulated signals are transmitted using N antennas. The individual signals only differ in an antenna specific delay shift δ_i. After the insertion of the cyclic prefix or Guard Interval (GI), the delay δ_i is inserted.

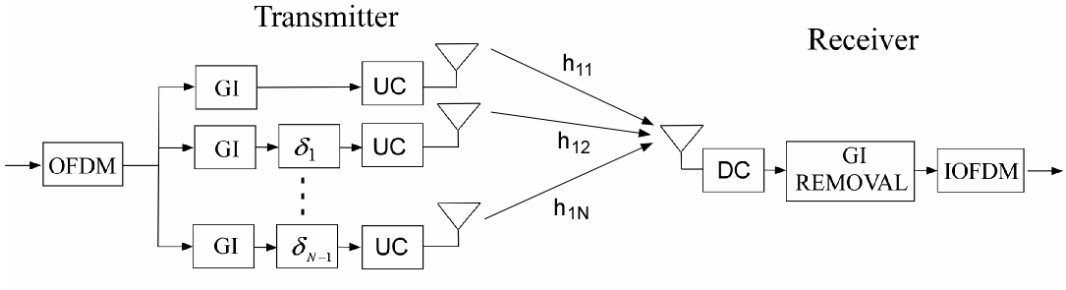

Figure 1-2: Transmit delay diversity applied to an OFDM system

The DD transmitted $N \times K$ matrix codeword C is defined as

$$C = \begin{pmatrix} s(0) & s(1) & \dots & s(K-1) \\ 0 & s(0) & \dots & s(K-2) \\ \dots & \dots & \dots & \dots \\ 0 & 0 & \dots & s(K-N) \end{pmatrix}_{N\,x\,K} \tag{1-1}$$

where the transmitted symbols are denoted by $s(t),\ t = 0,\dots K-1$ and K is the number of subcarriers. At the receiver side, the overlap of these sequences that passed through N uncorrelated channels results as one sequence that passed through a propagation channel with richer multipath components and thus higher frequency selectivity can be obtained than from a every single channel. This results in a "mitigation" of the channel severity by reducing the occurrences of channel flat deep fading. A coded OFDM system exploits this frequency selectivity and maximum diversity gain results if an interleaved signal is employed. The transmit DD code is transparent at the receiver side, e.g. any standard DVB-T/H demodulator can be used with any modifications. It is envisaged that under particular conditions, the same effects can be achieved by receiving multiple signals transmitted from several base stations of a Single Frequency Network (SFN) [7]. As it will be discussed in Chapter 3 and 6, DD is effective in Non Line of Sight (NLOS) channels characterized by a strong Rayleigh component, while it produces losses for Line of Sight (LOS) reception conditions. A more sophisticated version of DD which overcomes some severe limitations of DD is cyclic delay diversity (CDD). In CDD, symbols are cyclically shifted between respective N transmit antennas. The CDD coding is achieved before the GI insertion; thus, unlike the DD coding, CDD processing needs to be integrated into the DVB-T/H modulator itself. The resulting CDD $N \times K$ matrix codeword C is

$$C = \begin{pmatrix} s(0) & s(1) & \dots & s(K-1) \\ s(K-1) & s(0) & \dots & s(K-2) \\ \dots & \dots & \dots & \dots \\ s(K-N+1) & s(K-N+2) & \dots & s(K-N) \end{pmatrix}_{N\,x\,K} \tag{1-2}$$

The advantage of CDD consists of not introducing any additional channel delay as is the case for DD. This concept is clarified by Figure 1-3, where DD and CDD signal construction is shown for 2×1 transmit antennas diversity system. The antenna 0 transmits the OFDM sequence $s_0(t)$ while the antenna 1 transmits the sequence $s_1(t)$. Both symbols have a cyclic prefix (e.g. a guard interval) of length equal to N_g. The

channel multipath maximum delay is $\tau_{\max}$. The time section for OFDM modulation is synchronized with $s_o(t)$ sequence. The guard interval protects $s_o(t+1)$ from the multipath channel influence of $s_o(t)$. The sequence $s_1(t)$ with DD code causes inter-symbol interference (ISI), because N_g is not large enough to protect $s_o(t+1)$ from the multipath channel influence of $s_1(t)$. However, if $s_1(t)$ is substituted with CDD code, no ISI will occur because the cyclic shift does not introduce any additional delay.

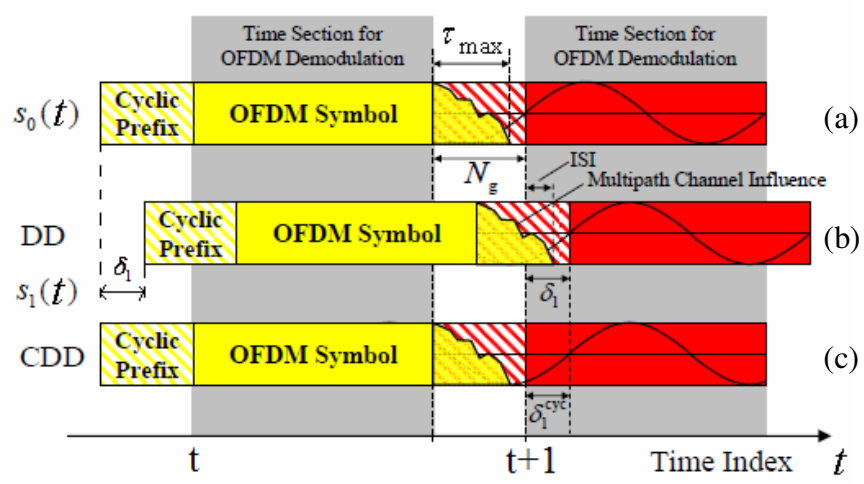

Figure 1-3: Signal construction for SISO (a), DD (b) and CDD (c) [27]

Thus, the main drawback of DD is the reduction of guard interval effectiveness. This is a severe limitation for real-life deployment of this technique, especially if used with Single Frequency Network (SFN) where the guard interval effectiveness is one of the key design parameters in determining the maximum transmitter separation. However, no ISI occurs for DD coding if:

$$\delta_i \le N_g - \tau_{\max}, \quad i = 0,1,\ldots N-1 \qquad 1\text{-}3$$

If this condition stands, it can also be proven that DD is equivalent to other diversity techniques, e.g. Cyclic Delay Diversity (CDD) and Phase Delay (PD). Since it was planned to test a network with a single base station, the DD coding was implemented for its simplicity for all tests. The laboratory and the field experimental set-up were studied to fulfill condition 1-3.

1.5 Software simulations on DVB standard compatible diversity codes

There has been much work published relating to application of transmit diversity for OFDM systems applying the techniques to non-standard implementations or to wireless LAN standards. However, by the time of starting this research (e.g. early 2006), there has been little work published on the application of standard compliant diversity techniques for broadcast and no evidence of real world trials, except DLR's paper which refers to applicability of the standard compliant diversity techniques for DVB [8]. A first analysis of transmit delay diversity has been made in [9] for single carrier systems with linear modulation schemes. In [10], a survey on compatible diversity techniques was presented, including subcarrier diversity (SD), delay diversity (DD), cyclic delay diversity (CDD), phase diversity (PD), and time-variant phase diversity (TPD) in [11], and Discontinuous Doppler Diversity (DDoD) in [12]. These techniques can be applied on top of already existing standards and are applied and investigated for OFDM based systems in [13] [14] [15]. Although the commonly known techniques (e.g. space-time block codes (STBC) [16][17] or space-time trellis codes (STTC) [18][19]) are not compatible with DVB standards, in [20] a comparisons of CDD and space-time block coding were presented. In [21], it was shown that CDD systems have similarities with traditional space-time diversity schemes in terms of full spatial diversity achievements. STBCs can be used in combination with beamforming as shown in [22]. Using transmit beam-forming typically implies an additional gain for antenna directivity and narrows delay and Doppler spread of the channel. This reduces the effect of interferences such as inter symbol interference (ISI) and the data rate could be increased by minimizing the guard interval. However, this means a concurrent reduction of multipath diversity. Thus CDD can be effectively adopted to combat the diversity loss and still have a higher data rate. In [23], beamforming and STBCs are compared in terms of channel capacity and Forward Error Correction (FEC) capabilities. Several works based on software simulations, extended the preliminary results presented in [8]. A study on CDD applied to DVB-H systems appeared in 2006 [24], while the impact of channel cross-correlation on system performances was first investigated in the early 2007 [25]. The analysis of signal degradation on Ricean channels due to diversity was reported in May 2007 in [26]. The estimation of diversity gain in terms of comparison of the seconds containing MPEG packet lost after the Reed-Solomon decoder and the MPE-FEC error rate appeared in June 2008 as a PLUTO project report [27]. Concurrently to this PhD investigation, transmit DD applied to DVB-T/H has been

evaluated though laboratory experiment in [28] while field trials for mobile reception and diversity loss for rooftop reception were performed by TéléDiffusion de France (TDF) in Metz (FR) and reported in [29]. The diversity gain for fixed indoor reception was estimated through field trials by Tampere University of Technology (TUT) in Tampere (FI) [30].

1.6 Thesis Aim and Objectives

The aim of this thesis is to investigate the effectiveness of novel diversity techniques for broadcast transmitter networks in real-word environments for real world applications. These techniques will improve reception in areas of poor coverage such as for mobile reception, indoors and obscured locations. Several measurement campaigns were planned and were focused mostly in places where the OFDM system presents poor performances, that is in rich scattering environments like indoor and urban. These experiments validated the improved system performances of DVB-T/H predicted through simulation results. It was beneficial to study the relationships between the system's performances enhancement and the different transmission environments. Thus post-processing was used to model the channels and to estimate their characteristics. These analysis included the effect of real word parameters such as antenna radiations patterns and mutual coupling, non-Gaussian noise sources, receivers channel estimation algorithm that usually are not modelled in the software simulation analysis The following are considered to achieve the aim:

1. Planning and designing an experimental laboratory and field trial measurement campaign;
2. Developing an effective approach for gain estimation in real word conditions;
3. Validating that the diversity gain estimated by simulation analysis which was achieved by using actual receivers;
4. Completing and extending the existing predictions with real word measurement results;
5. Characterizing the propagation conditions for DVB-T/H networks with field measurements and identify the relative channel models;
6. Identifying the relationship between the transmit antenna separations and the diversity gain;

7. Validating the effectiveness of techniques for mitigating diversity loss for rooftop reception.

1.7 Main Contributions

The main contributions of this thesis are[1]:

1. Measuring the performance enhancement due to diversity schemes in real word scenarios and relating the results to the particular transmit, environmental and reception conditions [1,2] [6,7] [10,11];
2. Developing different and effective approaches for estimation of transmit diversity gain in mobile, indoor and rooftop real word deployments [5-8] [11];
3. Planning and setting-up an experimental laboratory and field test bench to simulate a DVB-T network with transmit Delay Diversity (DD) and receiver Maximum Ratio Combiner (MRC) diversity scheme [1] [10];
4. Analyzing the transmit DD diversity performances loss for LOS DVB-T network and testing experimental spectrum shaping mitigation techniques [11];
5. Analyzing the impact of diversity gain of Reed Solomon encoder and Multi Protocol Encapsulation Forward Error Correction Code (MPE-FEC) [2].

1.8 Thesis Outline

The thesis is arranged as follows: Chapter 2 describes the DVB-T/H transmitter and receiver model design including outer coder/decoder, inner coder/decoder, QAM mapping, Frame adaptation and TPS insertion, OFDM and up/down converter. Chapter 3 describes the MIMO (Multiple Input Multiple Output) channels for the DVB-T/H systems and the main diversity technologies. Chapter 4 documents measurements made using actual receiver equipment in simulated laboratory conditions. The laboratory set-up includes a DVB modulator, a wireless channel emulator and a DVB receiver. Chapter 5 presents DVB-T field trial with CDD transmits diversity. The experiments were also extended to DVB-H to verify generically that diversity gains predicted by theory can be exploited by any OFDM system. Chapter 6 describe a long-term measurement campaign with the objective of analyzing the effect of diversity techniques on the DVB system over

[1] References are relative to the numbered list of Section 1.9

a long period of time through a monitoring network. Chapter 7 gives the conclusions and provides future research work for the field trials on diversity.

1.9 Papers Published and Submitted

The following papers have been published and submitted to journals and conferences that report results of this thesis:

1. R. Di Bari, Y. Zhang, K. Nasr, J. Cosmas, R. Nilavalan, M. Bard "Laboratory Measurement Campaign of DVB-T Signal with Transmit Delay Diversity", IEEE Transactions on Broadcasting on volume 54, Issue 3, Part 2, Sept. 2008 Page(s):532 – 541
2. R. Di Bari, Y. Zhang, K. Nasr, J. Cosmas, R. Nilavalan, M. Bard "Measurement Campaign on Transmit Delay Diversity for Mobile DVB-T/H Systems" submitted to IEEE Transactions on Broadcasting on Oct. 2008.
3. Y. Zhang, J. Cosmas, K.-K. Loo, M. Bard, and R. D. Bari, "Analysis of Cyclic Delay Diversity on DVB-H Systems over Spatially Correlated Channel", IEEE IEEE Transactions on Broadcasting, vol. 53, No. 1, March 2007.
4. Yue Zhang, C.H. Zhang, J. Cosmas, K.K. Loo, T. Owens, R.D. Bari, Y. Lostenlan, M. Bard, "Analysis of DVB-H Network Coverage with the Application of Transmit Diversity", IEEE Transactions on Broadcasting, Sept. 2008, Volume: 54,Issue: 3, Part 2, On page(s): 568-577
5. R. Di Bari, John Cosmas, MauRicean Bard, Kok-Keong Loo, Raj. Nilavalan, Hamidreza Shirazi "Measurements, Processing functions and Laboratory test-bench Experiments for Evaluating Diversity in Broadcast Network" IEEE International Symposium on Broadband Multimedia Systems and Broadcasting, March 2007, Orlando (USA).
6. Raffaele Di Bari, J. Cosmas, R. Nilavalan, H. Shirazi, K. Krishnapillai, M. Bard, K.K.Loo "Field Trials and Test Results of DVB-T Systems with Transmit Delay Diversity", IEEE International Symposium on Broadband Multimedia Systems and Broadcasting, March 2008, Las Vegas (USA).

7. Raffaele Di Bari, J. Cosmas, R. Nilavalan, H. Shirazi, K. Krishnapillai, M. Bard, K.K.Loo “Field trials and test results of portable DVB-T/H systems with transmit delay diversity”, ISCE 2008 - International Symposium on Consumer Electronics, April 2008, Algarve (PO).
8. Shirazi H, Di Bari R, Cosmas J, Nilavalan R, Zhang Y, Loo J, Bard M “Test-bed Development & Measurement Plan for Evaluating Transmit Diversity in DVB Networks” 16th IST Mobile and Wireless Communications Summit, Budapest (UN).
9. Shirazi H., Cosmas J., Krishnapillai K., Gledhill J., Bard M., Bradshaw D., Di Bari R. “Evaluating Existing Set-top Boxes Versus Transmit Diversity Schemes”, ISCE 2008 - International Symposium on Consumer Electronics, April 2008, Algarve (PO).
10. R. Di Bari, M. Bard, K.M. Nasr, Y. Zhang, J. Cosmas, K.K. Loo, R. Nilavalan, H. Shirazi, K. Krishnapillai, Gerard Pousset, Vincent Recrosio “Evaluation of Diversity Gains for DVB-T Systems” accepted for NEM 2008 Summit, Oct. 2008, Saint-Malo, (Fr)
11. R. Di Bari, M. Bard, A. Arrinda, P. Ditto, J. Cosmas, K.K. Loo, and R.Nilavalan, “Rooftop and Indoor reception with transmit diversity applied to DVB-T Networks: a long term measurement campaign”. Accepted for IEEE International Symposium on Broadband Multimedia Systems and Broadcasting, May 2009, Bilbao (ES)

2. The physical link structure of DVB-T/H systems

Chapter 1 mentions that the effectiveness in real-word applications of novel diversity techniques for broadcast transmitter networks needs to be proven. Although transmit delay diversity can be applied to several OFDM-based broadcasting systems, in this thesis the concept was proved by applying transmit DD to DVB-T/H networks. The Digital Video Broadcasting - Terrestrial (DVB-T) [2] is a standard of the European consortium DVB based on the transmission of audio/video MPEG-2 streaming by using of the Coded Orthogonal Frequency Division Multiplexing (OFDM) system. The Digital Video Broadcasting - Handheld (DVB-H) adds to the existing DVB-T architecture new features at physical and link layer to enable handheld and mobile reception. These networks are currently being deployed in a steadily growing number of countries in Europe. This chapter describes the basic physical elements that are used in DVB-T/H systems. An outline of the DVB-T system is provided, describing the main features of the transmission standard. Then, the architecture for a receiver decoder compliant with the DVB-T standard will be presented. Some of the challenging tasks facing OFDM demodulation will be described, in particular the coarse and fine frequency acquisition, FFT-window timing recovery and frequency domain channel estimation. The differences between DVB-T and DVB-H will also be presented. Finally a section dedicated on DVB-H/DVB-T compatibility issues concludes the chapter.

2.1 Schematic of DVB-T transmission system

The basic DVB-T schematic diagram includes the outer coder/decoder, inner coder/decoder, QAM mapping, Frame adaptation and TPS insertion, OFDM and up/down converter as shown in Figure 2-1. All the blocks presented below are implemented within the digital circuits stage of actual receiver/transmitter systems. The measurements of DVB-T with transmitter diversity are based on this platform.

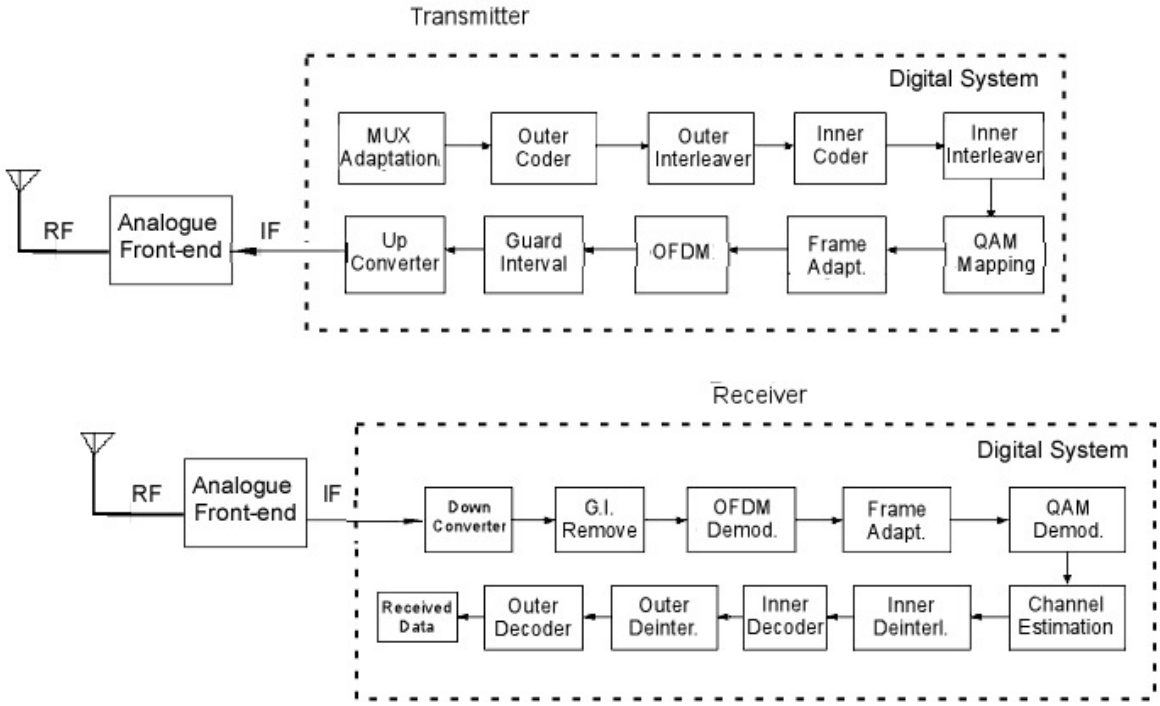

Figure 2-1: Schematic of DVB-T transmission system

2.2 MUX Adaptation stage

The MUX adaptation (or energy dispersal) stage is a randomizer with eight packet period. The input stream of DVB system is a 188-byte MPEG-2 TS, which is randomized by Pseudo Random Binary Sequence (PRBS) generator with generator polynomial $1+X^{14}+X^{15}$. The PRBS register is loaded with initial sequence "100 1010 1000 0000" (Figure 2-2) and is re-initialized at the start of every group of 8 MPEG2-TS packets. The first sync byte in a group of 8 packets is inverted from 47_{HEX} to $B8_{HEX}$ for identification of every randomized group of packets (Figure 2-3-b). The first bit at the output of the PRBS generator is applied to the first bit (e.g. Most Significant Bit) of the first byte following the inverted MPEG-2 sync byte (e.g. $B8_{HEX}$). To aid other synchronization functions, during the MPEG-2 sync bytes of the subsequent 7 transport packets, the PRBS generation continues, but its output is disabled, leaving these bytes unrandomized (Figure 2-3-b). Thus, the period of the PRBS sequence is 1503 bytes. The randomization process is active even if the modulator input bit-stream is non-existent or non-compliant with the MPEG2-TS format (1 sync byte + 187 packet bytes). Reverse operation is carried out in descrambler at the receiver in order to obtain the sink MPEG-2 TS. DVB-T and DVB-H have the same MUX part in the transmitter. In order to obtain the MPEG-2 TS

synchronization the reverse operation is carried out in the descrambler at the receiver. The DVB-T and DVB-H have the same MUX part in the transmitter.

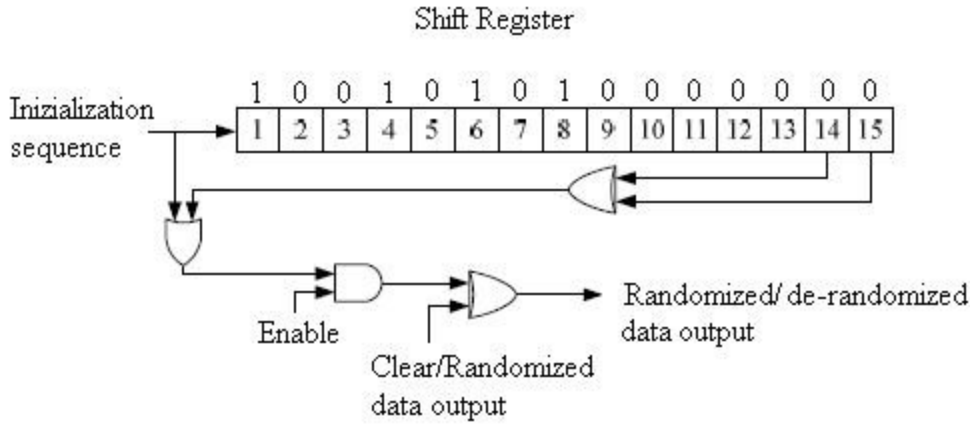

.

Figure 2-2: Scrambler/descrambler schematic diagram [2]

2.3 Outer coder and outer interleaver

A Reed-Solomon (RS) code is applied to each randomized transport packet (188 byte) to generate an error protected packet with 16-byte parity block. Thus, the RS block allows to correct up to t=8 random erroneous bytes in a received word of N=204 bytes (Figure 2-3-c). The RS code uses a generator polynomial, $g(x)=(x+\lambda^0)(x+\lambda^1)(x+\lambda^2)...(x+\lambda^{15})$, where $\lambda=02_{HEX}$, and a primitive field generator polynomial is $p(x) = x^8 + x^4 + x^3 + x^2 + 1$, that has the capability of correcting up to 8-byte random errors. This Reed-Solomon code may be implemented by adding 51 bytes, all set to zero, before the information bytes at the input of an NASA standard RS (255,239, t = 8) encoder. After the RS coding procedure, these null bytes are discarded, leading to a RS code word of N = 204 bytes. The RS coding is also applied to the packet sync byte, either non-inverted (i.e. 47_{HEX}) or inverted (i.e. $B8_{HEX}$). The outer interleaving is described in section 2.14.5. The data structure after the outer interleaver is shown in Figure 2-3-d

SYNC 1 byte	MPEG-2 transport MUX data 187 bytes

- MPEG-2 Transport Stream MUX packet

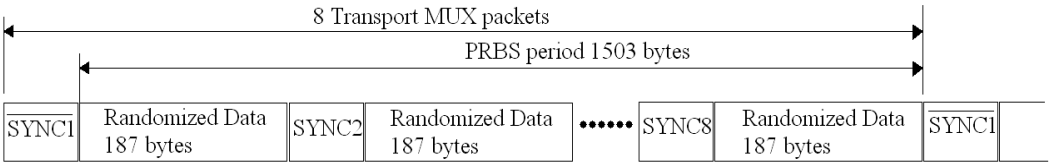

- Randomized MPEG-2 transport MUX packets

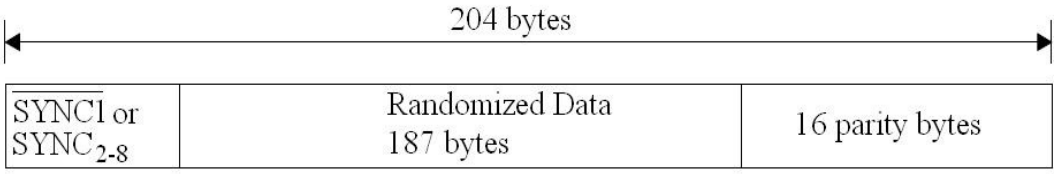

- Reed Solomon error protected packet

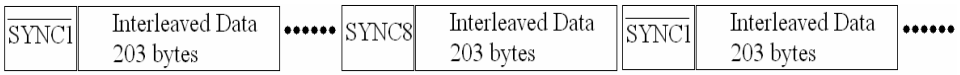

- Data structure after outer interleaving

Figure 2-3: Outer code and interleaving processing [2]

2.4 Inner coding

DVB-T/H system uses a convolutional code of rate 1/2 with 64 states to create a range of punctured convolutional codes. The generator polynomials of the mother convolutional codes are $G1=X+X^1+X^2+X^3$ for X output stream, and $G2=X+X^2+X^3+X^5$ for Y output stream (Figure 2-4). With mother code of rate 1/2, the input bitstream is doubled by the convolutional coder and the output is reduced by using puncturing method to provide an appropriate punctured rate such as 2/3, 3/4, 5/6 and 7/8. For instance, to obtain rate 2/3, one of each 4 bits data will be punctured. Similarly, to obtain rate 3/4, two of each 6 bits data will be punctured. At the receiver, the punctured bits are padded with zeroes such that the decoding is carried as if a rate 1/2 code. The punctured bits are lost bits which increases system BER (Bit Error Rate).

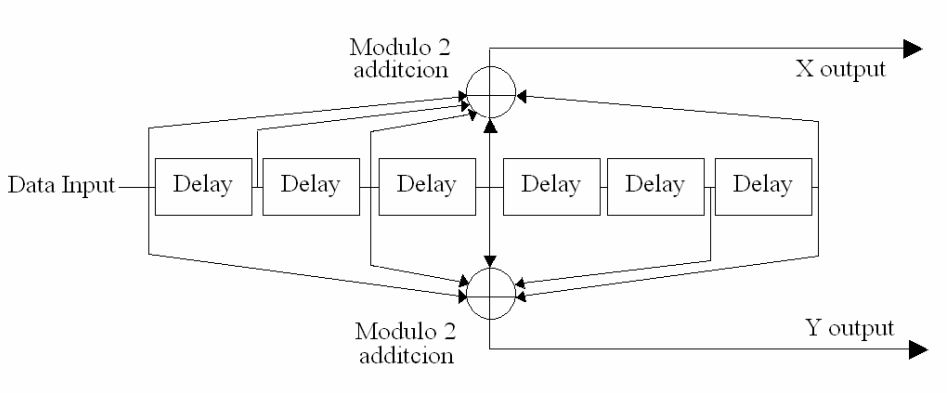

Figure 2-4: The mother convolutional generator

2.5 Inner Interleaving

Data sequence is rearranged after the inner encoder, aiming to reduce the influence of burst errors. A block interleaving technique is adopted, with a pseudo-random assignment scheme. Firstly the output of convolutional encoder (consisting of two streams) is split into v sub-streams, where $v = 2$ for QPSK, $v = 4$ for 16-QAM, and $v = 6$ for 64-QAM. Each sub-stream is then processed by a separate bit-interleaver. Bit-interleaver maps 128-bit input block onto 128-bit output block. The outputs of the six bit-interleavers are sequentially grouped to form six-bit symbols. These six-bit symbols are again interleaved by symbol-interleaver. In 2K mode, the symbol-interleaver interleaves 12 sets of 126, six-bit symbols, and in 8K mode, it interleaves 48 sets of 126 symbols. Figure 2-5 shows a Bits and Symbols inner interleaver for QPSK.

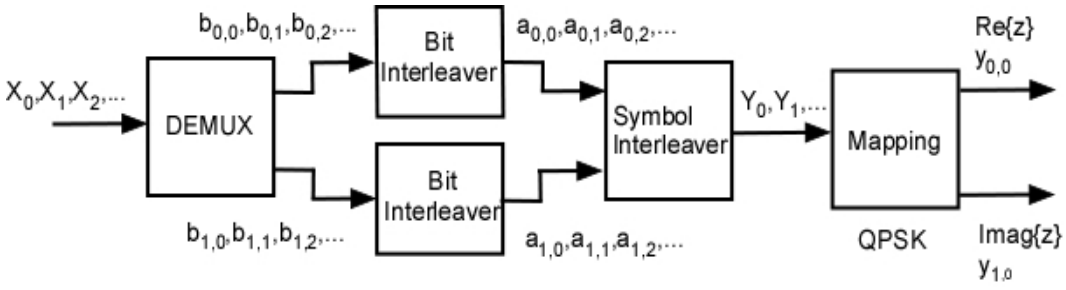

Figure 2-5: Bits and symbols inner interleaver for QPSK [2]

2.6 QAM Mapping

After the interleaver, the bits are almost random distributed in one OFDM symbol. The system uses Orthogonal Frequency Division Multiplex (OFDM) transmission. All data carriers in one OFDM frame are QPSK, 16-QAM, 64-QAM, non-uniform-16-QAM or non-uniform-64-QAM using Gray mapping. A non uniform constellation is used with the hierarchical modulation, where two separate data streams with different priority are modulated onto a single DVB-T stream. MPEG transport streams, referred to as the high-priority and the low priority stream are mapped onto the signal constellation by the mapper and the modulator which therefore has a corresponding number of inputs. A uniform QPSK mapping is shown in Figure 2-6.

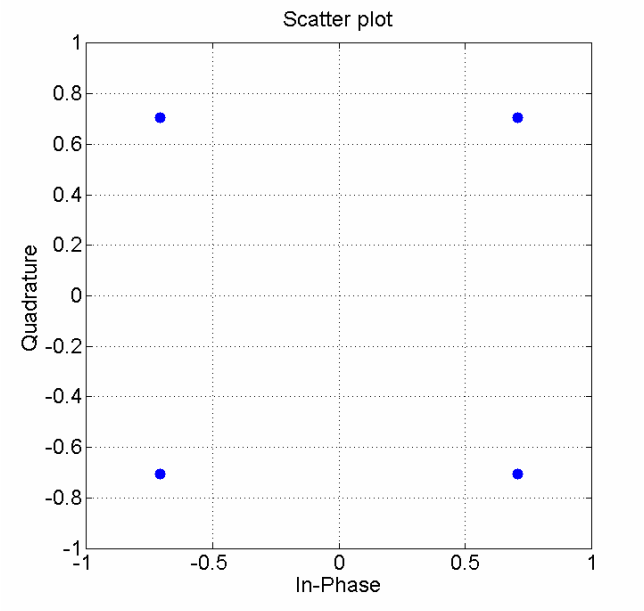

Figure 2-6: Uniform QPSK mapping

A 16-QAM and 64-QAM mapping is shown in Figure 2-7 and Figure 2-8.

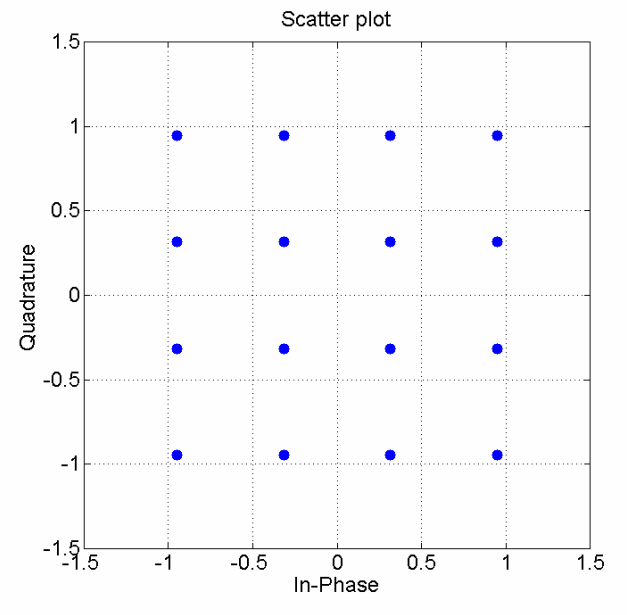

Figure 2-7: Uniform 16 QAM mapping

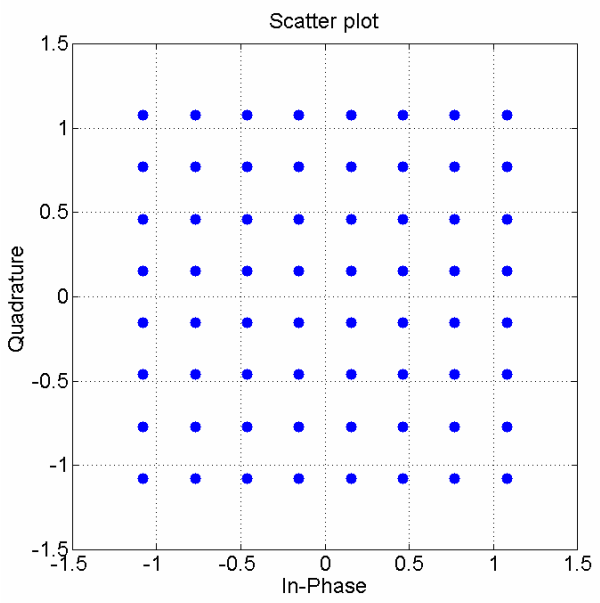

Figure 2-8: Uniform 64QAM mapping

2.7 Frame adaptation and Transmission Parameters Signalling (TPS)

The transmitted signal is organized in frames. Each frame has duration of T_F, and consists of 68 OFDM symbols. Four frames constitute one super-frame. Each symbol is constituted by a set of K = 6817 carriers in the 8k mode and K = 1705 carriers in the 2k mode and transmitted with a duration TS. Each symbol can be considered separated into cells, each

corresponding to the modulation carried on one carrier during one symbol. Various cells within the OFDM frame are modulated with reference information whose transmitted value is known to the receiver. Thus, in addition to the transmitted data, an OFDM frame contains scattered pilot carriers, continual pilot carriers and TPS carriers. The scattered pilot and continual pilots are used at receiver stage for channel estimation, and for the frame adaptation by using the frame synchronization, frequency synchronization, and time synchronization (Figure 2-16). The value of the scattered or continual pilot information is derived from the PRBS which is a series of values, one for each of the transmitted carriers. The TPS carry information on modulation, hierarchy, guard interval, inner code rates, transmission mode and frame number in a super-frame. The TPS is defined over 68 consecutive OFDM symbols, allocating 17 TPS carriers for the 2k mode and on 68 carriers for the 8k mode. Each OFDM symbol transports one TPS information bit, differentially encoded over the TPS carriers of the same symbol. It should be noted that the receiver must be able to synchronize, equalize, and decode the signal to gain access to the information held by the TPS pilots.

2.8 OFDM

Orthogonal Frequency Division Multiplexing (OFDM) is a multicarrier transmission technique, which divides the available spectrum into many carriers, each one being modulated by a low rate data stream. The ortogonality between the sub-carriers is achieved by positioning nulls of each sub-carrier spectrum at the center of the other sub-carrier and thus minimizing inter-carrier interference (ICI). The close spacing and the overlapping of the subcarrier spectrums allow high bandwidth efficiency. The OFDM symbol can be generated in an efficient way by using an IFFT algorithm. The OFDM modulation shows its robustness in multipath propagation environment. By transmitting the data stream with bandwidth B into N sub bands of bandwidth B_F=B/N, the channel transfer function per each sub band can be considered flat (if N is high enough) and the equalization function is not necessary or very simplified, as compared to single carrier modulation. Intersymbol interference is avoided through the use of a guard interval. The using of N sub-carriers makes the OFDM symbol duration N times longer than the duration of single carrier modulation symbol with the same bit rate. This configuration requires a smaller fraction of time needed to eliminate the ISI compared to a single carrier

system, making the OFDM modulation more efficient to prevent the delay spread effects. Disadvantages of OFDM systems include a peak–to-average power ratio (PAPR) of OFDM higher than a single carrier system and OFDM is sensitive to a flat fading channel. The OFDM baseband signal consists of *K* orthogonal sub-carriers modulated by *K* parallel data streams:

$$s(t) = \sum_{k=K_{min}}^{K_{max}} c_k \, e^{j 2\pi k' (t-\Delta)/T_u}, \qquad 0 \le t \le T_S \tag{2.1}$$

where $k'=k-(Km_{ax+}Km_{in})/2$, k denotes the carrier index, Δ is the guard interval, T_u is the inverse of the carrier spacing (or symbol duration), and c_k is the complex symbol for carrier k. The total duration of the symbol is defined as $T_S = \Delta + T_U$. The OFDM signal in equation 2.1 can be derived by using the inverse Discrete Fourier Transform (DFT):

$$x_n = \frac{1}{N} \sum_{q=0}^{N-1} X_q \, e^{j 2\pi q n / N} \tag{2.2}$$

where N is the number of DFT coefficients. A convenient form of implementation of equation 2.2 is to use the Inverse FFT (IFFT) to generate N samples x_n corresponding to the useful part, T_U long, of each symbol. The 2K mode is Doppler tolerant at extremely high receiver speeds because of the large spacing of the subcarriers which it implements. However, the short duration of the associated Guard Interval (GI) makes the 2K mode suitable only for small size SFN, making it difficult for network designers to build spectrally efficient networks. An 8K mode implements a longer duration of the associated GI than the 2K, making this mode suitable for large size SFN. However, the performances at high speed reception are unsatisfactory, especially with reasonable receiver cost/complexity. A compromise mode between the 2K and 8K, allows acceptable mobile performance on the receiver side whilst allowing more economical and flexible network architectures. The DVB-H includes a new transmission in the DVB-T physical layer using a 4K mode inner interleaver. In addition to the 2K and 8K transmission modes provided originally by the DVB-T standard, the 4K mode brings additional flexibility in network design by trading off mobile reception performance and size of SFN networks. DVB-H systems use a 4K mode in-depth interleaver, which interleaves 24 sets of 126 symbols. The 4K mode provides about 2 times better Doppler performance than 8K [4]. The max

Doppler $D_{\max}^{f}$ shift can be expressed as percentage of the sub-carrier spacing D_{c}^{f} as $D_{\max}^{f} / D_{c}^{f}$. A Doppler shift in frequency has an ISI effects on the signal. According simulation presented in [27], a relative shift smaller then 5% produce ICI with a negligible effect on the system performances. The guard interval is added by taking copies of the last $N\Delta / Tu$ of these samples and appending them in front (Figure 2-9). As shown in chapter 1, the transmit Delay Diversity coding reduces the effectiveness of the guard interval.

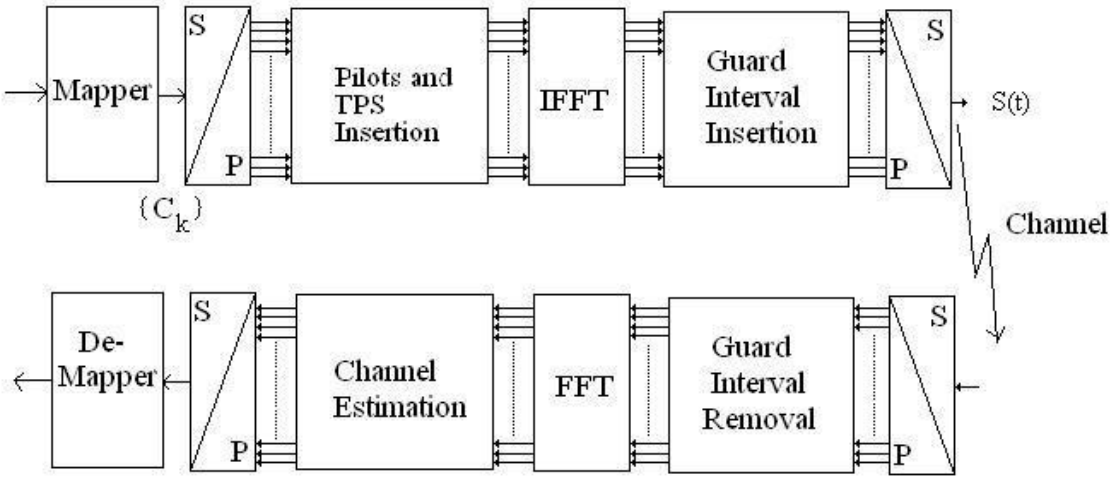

Figure 2-9: The OFDM baseband structure

In DVB standard, the sequence of blocks is modulated using *N*=2048, 4096, or 8192 carriers (2k, 4k, and 8k mode, respectively). The K values c_k are padded with a convenient number of zeros before being mapped onto the N IFFT coefficients X_q.

2.9 Digital Up Conversion

The Digital Up Converter (DUC) is a digital circuit which implements the conversion of a complex digital baseband signal to a real pass-band signal. The DUC implementation detailed in this section is merely for reference purposes. It includes two main blocks: the interpolation filter and the direct digital synthesizer (DDS) as shown in Figure 2-10.

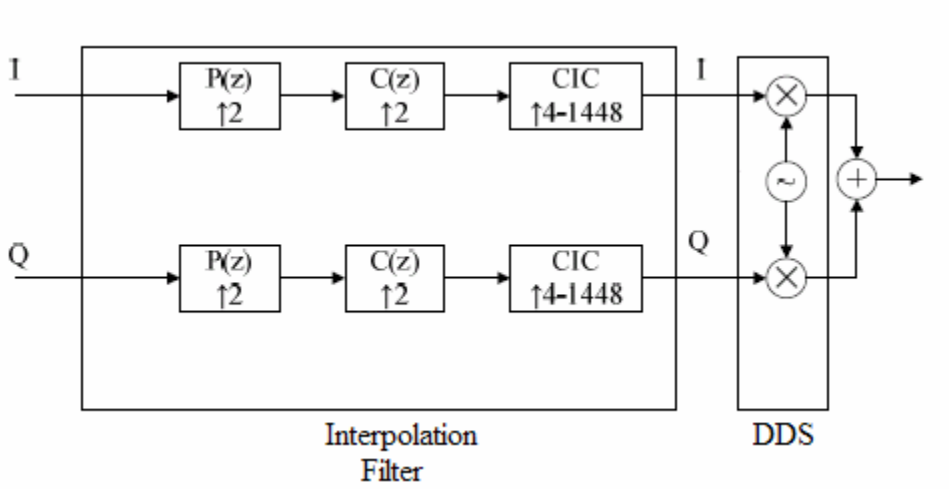

Figure 2-10: The digital up converter [1]

The interpolation filter is composed of three filters, each of which performs a sampling rate change and associated low pass interpolation filtering. At the input of the DUC circuit, the input complex baseband signal is sampled at a relatively low sampling rate, yielding a symbol rate of 9.14 Mega Symbol per Second (MSPS). The sampling rate comes from the elementary period (equal to the system clock) T of 7/64 μs as defined in [2]. The pulse shaping FIR filter P(z) provides a sampling rate increase of 2 and performs transmitter Nyquist pulse shaping. The compensation FIR filter C(z) provides a sampling rate increase of 2 and is used to compensate for the pass-band distortion of the third stage cascaded integrator-comb (CIC) filter [1]. The final CIC filter performs efficiently a sampling rate increasing from 4 to 1448 [31]. The complex data stream from the filtering stages is up-converted to an IF band by a mixing operation with a local oscillator generated by DDS in digital domain. The I and Q mixer outputs are combined to form the final pass-band signal centered at 36.16 MHz.

2.10 Analogue front end

The analogue front-end circuit for the transmitter mainly consists of signal amplification, bandwidth filtering and conversion from IF to the radio frequency (RF) of interest. Figure 2-11 shows an example of a transmitter digital system and analogue front end. The analogue front-end deployed for the transmit diversity experiment of this thesis is fully detailed in Chapter 5.

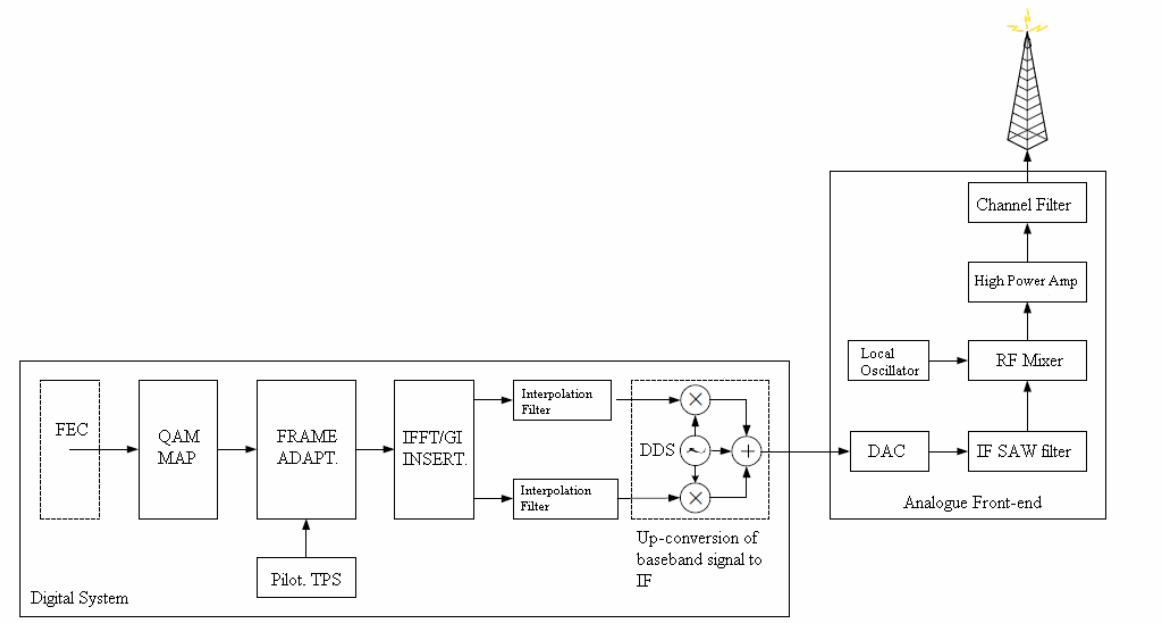

Figure 2-11: The transmitter digital system and analogue front-end [1]

2.11 DVB-T/H Receiver Design

DVB-T specifications [1] do not provide guidelines for the receiver design. Thus, the receiver design in this section will be referred to a typical implementation Set Top Box receiver (STB) used in the measurement campaign, consisting of a single conversion full band Network Interface Module (NIM) [32] with a built in low phase noise phase locked loop (PLL) tuner and a single chip DVB-T channel decoder. The module also provides MPEG-2 Transport Stream as output.

The receiver module can be split into two stages: the analog front end (including the tuner and the IF interface) and the digital system (e.g. the demodulator chipset). Figure 2-12 shows the reference receiver block diagram. The tuner part delivers the received signal located at Intermediate Frequency (IF). The digital receiver part can be divided itself into several stages, including Digital Down Converter (DDC), symbol, carrier and timing recovery, OFDM demodulation, channel equalization, QAM demodulation and FEC (Forward Error Coding).

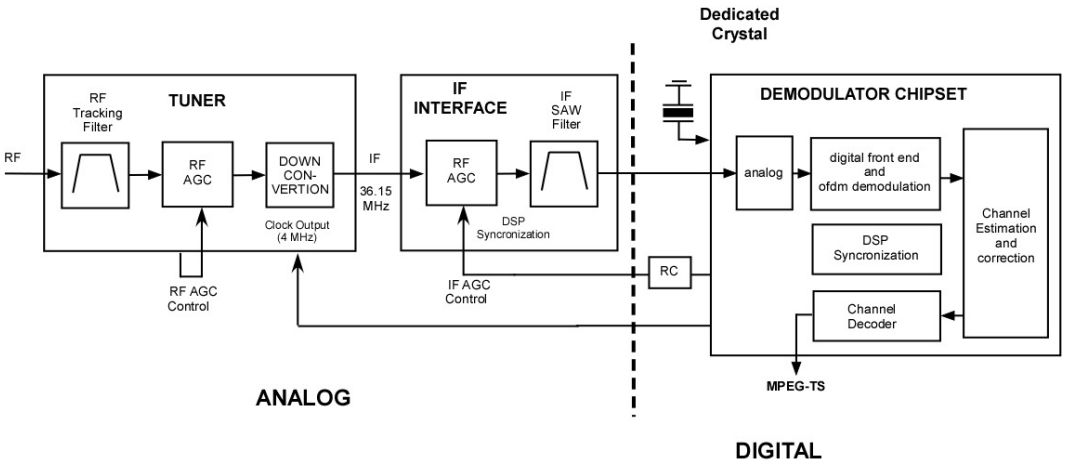

Figure 2-12: Reference receiver block diagram [32]

2.12 Tuner

The tuner performs one stage down conversion. A RF tracking filter tracks the RF wanted frequency and suppresses the image. A first wide-band automatic gain control (AGC) is processed at RF level. The RF AGC is driven from within the RF section. The down-converter translates the RF signal to the IF, typically 36.16 MHz. A phase locked loop (PLL) generates the Local Oscillator that is mixed with the RF signal to downconvert it to IF. The PLL is driven by an external 4 MHz clock (given by a crystal oscillator) feeding the demodulation chipset (Figure 2-12).

2.13 IF interface

The IF interface block consists of an IF AGC and a surface acoustic wave (SAW) filter. The 8 MHz surface acoustic wave SAW filter eliminates part of the power of the adjacent channels around IF. The IF AGC gets the control signal from the digital AGC embedded in the demodulator chipset. The IF AGC control is analogue converted by using low pass RC filter (Figure 2-12). The AGC controls are used to estimate the Received Signal Strength Indication (RSSI) used in several experiments in chapter 5.

2.14 COFDM Demodulator Chipset

The demodulator chipset can be divided into 5 main stages: analogue section, digital front end and COFDM demodulation, synchronization block, channel estimation and correction, and FEC decoder. The internal DSP synchronization core manages the control of the demodulation process. The module offers capabilities to monitor parameters such as BER, $ESR_{\%}$, SNR, RSSI and Channel information.

2.14.1 Analogue block

This includes an analog to digital converter (ADC) and a PLL. The input IF analogue signal is sampled at the ADC and converted onto a 10-bit digital signal. An embedded PLL (locked to the 4 MHz crystal oscillator) delivers the sampling frequency to the ADC and to the digital core. The digital converter (ADC) has a sampling frequency of F_S=53 MHz to over-sample the IF signal at 36.16 MHz and thus help relax the analog anti-aliasing filtering requirements. Typically, the sampling frequency gives optimum performances around 53 MHz, corresponding to equal suppression (of adjacent channels) in the upper and lower aliased bands. This sampling frequency also is applicable for 6 and 7 MHz signal bandwidths.

2.14.2 Digital Front End and OFDM demodulation

Before the OFDM demodulation, the digital front end performs several synchronization tasks such as sampling clock, symbol clock, and carrier frequency recovery. A typical configuration is shown in Figure 2-13.

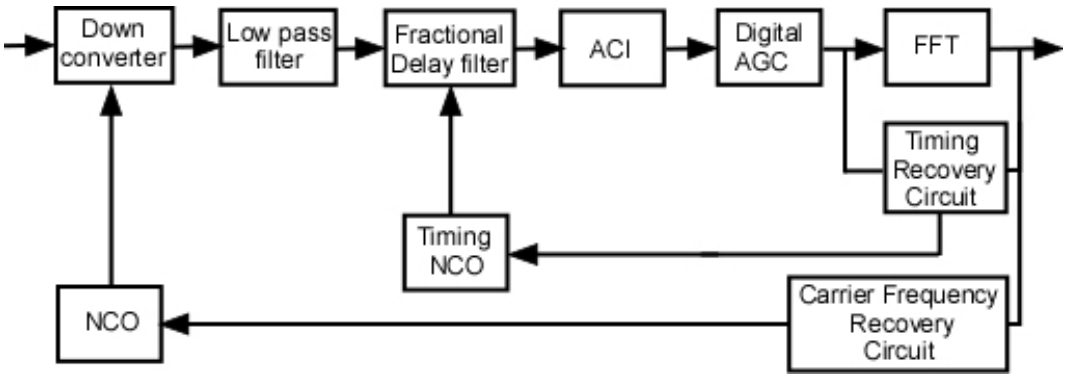

Figure 2-13: Frequency and timing recovery loop.
The I and Q arms are not shown

The signal passes through the downconverter where it is divided into its in-phase (I arm) and in-quadrature (Q arm) components and is low-pass filtered to remove the high frequency components. Then, the symbol timing is synchronized by using a timing recovery circuit, a Numerical Control Oscillator (NCO) and a Digital fractional delay filter. The fractional filter is a useful tool for fine-tuning of the symbol timing synchronization (e.g. FFT window opening time). A Digital Adjacent Channel Interference (ACI) filter suppresses the remaining adjacent signal and thus eliminates the need for multi-bandwidth SAW IF channel filters providing 6, 7, and 8 MHz operation using a single 8 MHz SAW filter. A digital AGC is placed behind the ACI filter in order to compensate for the bandwidth reduction performed by the filter to re-adjust the level of the useful DVB-T wanted signal to the level required before FFT demodulation. A FFT (Fast Fourier Transform) processor carries out an FFT operation for the useful data duration of input signals, converts time domain signals into frequency domain signals, and outputs the frequency domain signals.

2.14.3. Synchronization block

2.13.3.1 Time recovery (e.g. symbol and sampling recovery)

In general, to get a precise timing in a wide range, the synchronization process must be divided into two modes: coarse synchronization and fine synchronization. The coarse symbol synchronization typically uses the correlation method based on the guard interval. The estimation of the starting position of the symbol k_{est} can be found as:

$$k_{est} = arg\ \max_{k} \left| \sum_{i=0}^{L-1} r(k-i) r^{*}(k-i-N) \right| \qquad 2.3$$

where N is the number of the sub-carriers and L is the size the guard interval in samples. This coarse symbol timing estimation is biased and has a large standard deviation [33]. So the fine synchronization process is needed to further improve its accuracy. After coarse timing synchronization, the received demodulated signal with incorrect FFT-window position can be described as:

$$\tilde{X}(n) = \frac{1}{N} \sum_{n=0}^{N-1} x(n) e^{j2\pi k \frac{\varepsilon}{N}} e^{-j2\pi k \frac{n}{N}} \qquad 2.4$$

where ε is the offset of the fine FFT-window in samples. Figure 2-13 shows a timing fine-estimation based on the scattered pilots. Since ε is constant for each k, it can be seen as a time shift of the impulse response. It is assumed that the offset ε is in the direction that causes no ISI. A first step consists of collecting the received scattered pilots. By comparing the received values with the known amplitude and phase, the channel can be estimated in frequency domain. By taking the IFFT, the Channel Impulse Response (CIR) can be estimated. The FFT-window can be "open" at the optimal time which is assumed to be the first tap of CIR. The place of the first tap of CIR can be detected by using a threshold and detecting the parts where CIR values are over this threshold. After the timing synchronization, the removal of the guard interval can be done with the required accuracy.

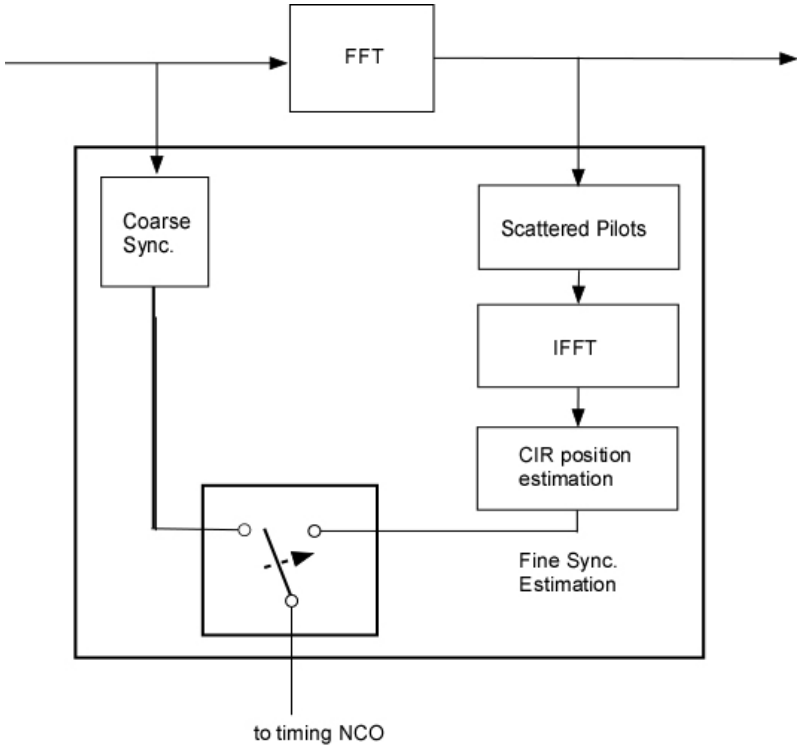

Figure 2-13: Fine and coarse symbol synchronization design

2.14.3.2 Frequency synchronization

Besides the symbol synchronization, the frequency synchronization is also necessary for the DVB receiver implementation. If the receiver frequency differs from the transmitted frequency, all the constellation diagrams will rotate by an angle proportional to the frequency offset between the received and transmitted frequency. The frequency offset might have been caused by Doppler effects or inaccuracies in frequency recovery. The carrier frequency recovery circuit estimates the residual frequency offset from outputs of the FFT processor, and yields a value of the estimated residual frequency offset to the NCO. The NCO converts the estimated residual frequency offset value into the sinusoidal wave signals sine and cosine. The sinusoidal wave signals are fed into the complex multiplier. The NCO output frequency is changed until the phase difference becomes zero. The frequency offset is usually estimated by correlating the received pilot tones with the complex conjugate of the transmitted ones, and searching for the frequency shift for which the correlation value is highest. The continuous pilots are located on the real axis, i.e. I (in phase) axis, at either 0° or 180° degrees, and has a defined amplitude. The continuous

pilots are boosted by 3 dB compared with the average signal power. It is assumed that a coarse timing estimation has been performed in order to position the FFT.
This approach is presented in the following expressions:

$$\mu(d) = \sum_k w(k-d) \cdot b_k, \quad w(k) = \begin{cases} a_k^{\,*} \; if \; k \in K_{fpt} \\ 0 \; otherwise \end{cases} \qquad 2.5$$
$$d_{opt} = \arg\max\{\mu(d)\}$$

where d_{opt} is the coarse estimate for the normalised sub-carrier spacing, b_k are the received symbols, a_k are the transmitted fixed pilot tones [4], k the sub-carrier index and K_{fpt} the set of indexes of the fixed pilot tones [34]. In theory, the range of this algorithm is infinite, since there is no periodicity in the frequency assignment of the fixed pilot tones. In general, the coarse carrier offset can be further categorized as fine carrier offset and coarse carrier offset. For the coarse carrier offset, the frequency offset is a multiple number d of sub-carrier spacing frequency offsets, that is, multiple times of OFDM symbol rate. Whereas the fine carrier offset means the frequency offset is smaller than one subcarrier spacing. A fine carrier offset estimator can be found in [34].

2.14.4 Channel Estimation and correction

The channel estimation and correction schema is presented in Figure 2-15.

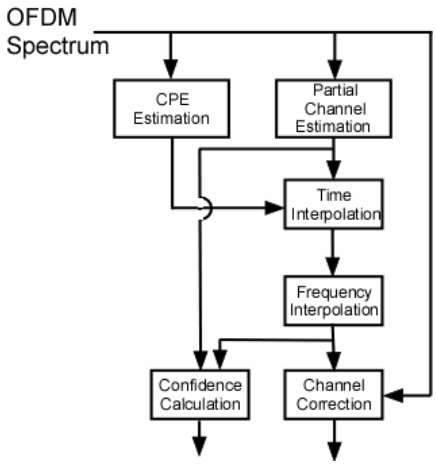

Figure 2-15: Channel estimation and correction [32]

After the base band conversion and FFT demodulation, the channel frequency response is estimated by using known symbols, referred to as the pilots, as shown in Figure 2-16.

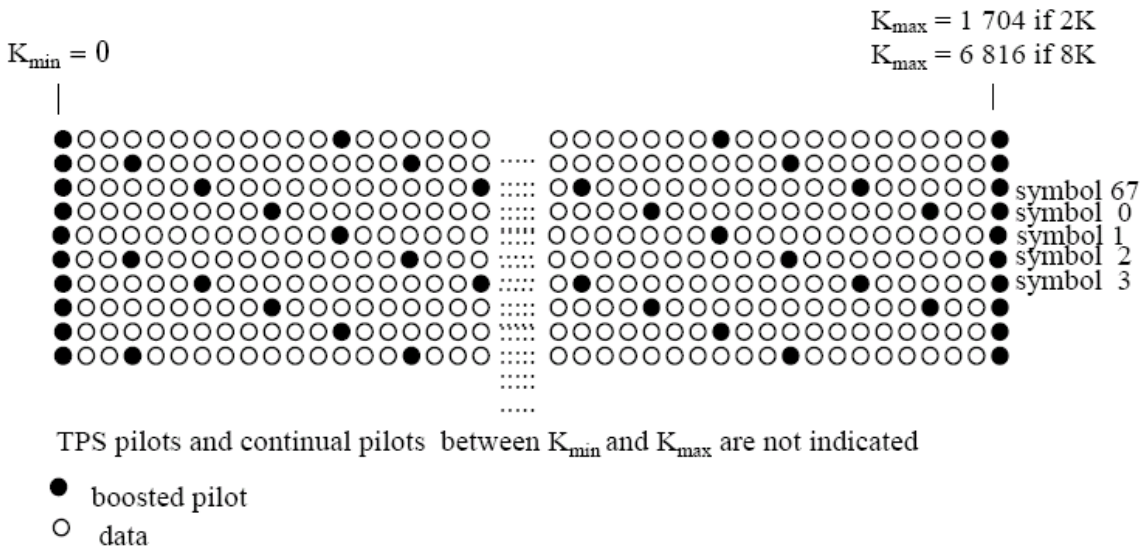

Figure 2-16: Pilots arrangement in DVB systems [2]

The relationship between received signals *Y(n,k)*, transmitted signals *X (n,k)* and the channel transfer function *H(n,k)* can be formulated as:

$$Y(n,k) = H(n,k)\,X(n,k) + W(n,k) \qquad 2.6$$

where *n* is the OFDM symbol index, *k* is the subcarrier index, *W(n,k)* is the 2-D Additive White Gaussian Noise (AWGN) whose power *s(n,k)* may vary with respect to carrier *k*.
In 2.6 the phase noise was ignored and it will be discussed later in this chapter. The received pilot signals are estimated from *Y (n,k)*. For the pilot sub-carriers, the transmitted information $X(n_p,k)$ is known to the receiver and it can be used to estimate the channel coefficients. The channel estimation $\tilde{H}(n_p,k)$ is used to equalize the signal as:

$$D(n_p,k) = \frac{H(n_p,k)X(n_p,k)}{\tilde{H}(n_p,k)} + \frac{W(n_p,k)}{\tilde{H}(n_p,k)} = X(n_p,k) + \frac{W(n_p,k)}{\tilde{H}(n_p,k)} \qquad 2.7$$

Several pilot-aided channel-estimation schemes for equation 2.7 have been studied based on least-squares (LS) and minimum mean–square error (MMSE) algorithms for OFDM applications. The LS estimator has low complexity but its performance is not as good as that of the MMSE estimator [35] that requires a priori knowledge of the channel statistics and the signal-to-noise ratio (SNR) [36]. For those reasons, the LS estimator has been commonly used for channel estimation.

Results presented in Chapter 4 shows that the particular channel estimation implementation and optimization can also affect the achievable diversity gain. The values of the channel in between the samples can then be obtained via an interpolation procedure. Generally the interpolation is a two dimensional interpolation problem that can be separated into an interpolation in time and in frequency. Thus the channel responses of data tones can be interpolated by a cascade of 1-D filters using linear interpolation and Gaussian [37], Cubic [38] or Lagrange interpolation [39]. Interpolations in both frequency and time domain must agree with the sampling theorem [40]. In the *time domain*, the interpolation is band limited by the time-variant behavior of the channel. This is caused by a movement of the receiver and by uncompensated synchronization errors. Time interpolation takes into account an estimate of the Common Phase Error (CPE). The CPE is a random phase error, common to all carriers, that is due to the local oscillator's phase noise [41]. The CPE is estimated in a block separate from ICI recovering, using continual pilots that are inserted in the DVB-T signal. In the *frequency domain,* the interpolation in frequency is band limited by the length of the Channel Impulse Response (CIR). The maximum allowable CIR-length thus is not only determined by the length of the guard interval but also by the number of training symbols in one OFDM symbol [42]. The estimation is then used as a correction on the signal, carrier by carrier.

2.14.4.1 Confidence calculation

The estimation of signal-to-noise power on D(n,k) from equation 2.7 is

$$\left|\tilde{H}(n_p,k)\right|^2 / \left|s(n_p,k)\right|^2 \qquad 2\text{-}8$$

This value will be passed to the channel decoder as a confidence estimate, together with D(n,k). Several methods can be adopted to calculate the signal-to-noise power. The SNR can be estimated using pilot data or data symbols (blind estimation). For instance, [43] suggests a pilot aided SNR estimator based on subspace algorithms, while [44] proposes a MMSE Noise Power and SNR estimation restricted to data aided estimation. The SNR estimated by the receiver will be used to evaluate the diversity gain in chapter 5 experiments.

2.14.5 FEC decoder

The FEC decoder implementation in the receiver includes demapper, symbol/bit deinterleaver, Viterbi decoder and convolutional deinterleaver. Channel State Information (CSI) is computed for each carrier and is fed to the FEC to get optimum performances. CSI consists of extra reliability information bout the noise level per each subcarrier and must take account of the soft decision. Frequently, CSI is defined as SNR (Signa1 to Noise Ratio) in a carrier position. Typically the CSI is first calculated over the pilots' sub-carrier and then interpolated to get CSI in the useful data positions. The demapper generates soft decision information as a function of the modulation and the channel reliability. The value of each noisy sample yielded by the FFT and channel correction processing is converted into a number of soft decision metrics that can be optionally weighted by the (CSI) of the related sub-carrier [45]. The de-interleaving step performs the inverse addressing operation described in section 2.3. Internal decoding is performed by using a Viterbi algorithm. The implementation of the Viterbi decoder consists of three main blocks: the branch metrics calculation unit (BMU), the add-compare-select unit (ACS), the Back-trace unit (TBU) and a (First-In-Last-Out) FILO buffer (Figure 2-17).

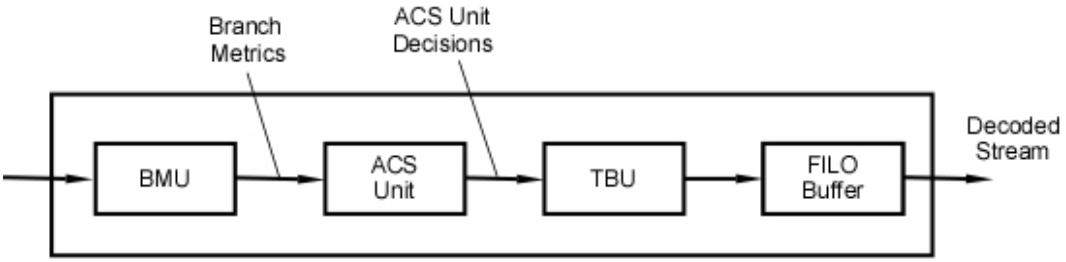

Figure 2-17: The Viterbi decoder block diagram

The BMU performs the calculation of distances of sampled signals from constellation symbols which computes 2N possible branch metrics for every set of N received symbols, where N is 2 or 3 for most practical cases. The receiver can deliver either hard or soft symbols to the Viterbi decoder. A hard symbol is equivalent to a binary ± 1 while a soft symbol is multi-leveled to represent the confidence in the bit being positive or negative. Soft coded data gives a significantly better BER performance compared with hard coded data. Soft decision offers approximately a 3 dB increase in coding gain over hard decision decoding. The BMU can be fed also with the CSI information. The CSI can be considered

as weighting factor during the calculation of the metrics and thus improving the decoding performances up to 2.7 dB [46]. The second block in the decoder is the ACS unit. This block is used to determine the shortest of possible trellis paths for each state and receiving symbol. There is an ACS sub-block per each state. The basic ACS operation is demonstrated in Figure 2-18. For a radix-2 trellis, the computation of the shortest path to a state requires two additions and one comparison. The addition computes the value of each of the two possible paths from the current path metrics and the receiving symbol. The comparison selects the smaller of the two to be updated in the path metric. The decision path is forwarded to the TBU that is used later to decode the receiving symbols. The path metric is then updated with the new selected value [47]. For a given trellis constraint length L, the number of an ACS sub-block is 2^{L-1}.

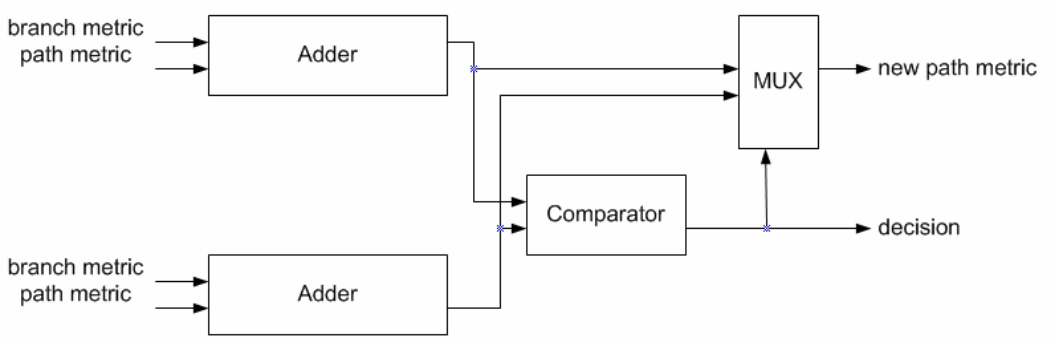

Figure 2-18: The ACS sub-block diagram

The last block is the TBU. The actual decoding of symbols in order to obtain the original data sent is accomplished by tracing the maximum likelihood path through the trellis in a backward manner. The general approach to TBU is to accumulate path metrics for up to five times the constraint length, find the node with the largest accumulated cost, and begin traceback from this node. After a number of symbols equal to at least five times the constraint length (e.g. traceback length), the decoded data is outputted. Since it does this in inverse direction, a Viterbi decoder comprises a FILO buffer to reconstruct a correct order. After the Viterbi decoder, the output data is sent to the convolutional deinterleaver. Figure 2-19 illustrates the operation of the convolutional interleaver/de-interleaver. The interleaver operates as a series of delay line shift registers given the DIN input and DOUT output symbols. Both commutator arms start at branch 0 and advance to the next branch

after the next rising clock edge. After the last branch has been reached, the commutator arms both rotate back to branch 0 and the process is repeated. The only difference between an interleaver and a deinterleaver is that branch 0 is the longest in the deinterleaver and the branch length is decremented by L rather than incremented and Branch (B-1) has length 0. There are I=12 branches [48].

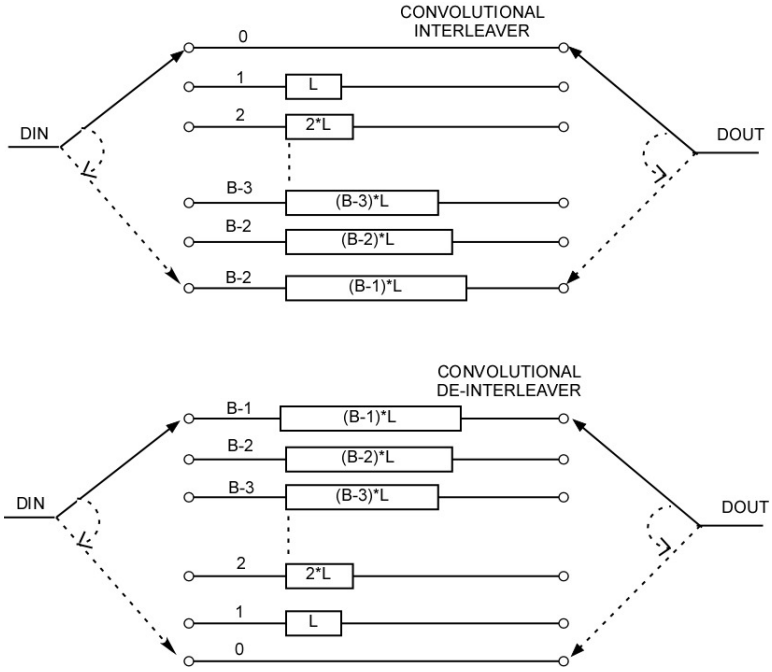

Figure 2-19: Conceptual diagram of the Interleaver and de-interleaver [2].

The outer decoding block includes mainly a shortened Reed-Solomon RS(204,188) decoder. The FEC chip also includes a de-scrambling and a smoothing buffer at the MPEG-2 TS output (for delivering a jitter-free MPEG-2 compliant sample stream). Software simulation typically compares the diversity gain in terms of dB by comparing the Bit Error Rate after Viterbi decoder. However, it was found to be impractical to base laboratory and field trials measurements on the normally used BER metrics due to the bursty nature of the errors. Hence a criterion called $ESR_{\%}$ (Errored Seconds Ratio) defined n chapter 4 was adopted. $ESR_{\%}$ is based on the number of faulty packets after the Reed-Solomon decoder occurring in a time interval.

2.15 Differences between DVB-T and DVB-H

There are few differences between DVB-T and DVB-H in physical and link and layer elements. The first difference in physical layer is the 4K mode. The 4K mode is

architecturally compatible with existing DVB-T infrastructure, requiring only minor changes in the modulator. The 4K mode constitutes a new FFT size added to the native DVB-T 2K and 8K FFT sizes, all other parameters being the same. As the C/N (Carrier to Noise Ratio) performance is FFT size independent, so the 4K size provides the same performance as the other two modes in AWGN, Ricean and static Rayleigh channels [49]. The DVB-T provides a 2K mode with excellent performances well in mobile environment, while the 8K-mode is unsatisfactory especially with reasonable complexity of the receiver. A 4K mode solution achieves better Doppler performance by doubling the carrier spacing of the 8K mode. On the other hand, the longer symbol duration of 8K mode allows the design of small, medium and large Single Frequency Networks (SFNs) while the 2K can be used only for small SFNs. The 4K duration allows the design of small and medium SFNs. Thus the 4K introduces a trade off between mobility and SFN cell size, allowing single antenna reception in medium SFNs at very high speed, adding flexibility for the network design. 4K mode is not mandatory for DVB-H. To further improve robustness of the DVB-H 2K and 4K modes in a mobile environment and impulse noise reception conditions, an in-depth symbol interleaver has also been designed for the DVB-H. For 2K and 4K modes, the in-depth interleavers take benefit of the 8K symbol interleaver's memory to effectively quadruple (for 2K) or double (for 4K) the symbol interleaver depth, therefore improving reception in fading channels. This also provides an extra level of protection against short noise impulses caused for instance by ignition interference. DVB-H signaling in the TPS-bits is used to enhance and speed up service discovery. A cell identifier is also carried in the TPS-bits to support quicker signal scan and frequency handover on mobile receivers. DVB-H signalling is mandatory for DVB-H [5]. A first difference in the link layer is the time slicing. Time slicing consists of a burst transmission of data in order to reduce the average power consumption of the receiving terminal. Time slicing also supports the possibility for the receiver to monitor neighbouring cells during the off-times between bursts, enabling enable smooth and seamless frequency handover. Time slicing is mandatory for DVB-H. A second difference consists of the adoption of the forward error correction for multiprotocol encapsulated data (MPE-FEC). It provides a method to allow DVB systems to transmit IP datagrams. IP datagrams are filled column after column and padded with zeros. The IP packets are arranged frames having 191 columns and a variable number of rows (e.g. 256, 512, 768 or 1024). Once all the packets

are loaded, the parity data section is computed by a Reed Solomon (RS) code as depicted in Figure 2-20. MPE-FEC improves in C/N and Doppler performance in mobile channels. Moreover, it enhances the tolerance to impulse interference. MPE-FEC is not mandatory for DVB-H and must be signalled with two bits of TPS. As it will be shown in chapter 5, the MPE-FEC greatly reduce the achievable diversity gain, since this already partly exploits time diversity by introducing a virtual time-interleaving.

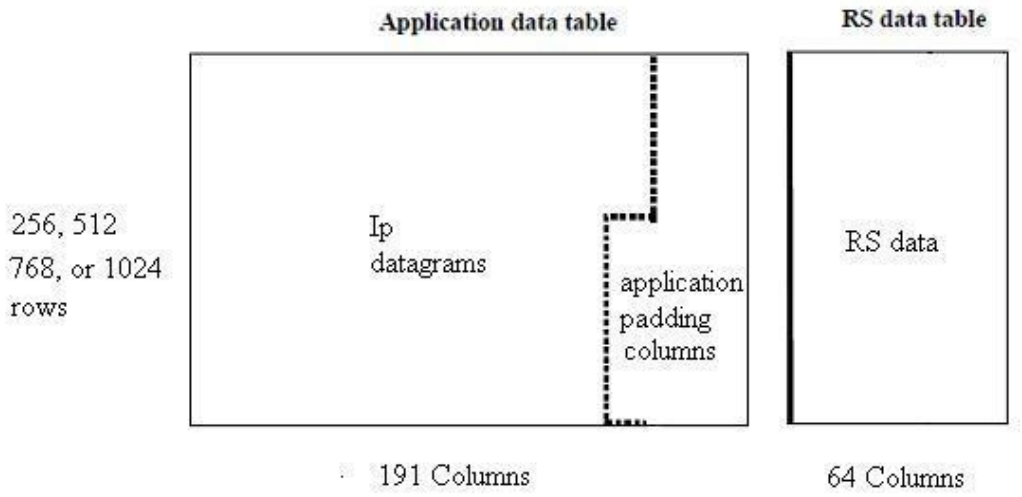

Figure 2-20: MPE Tables and parity check data

2.16 DVB-H/DVB-T compatibility issues

The new DVB-H components are compatible to the existing DVB-T systems [4]. First, as time slicing and MPE-FEC constitute processes applied at the Link layer (Open Systems Interconnection (OSI) Layer 2), they do not raise any incompatibility issues and are fully compatible with the existing DVB-T/S/C Physical layer (OSI layer 1). Moreover, the interface of the network layer (OSI layer 3) of DVB-T supports bursty incoming of IP datagrams, and is therefore fully compatible with time slicing. Time slicing and MPE-FEC modify the MPE protocol in a fully backward compatible way. Allocating bytes of the MAC_address fields, located in the MPE section header, for delivering DVB-H specific parameters is fully supported by the DVB-SI standard [50]. Time slicing and MPE-FEC may be used in a multiplex together with non-Time Sliced and non-MPE FEC services. Furthermore, as for DVB-H signaling, DVB-H signaling is fully backward compatible as

is all signaling in “reserved for future use” bits and these unused bits are ignored by the DVB-T receivers. Therefore, even though some diversity techniques are based on DVB-T system, they can still be applied in DVB-H systems without any modification. However, the 4K mode and in-depth symbol interleaver for the 4K modes affects the compatibility with the current DVB-T physical layer specification. At the system level, the new 4K mode could be considered just as an interpolation of the existing 2K and 8K mode, requiring only an additional parameter in the DVB-T system and a little control logic in the equipment. At the receiver level, 2K or 8K receivers are unable to receive 4K signals, but this is not a severe restriction as any new DVB-H network using the 4K mode is targeted towards new services and new types of hand portable terminals. The only restriction in this case arises when sharing the multiplex between traditional DVB-T and DVB-H services. The standard allows new 4K capable receivers to receive both 2K and 8K transmissions [4]. The integration of DVB-H with DVB-T on the same chipset can be questionable. The DVB-T might not be suitable for hand-held reception since the high power consumption. Moreover, DVB-T standard does not support seamless handover for mobile reception. Finally, the different nature of the services can make not worthy to integrate the two standards on the same chip. A recently-released commercial chip supporting DVB-H and DVB-T standards is presented in [51].

2.17 Summary

The section described the DVB-T/H physical system, including outer coder/decoder, inner coder/decoder, QAM mapping, Frame adaptation and TPS insertion, OFDM and up/down converter. DVB-T/H allows different levels of QAM modulation including QPSK, 16-QAM and 64-QAM and different inner code rates to be used to trade bit rate versus ruggedness. DVB-T/H also allows two level hierarchical channel coding and modulation, including uniform and multi-resolution constellation. Convolutional code and Reed-Solomon code are used in the channel code. MPEG transport streams, referred to as the high-priority and the low priority streams are mapped onto the signal constellation by the mapper and the modulator which therefore has a corresponding number of inputs. Frame adaptation provides synchronization to frame structure of the signal. The OFDM is the major technique for DVB-T/H systems. OFDM is a proven technique for achieving high

data rate whilst overcoming multipath fading in wireless communications. There are 2K and 8K modes for DVB-T system and 4K mode for DVB-H system. One complex number of data symbol modulates one OFDM carrier in DVB-T/H systems. Besides data carriers, each OFDM symbol carries scattered pilots, continual pilots, and TPS carriers. Scattered pilots and continual pilots are used for estimating channel condition together with timing and frequency recovery at receiver side. DVB-H system can be fully compatible with DVB-T system. Differences between the DVB-T and DVB-H consists of the 4K FFT size added to the native DVB-T 2K and 8K FFT sizes, the in-depth symbol interleaver, additional DVB-H parameters signaling in the TPS-bits, time slicing and MPE_FEC correction code. The diversity techniques in DVB-T systems can also be applied into DVB-H system without modifications. The only restriction in compatibility arises when sharing the multiplex between traditional DVB-T and DVB-H services, because of 2K or 8K receivers are unable to receive 4K signals. In the following chapter, a mathematical framework of the MIMO channels and the main propagation characteristics and mechanisms are discussed.

3. Optimization with Diversity

3.1 Introduction

One of the most commonly used and effective technique to combat multipath fading in wireless communication is interleaved coded modulation. This coding adds redundancy, and the interleaving separates the code symbols in time domain to provide independent fading statistics on each of the codeword symbols. However, when the motion in the link is very small (e.g., pedestrian or stopped vehicle), either a very long interleaver is needed to achieve quasi-independent code symbols or interleaving is not effective [52]. Moreover, reception at low SNR needs a robust coding, resulting in a loss of throughput efficiency. A solution to optimize the system is to combine interleaving and coding with transmit and/or receiver diversity. The main idea of diversity consists of transmit several redundant signal replicas in time, space and frequency direction that undergo different multipath profiles. The receiver decoder improves the system performances by exploiting the reception of diversity codeword symbols that experienced independent fading statistics. Diversity can be used to increase the achievable throughput while maintaining the same reception quality, thus providing the so called multiplexing gain. The characteristics of the channel can greatly affect the potential diversity gain. For instance, the Alamouti code achieves optimal gain assuming that the channel does not change within the time interval of the two coded symbols. Thus, a time variant channel can reduce appreciably the achievable gain. On the other hand, the maximum achievable gain in CDD and DD is greatly affected by the coherence bandwidth of the channel. This chapter first provides a mathematical framework of the MIMO channels. The main propagation characteristics and mechanisms are also discussed. These fundamental concepts are also needed to characterize the experimental tests of the next chapters. Then, several indoor and outdoor channel models of interest are presented. These channel models will be employed in hardware simulations presented in chapter 4. A non selective reference channel model is also detailed, to discuss the link between the channel propagation characteristics and the cross correlation in a MIMO channel. This analysis is required to justify the transmit antenna separation deployed for tests of chapter 5 and 6. A brief literature review details the benefits of general space-time-coding techniques with particular reference to

techniques compliant for DVB standard, providing a reference for all results produced in chapter 4, 5 and 6.

2.2 Diversity Theoretical Background

Diversity is a collection of techniques that can be used to improve reception, particularly for mobile/portable devices by overcoming degradations caused mainly by scattering environments, interference, Doppler effects, etc. The advantages provided by diversity consist of increasing the quality of transmission and bandwidth efficient while maintaining a low decoding complexity. Diversity consists of the transmission of several redundant replicas that undergo different multipath profiles. Three types of diversity are usually adopted: frequency, time diversity and space (or antenna) diversity. Frequency diversity consists of transmitting the same information on different frequency channels or spread over a wide spectrum that is affected by frequency-selective fading. In time diversity techniques, the replicas of the signal are provided in the form of redundancy in the time domain by the use of an error control code together with a proper signal interleaver. In space diversity, the redundancy is provided by employing an array of antennas, with a minimum spatial separation between neighbor antennas. Different polarization can also be used. The three diversity techniques can be combined together; although latest wireless communications researches are focusing on the combination of time-space diversity techniques because of the bandwidth efficiency. The use of Multiple Input-Multiple Output (MIMO) technology in wireless communication systems enables high-rate data transfers and improved link quality through the use of multiple antennas at both transmitter and receiver. MIMO technology is a well-documented technique where each pair of transmit and receive antennas provides a different signal path from the transmitter to the receiver. By sending signals that carry the same information through these different paths, multiple independently faded replicas of the data symbol can be obtained at the receive end. Figure 3-1 shows a schematic diagram of a typical MIMO system deploying N transmit and M receiver antennas.

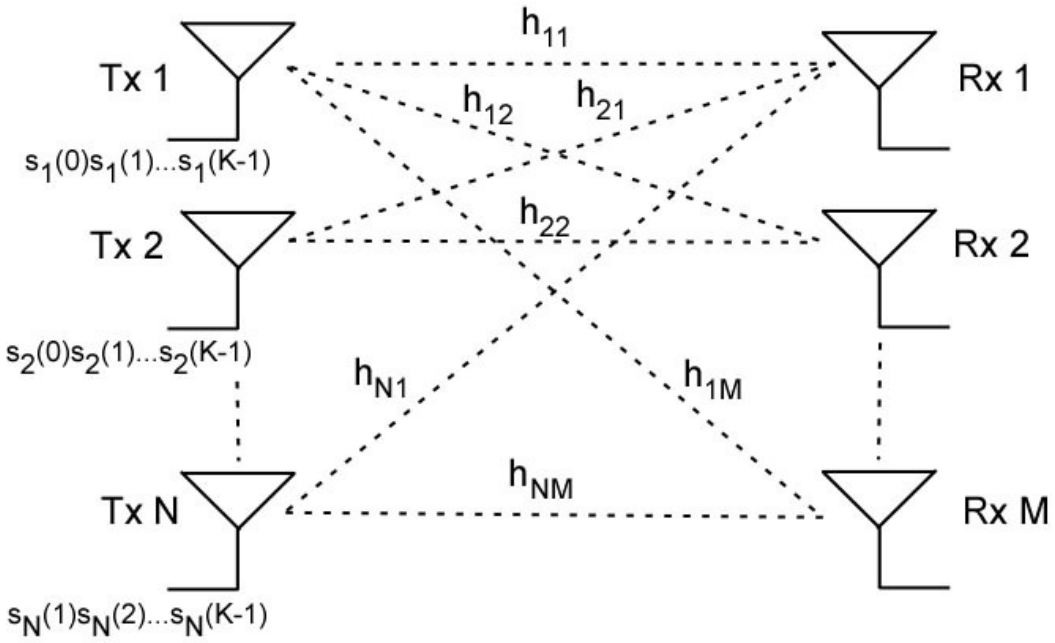

Figure 3-1: A schematics of a MIMO channel

Considering discrete baseband signal processing, the complex symbol $s(t)$ with sample index $t = 0,1,....., K-1$ is sent by N transmit antennas and is detected by j^{th} receive antenna is denoted as $r_j(t)$. The fading coefficient h_{ji} for each channel is the complex path gain from the transmit antenna j to the receive antenna i. h_{ji} is independent complex circular symmetric Gaussian. h_{ji} is assumed to be known to the receiver and constant within the channel estimation process at receiver, thus the receive signal in time-domain can be represented as [53]

$$r_j(t) = \sqrt{\frac{SNR}{N}} \sum_{i=1}^{N} h_{ji}(t) \otimes s_i(t) + \eta_j(t) \qquad 3\text{-}1$$

where SNR is the average Signal-to-Noise Ratio at the receiver antenna, $h_{ji}(t)$ is the path gain from transmit antenna i to receiver antenna j, $s_i(t)$ is the modulation symbol transmitted by antenna i, and $\eta_j(t)$ is an independent Gaussian variable (e.g. AWGN channel). The MIMO channel is defined as a linear superimposition of SISO channels. The relations between these SISO channels will be discussed later.

Each SISO channel is assumed to be Wide-Sense-Stationary-Uncorrelated-Scattering (WSSUS) channel [54]. A WSSUS channel assumes the channel correlation function is invariant over time, and scatterers with different path delays are uncorrelated. This channel model is fully determined by the several echo delay due to multipath, and the Doppler shift due to the vehicle movement. Assuming that the channel is composed of D echoes, the baseband equivalent of instantaneous Channel Impulse Response (CIR) can be expressed as

$$h(t,\tau)=\sum_{n=0}^{D}\alpha_n e^{j\theta_n}e^{j2\pi f_{Dn}t}\delta(\tau-\tau_n) \qquad 3\text{-}2$$

where α_n are the path amplitudes, D is the number of echoes, θ_n are the path random phases, f_{Dn} are the random Doppler frequencies, τ_n are the random delays. The path phases are randomly uniform distributed within the interval of $[0,2\pi]$. Doppler shift in the received signal components is determined by the receiver motion and is defined as

$$f_{Dn}=\frac{v}{\lambda}\cos\phi_n \qquad 3\text{-}3$$

Where n is the index of the incoming wave, v is the receiver speed, λ is the carrier wavelength and ϕ_n is the arrival angle of the n^{th} incoming wave with the motion direction. When the impulse response $h(t,\tau)$ is modeled as zero mean complex valued Gaussian process, the envelope $\rho=|h(t,\tau)|$ at any instant t is Rayleigh-distributed [55]. In this case, the channel is said to be *Rayleigh fading channel.* If the process does not have a zero mean, the envelope has a Ricean distribution and the channel is said to be a Ricean fading channel. In a Rayleigh channel, the phases can be assumed as uniform distributed while for Ricean channels this assumption doe not hold. The transfer function for the channel model is given by [24].

$$H(f,t)=\int_{-\infty}^{+\infty}h(\tau,t)e^{-j2\pi f\tau}d\tau \qquad 3\text{-}4$$

In frequency domain, the received signal is represented

$$\tilde{R}(m)=\sqrt{\frac{SNR}{N}}\tilde{H}(m)\tilde{S}(m)+\tilde{V}(m) \qquad 3\text{-}5$$

where m is the frequency index and

$\tilde{R}(m) = [R_1(m), R_2(m), ...R_M(m)]^T$,

$\tilde{S}(m) = [S_1(m), S_2(m), ...S_M(m)]^T$,

$$\tilde{H}(m) = \begin{bmatrix} H_{11}(m) & H_{12}(m) & ... & H_{1N}(m) \\ H_{21}(m) & ... & ... & ... \\ | & | & | & | \\ H_{M1}(m) & ... & ... & H_{MN}(m) \end{bmatrix}$$

For the case of uncorrelated MIMO channel, it is assumed the channel is sufficiently spatially separated to ensure decorrelation of the multipath signals. The benefits of MIMO diversity are realized when the fading on received signals from the two channels are decorrelated, that is, the signals are faded independently. If LOS are considered, each tap of the MIMO channel matrix can be separated into LOS (fixed) and NLOS (time variant) components according to [56]. The matrix $\tilde{H}$ can be described as

$$\tilde{H}(m) = \sqrt{P}\left(\sqrt{\frac{K}{K+1}}H_V + \sqrt{\frac{1}{K+1}}H_F\right) \qquad 3\text{-}6$$

$$\tilde{H}(m) = \sqrt{P}\left(\sqrt{\frac{K}{K+1}}\begin{pmatrix} e^{j\phi_{11}} & e^{j\phi_{12}} & ... & e^{j\phi_{1N}} \\ e^{j\phi_{21}} & ... & ... & e^{j\phi_{2N}} \\ | & | & | & | \\ e^{j\phi_{M1}} & e^{j\phi_{M2}} & ... & e^{j\phi_{MN}} \end{pmatrix} + \sqrt{\frac{1}{K+1}}\begin{pmatrix} X_{11} & X_{12} & ... & X_{1N} \\ X_{21} & ... & ... & X_{2N} \\ | & | & | & | \\ X_{M1} & X_{M2} & ... & X_{MN} \end{pmatrix}\right) \qquad 3\text{-}7$$

where X_{ji} (j^{th} the receiving and i^{th} the transmitting antenna) are uncorrelated zero-mean, unit variance, complex Gaussian random variables as coefficients of the variable NLOS (Rayleigh) matrix H_V, $e^{j\phi_{ji}}$ are the elements of the fixed LOS matrix H_F, K is the Ricean K-factor, and P represents the sum of the fixed LOS power and the variable NLOS power (sum of powers of all taps).

2.3 Fading distributions

As shown in the previous section, ρ depends on the propagation environment and on the receiver speed. A simple model for ρ was proposed by Clarke [57] assuming a fixed

elevated transmitter with vertical polarization, a mobile receiver with horizontal polarization antenna, and a large number of signals arriving at receivers with angle of arrivals uniformly distributed and equal average powers. Under this condition, is it possible to prove that ρ can be modeled as a Gaussian zero mean stationary processes, with real and imaginary part independent and normalized autocorrelation function equal to:

$$R(\tau) = P \cdot J_0(2\pi f_D \tau) \qquad 3\text{-}8$$

where $J_0(\ )$ is a 0^{th} order Bessel function of the first kind, f_D is the maximum Doppler shift and P is the signal power. The autocorrelation function of this fading channel with 10 Hz maximum Doppler shift is shown in Figure 3-2.

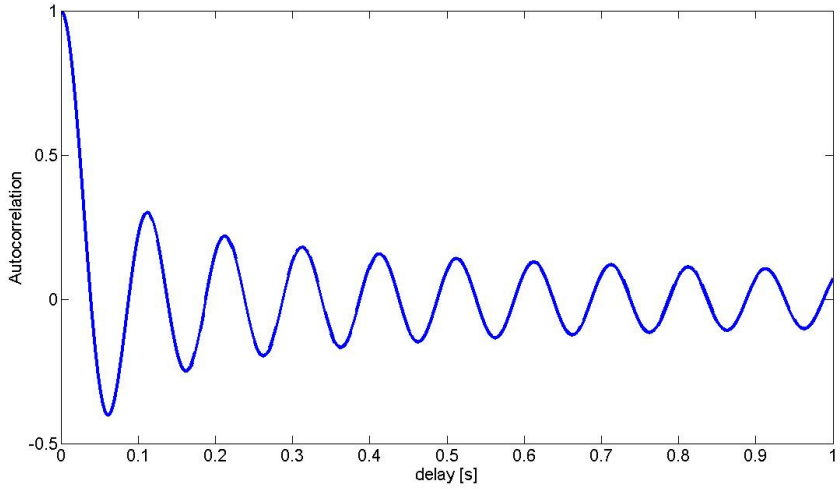

Figure 3-2: Normalized autocorrelation of a complex Gaussian zero-mean fading with maximum Doppler shift of 10 Hz

It is periodic with delay and its envelope decays slowly after the initial zero-crossing. The cross-correlation function between two Rayleigh or Ricean different channels exhibits a behavior similar to formula 3-7. The normalized transfer function for the channel model is given by: [58]

$$S(f) = \frac{P}{2\pi f_D \sqrt{1 - \left(\frac{f}{f_D}\right)^2}} \qquad 3\text{-}9$$

$S(f)$ is limited within the interval $-f_D \le f \le f_D$ and it approaches infinite at its borders. Figure 3-3 shows a normalized theoretical and a simulated version of $S(f)$.

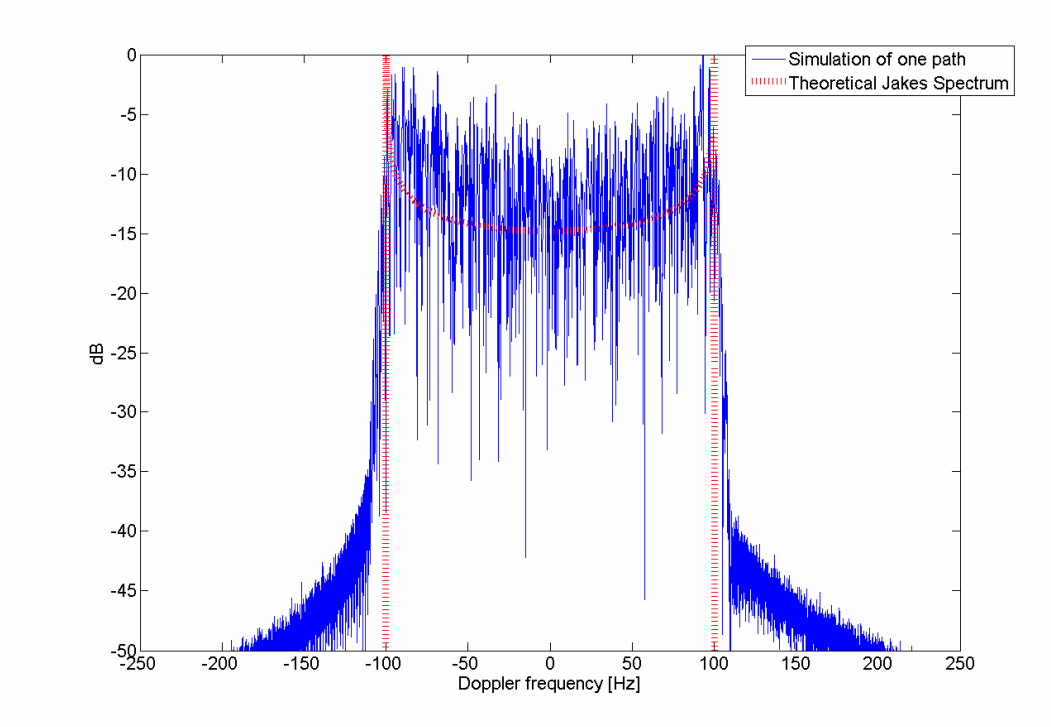

Figure 3-3: Normalized Clarke's model of power density spectrum

The Clarke assumptions of equal zero power of channel components, well represents the situation when there is no line of sight between the receiver and the transmitter. In this case, the Rayleigh fading is the most applicable distribution for the fading amplitude ρ. In the case of line of sight, one channel response component will be stronger than the others and the most applicable distribution is Ricean. The envelope of a Rayleigh channel has the following distribution:

$$P(\rho) = 2\rho e^{-\rho^2} \quad \rho \ge 0 \qquad 3\text{-}10$$

where the square mean value of ρ is supposed to be equal to 1. The requirement of many scatterers means that Rayleigh fading can be a useful model in heavily built-up city centers where there is no line of sight between the transmitter and receiver and many buildings and other objects attenuate, reflect, refract and diffract the signal. Early experimental work in Manhattan has found near-Rayleigh fading there [59]. Rayleigh fading is a small-scale effect; however, environment also shows properties such as path

loss and shadowing upon which the Rayleigh fading is superimposed. Figure 3-4 shows the power variation of two Rayleigh fading signals with a maximum Doppler shift of 100 Hz and 10 Hz using the classic shape of Rayleigh fading. The signal strength can drop by a factor of 20 dB.

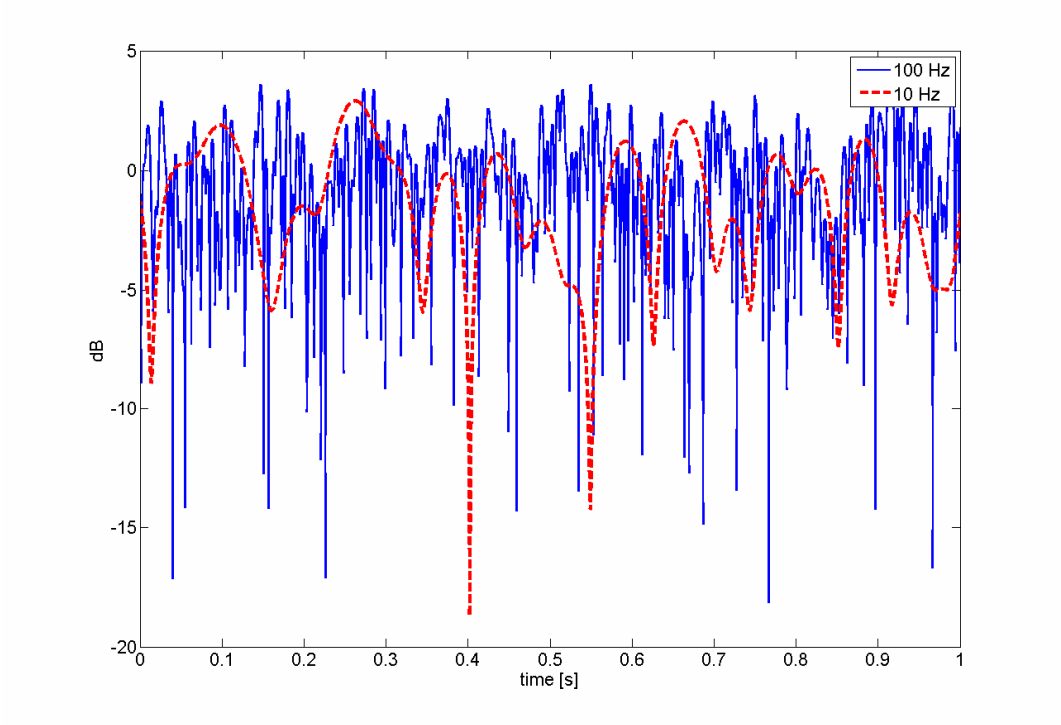

Figure 3-4: Rayleigh fading at 100 Hz and 10 Hz Doppler shift

A radio propagation characterized by a Ricean distribution is caused by partial line of sight signals. Signals arrive at a receiver by several different paths, and a parts of it is time-variant and the other is time invariant due to a fixed direct path. Ricean fading occurs when the direct path signal is much stronger than the others. The effect of the direct signal with many weaker multipath signals gives rise to the Ricean distribution. As the direct signal becomes weaker, the composite signal degenerates into a Rayleigh distribution where the dominant component reaches the same average power of the other components. The Ricean distribution is given by

$$p(\rho) = 2\rho(K+1)e^{-(K+1)\rho^2-K} I_0\left(2\rho\sqrt{K(K+1)}\right),\ \rho \geq 0 \qquad 3\text{-}11$$

where the square mean value of ρ is supposed to be equal to 1, and $I_0(\cdot)$ is the modified Bessel function of the zero-order. The Ricean distribution is often described in terms of a

parameter K which is defined as the ratio between the deterministic signal power and the variance of the multipath. The parameter K is known as the Ricean K-factor and completely specifies the Ricean distribution. For $K = \infty$, the Ricean distribution corresponds to a delta function while for K=0, the Ricean distribution degenerates to a Rayleigh distribution.

3.4 Multipath channel parameters

Together with the power distribution of the paths of a multipath channel, several other parameters are required to quantitatively characterize the radio channel. Multipath channels are grossly characterized by their mean excess delay $(\bar{\tau})$ and root mean square (RMS) delay spread σ. The former is the first moment of the power delay and is defined as [60]

$$\bar{\tau} = \frac{\sum_{n=0}^{D} \bar{\alpha}_n^2 \tau_n}{G_r} \quad where \; G_r = \sum_{n=0}^{D} \bar{\alpha}_n^2 \qquad 3\text{-}12$$

where $\bar{\alpha}_n^2 = E\{|\alpha(t)|^2\}$.

The latter, is the square root of the second central moment of the profile and is defined as

$$\sigma = \sqrt{\bar{\tau}_s - (\bar{\tau})^2} \; where \; \bar{\tau}_s = \frac{\sum_{n=0}^{D} \alpha_n^2 \tau_n^2}{G_r} \qquad 3\text{-}13$$

In the equation 3-12, the delays of each profile are measured relative to a first detectable signal arriving at $\tau_0 = 0$. The RMS delay spread is a measure of the temporal extent of the multipath delay profile, which relates to performance degradation caused by intersymbol interference. In the OFDM systems, the intersymbol interference is avoided by using guard interval. As it will be explained later, Delay Diversity approximately doubles the RMS delay spread seen by the receiver. Moreover, the multiple signals coming from a Single Frequency Network (SFN) can also increase this value. Equation 3-12 and 3-13 are mainly related to the presence and the distances of the scatterers around the receiver (i.e. buildings, indoor facilities, etc). Very large delays in this range might correspond, for

example, to an area surrounded by mountains. Another parameter of interest is the maximum excess delay D_E, indicating the time offset between the first and the last path of a channel model [60]. The first path can be selected as the strongest or the first path passing a defined power threshold. The last path is selected as the last path being above a power threshold. Last parameter of interest is the coherence bandwidth, defined as a statistical measure of the range of frequencies over which the channel can be considered "flat" [60]. For instance, if the coherence bandwidth is defined as the bandwidth over which the frequency correlation function is above 0.9, then the coherence bandwidth is approximately [61]

$$B_c \approx \frac{1}{50\sigma} \qquad 3\text{-}14$$

This formula will be referred to characterize the coherence bandwidth of the channels in Chapter 4. As it will be shown later, the RMS delay spread and the coherence bandwidth are closely linked to the Delay Diversity performances.

3.5 Multipath Channel models

A radio channel model allows the prediction of the performances of wireless communication system before performing field tests. Several radio channel model are derived from experimental estimation of parameters such as path relative amplitude and distribution, delays, Doppler profile, etc. These parameters are strongly dependant on the reception environment (e.g. indoor, outdoor, rooftop, etc.). One of the most used multipath radio channel for outdoor is the COST 207 reported in [62] and later detailed in this chapter. This channel considers various environments and determines the propagation scenarios by continuous exponentially decreasing delay power density profile. The DVB-T specification [2] also defines a channel to describe the portable indoor or outdoor reception conditions. However, this channel does not include any Doppler and should therefore be considered as a snapshot of a real time variant Rayleigh channel. This model has 20 taps, and is therefore difficult to use in any practical work. Reference [63] provides a possible 6 tap approximation. The so called portable indoor (PI) and portable outdoor (PO) channel models have been developed by the Wing-TV project [64] for describing the

slowly moving hand held reception for indoors and outdoors. The channel models are based on measurements in DVB-H Single Frequency Networks and have paths from two different transmitter locations. The Doppler spectra of various taps are also defined. Regarding indoor channels, the first multipath delay spread measurements within a large office building were reported by Devasirvatham [65] at the carrier frequency of 850 MHz using channel sounder transmitting a biphase-modulated pseudonoise coded signal. Rappaport [66] performed the first wide-band measurements at the carrier frequency of 1300 MHz in a factory environment, estimating a multipath spreads ranging from 40 to 800 ns. Saleh-Valenzuela [67] developed a simple statistical indoor multipath model based on Poisson's distribution of the path arrival times. Parameters are derived from measurements performed in a medium-size office building at 1.5 GHz. A more recent set of indoor channel models was developed in [68] [69]. In [68], five delay profile models were proposed for different environments, including residential homes, typical and small office, and large open spaces. The RMS delay spread varies from 15 to 250 ns. The models also define a path loss propagation law and the shadowing. Finally, [70] specified an indoor and an outdoor channel model, referred to as "Indoor Commercial Channel B" and "Outdoor Residential – High Antenna Channel B". According to the specification, the indoor model is dedicated for large open centers, such as shopping malls and airports, whereas the outdoor model covers scenarios with single and double store buildings as well as roads having two lanes and cars parked along the street sides. For hardware simulation of Chapter 4, few COST 207 models are used to simulate the outdoor channel while a modified version of "Indoor Commercial Channel B" is used for the indoor channel.

3.5.1 COST 207 Channel Models

The COST 207 model was first developed for simulating GSM systems, and it describes the channel impulse response in terms of a set of Doppler characteristics at various specified time delays. An adaptation of the COST 207 profiles to mobile DVB-T reception was done by the Motivate project [71]. MBRAI association [72] also defines in [63] a mobile SFN-channel based on the composition of two TU-6 channels. This channel profile has been proven to present fairly well the general mobile DVB-T reception by several field tests. Using this model as a basis for the hardware DVB hardware simulations of

chapter 4, a set of complex fading weights is used to describe the channel impulse response at a given instant. Equation 3-2 describes the discrete number of taps and these taps are determined by their time delay and their average power. The Rayleigh distributed amplitude of the each tap is varying according to a Doppler spectrum. The model has D individual paths and each path has its own random Doppler shift.

3.5.1.1 Doppler Spectrum Types

Four general classes of Doppler spectra are used to describe the variation of the channel weights at specific time delays of the impulse response. These are the classical Doppler spectrum (CLASS), two spectrum based on Gaussian distributions (GAUS1 and GAUS2) and a Ricean spectrum (RICEAN) being the result of the addition of a single direct path to a classical Doppler spectrum. This last distribution appears only in one type of model namely that for the rural non-hilly environment [62]. The classical Doppler distribution (CLASS) given in the COST 207 model corresponds to the Jakes Doppler spectrum (equation 3-9) and is defined in the frequency domain by

$$S(\tau_n, f) = \frac{a}{\sqrt{\left(1-(f/f_D)^2\right)}} \quad with \quad f \in]-f_D, f_D[\qquad 3\text{-}15$$

where f_D is the maximum Doppler frequency of the channel. This distribution will be used for paths with delays not in excess of 500 ns, where it is defined for the rural area channel without direct path. The Gaussian frequency spectrum is defined by [62]

$$G(f) = A\exp\left(-\frac{(f-f_1)^2}{2f_2^2}\right) \qquad 3\text{-}16$$

where f_1 and f_2 control the Centre and the width of the spectrum, respectively.

GAUSl is defined by

$$S(\tau_n, f) = G(A, -0.8f_D, 0.005f_D) + G(A_1, 0.4f_D, 0.1f_D) \qquad 3\text{-}17$$

where A_1 is 10 dB below A. These spectra are the results of a summation of two Gaussian spectra with different centre frequencies and magnitudes and are used for excess delay times in the range of 500 ns to 2 μs, where it is defined for the typical urban channel. Similarly, GAUS2 is defined as

$$S(\tau_n, f) = G(B, 0.7 f_D, 0.1 f_D) + G(B_1, -0.4 f_D, 0.15 f_D) \quad \text{3-18}$$

where B_1 is 15 dB below B. This distribution is used for paths with delays in excess of 2 μs, where it is defined for the hilly terrain channel. RICEAN is the sum of a classical Doppler spectrum and one direct path, such that the total multipath contribution is equal to that of the direct path. This spectrum is used for the shortest path of the model for propagation in rural areas:

$$S(\tau_i, f) = \frac{0.41}{2\pi f_D \sqrt{\left(1 - \left(\frac{f}{f_D}\right)^2\right)}} + 0.91\delta(f - 0.7 f_D) \quad \text{3-19}$$

3.5.1.2 TU6

The TU channel is typical urban channel. The power delay profile (PDP) is as follows:

$P(\tau) = \exp(-\tau)$ *for* $0 < \tau < 7\,\mu s$

The maximum delay of 7 μs for the TU channel is based on the measurement results in most of the urban environment. The phases of the TU channel belong to a uniform distribution. The TU model selected fro the laboratory experiments of Chapter 4 is composed of 6 fixed taps as shown in Table 3-1. According to the PDP of TU, the channel impulse response in time and delay domain is given at Figure 3-5.

Table 3-1: Power Delay Profile of COST 207 TU6

Taps	Delay (us)	Amplitude (dB)
0	0	0
1	0.1	-4
2	0.2	-8
3	0.3	-12
4	0.5	-16
5	0.7	-20

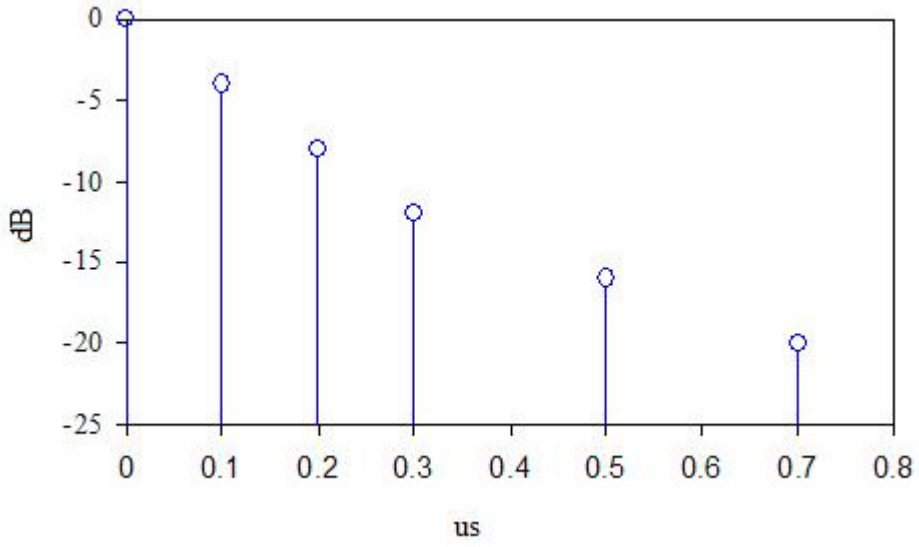

Figure 3-5: Magnitude impulse response of a sample COST 207 TU6

3.5.1.3 RA

The RA channel is typical for the non hilly terrain. The power delay profile is as follows:

$P(\tau) = \exp(-9.2 \cdot \tau)$ *for* $0 < \tau < 0.7 \mu s$

The maximum delay 0.7 of micro seconds for the RA channel is based on the measurement results in most of the rural area environment. The phases of the RA channel belong to a uniform distribution. The RA model selected for the laboratory experiments of Chapter 4 is composed of 6 fixed taps as shown in Table 3-2. According to the PDP of RA, the channel impulse response in time and delay domain is given at Figure 3-6. It is interesting to note that RA channel has a RMS delay spread and excess delay very similar to that of an Indoor channels' ones, as it will be shown later.

Table 3-2: Power Delay Profile of COST 207 RA

Taps	Delay (us)	Amplitude (dB)
0	0	-4.6
1	0.1	0
2	0.2	-4.3
3	0.3	-6.5
4	0.5	-3
5	0.7	-15.2

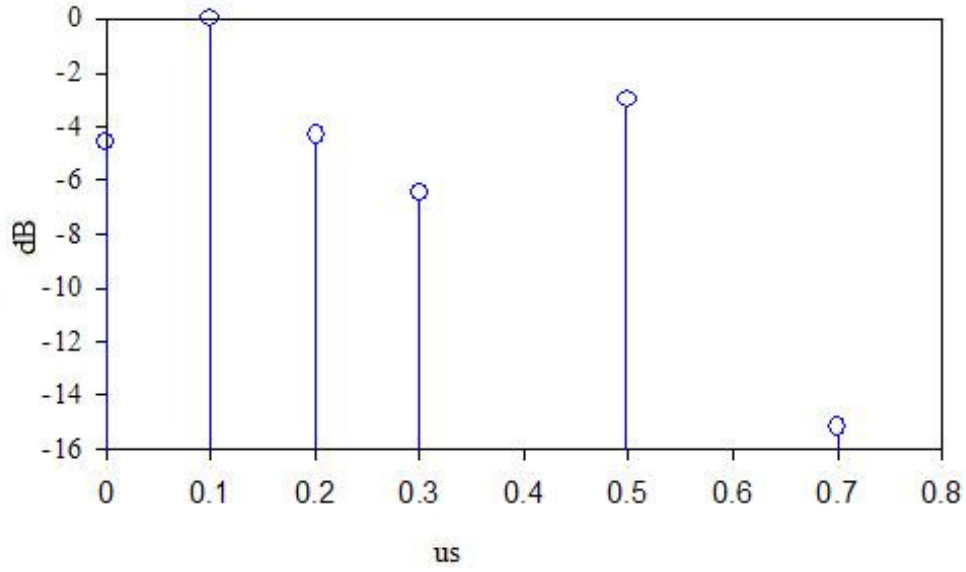

Figure 3-6: Magnitude impulse response of a sample COST 207 RA

3.5.1.4 BU12

BU channel is bad urban for the non hilly terrain. Path power does not decrease gradually in the delay domain as the TU model. The power delay profile (PDP) is as follows:

$$P(\tau)=\begin{cases}\exp(-\tau) & for\ \ 0<\tau<5\mu s\\ 0.5\exp(5-\tau) & for\ \ 5<\tau<10\,\mu s\end{cases} \qquad 3\text{-}20$$

The main difference between TU and BU channel is that there are two delay clusters in the delay domain of BU channel impulse response. The TU channel is mostly in the urban

environment without high and densely located buildings while the BU channel is in the urban environment with densely located buildings. The BU model presented is composed with 12 fixed taps as shown in Table 3-3. According to the PDP of BU, the channel impulse response in time and delay domain is given at Figure 3-7. The rich reflections and massive delays of some paths in BU cause the second clusters.

Table 3-3: Power Delay Profile of COST 207 BU12

Taps	Delay (us)	Amplitude (dB)
0	0	-7
1	0.2	-3
2	0.4	-1
3	0.8	0
4	1.6	-2
5	2.2	-6
6	3.2	-7
7	5	-1
8	6.0	-2
9	7.2	-7
10	8.2	-10
11	10.0	-15

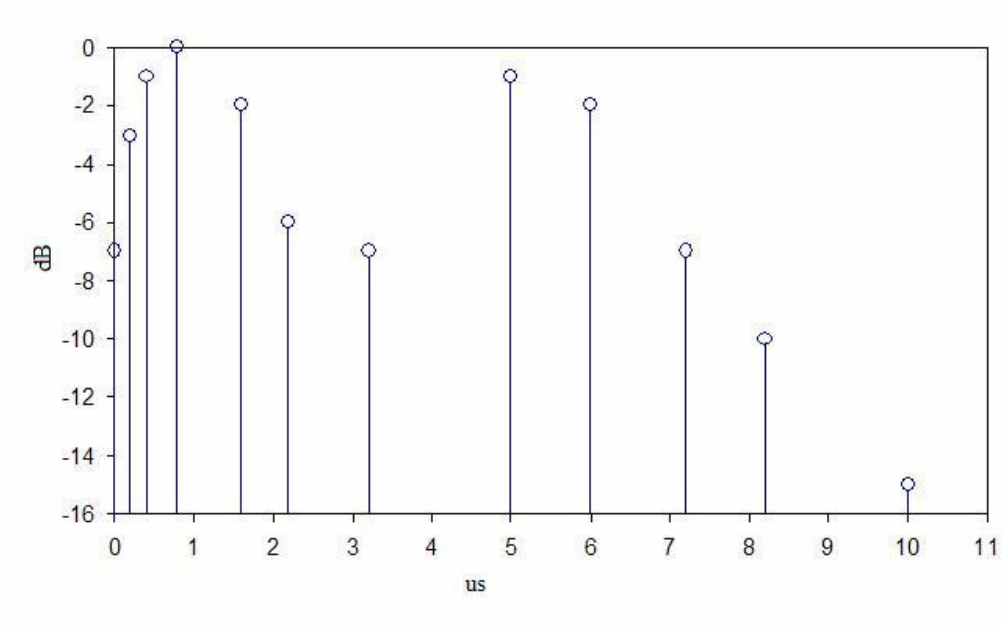

Figure 3-7: Magnitude impulse response of a sample COST 207 BU12

3.5.2 JTC Indoor and JTC Indoor Modified

The indoor radio channels differ from the outdoor channels in one important aspect. Unlike the outdoor radio channel scatterers, the indoor scatterers are typically very close to the receiver. In fact, the indoor propagation is strongly influenced by local features, such as floor layout and building construction materials for walls, floors and ceilings [73]. The local scatterers causes short delay echoes, resulting in a smaller RMS delay spread compared to outdoor. A smaller delay spread corresponds to a wider coherence bandwidth, or in other words, to a flat fading. Table 3-4 shows the power delay profile of Indoor JTC "Commercial B" used for the hardware simulations of Chapter 4 to estimate the diversity gain in indoor environment. The second tap has the shortest relative delay of $0.05\,\mu s$, representing the echo generated by the closest scatterers from the receiver. This delay corresponds to a distance from the scatterers of 15 m. This minimum distance suggests that the radio channel is more suitable for big mall and airports than houses or offices. Thus, two additional taps have been added to the existing channel model in order to represent the scatterers of typical a smaller indoor environment. These two additional taps produces flat fading and can cause severe OFDM signal degradation as it will be shown in chapter 4. The insertion of these two taps in the JTC indoor channel is a specific contribution of this thesis.

Table 3-5 shows the power delay profile of Indoor JTC "Commercial B" channel with the two additional taps (tap number 1 and 2). The second and third taps have a relative delay of 0.015 μs and 0.025 μs corresponding to 4.5 m and 7.5 m, respectively.

Table 3-4: Power Delay Profile of Indoor JTC "Commercial B"

Taps	Delay (us)	Amplitude (dB)
0	0	-4.6
3	0.05	0
4	0.15	-4.3
5	0.225	-6.5
6	0.4	-3
7	0.525	-15.2
8	0.75	-21.7

Table 3-5: Power Delay Profile of Indoor Modified JTC "Commercial B". The additional taps are marked with (*)

Taps	Delay (us)	Amplitude (dB)
0	0	-4.6
1*	0.015	-2
2*	0.025	-3
3	0.05	0
4	0.15	-4.3
5	0.225	-6.5
6	0.4	-3
7	0.525	-15.2
8	0.75	-21.7

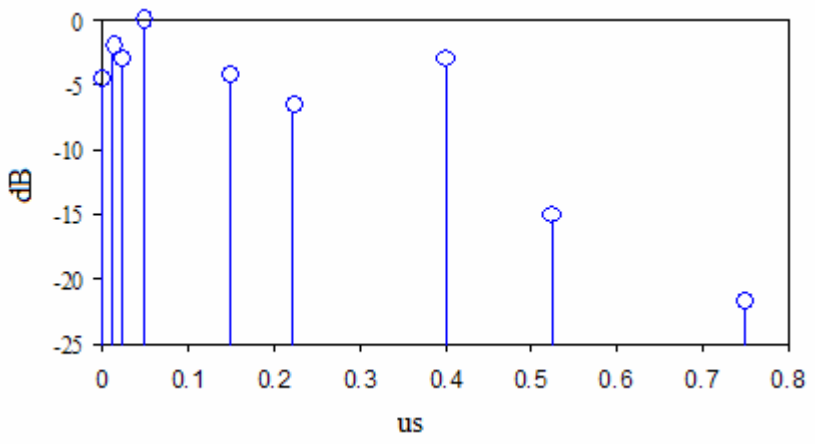

Figure 3-8: Power-delay profile of the modified "Indoor Commercial Channel B" channel model [70]

3.6 Channel Correlation Model

The MIMO is assumed to be composed of uncorrelated SISO channels. However, in real MIMO channels, the SISO channels are likely to be correlated. The performance of a MIMO OFDM system is thus highly related to the degree of correlation between the transmit diversity radio channels. The more decorrelated any two transmitted signals are relative to each other, the greater the diversity gain that can be obtained from a transmit diversity system. As it will be shown in chapter 5, highly correlated channels can make the performances of a DVB signal with a standard compliant diversity (e.g. CDD, DD, etc.) worse than SISO performances because of the destructive interference. The channel model presented in (1) is a finite sum of complex numbers, each of them corresponding to a

particular path of the signal transmitted through a scattered environment. The scatterers around the receiver cause a rotation of the signal phases according the relative position of the receiver and the transmitter, the disposition of the scatterers, the scattering typology (e.g. reflection, diffraction), shape of scattering surfaces, the frequency, etc. Each θ_n value depends on the unique scattering characteristics of each path, and thus they are likely to be uncorrelated. Transmitting two signals from two antennas with enough separation will result in the reception of two "cluster" of echoes. The phase angles of the paths within each cluster are typically modeled as random variables belonging to a uniform distribution within the range of $[0,2\pi]$ for Rayleigh channels. However, the paths of one cluster are likely to be correlated with the paths of the other cluster. A minimum antenna separation is required to generate paths with different propagation characteristics. If the antennas have enough separation, the absolute values of the path results in two uncorrelated (or with small correlation) signal fades as shown in Figure 3-9.

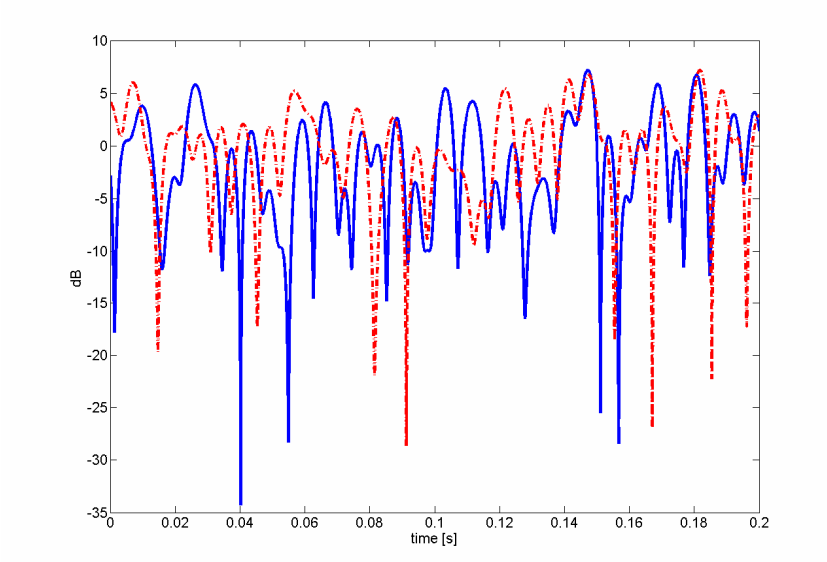

Figure 3-9: The two uncorrelated fadings

[74] show that a transmit antenna separation of the tens wavelength order is required to achieve diversity improvements. On the other hand, if two antennas are used to provide diversity signals at a remote receiver station, they must be on the order of three wavelengths apart to provide sufficient decorrelation. This is due to the difference in the

nature of the scattering environment in the proximity of the remote and near base stations. The remote stations are usually surrounded by nearby scatterers, while the base station is often placed at a higher altitude with no nearby scatterers; thus a larger antenna separation is required to generate uncorrelated paths. An analytical two dimensional MIMO space-time channel correlation model has been detailed in [75] will be used to illustrate the bound between the path cross correlations and the propagation characteristics. The model presents frequency non-selective Ricean fading channel and it is suitable for mobile reception. The cross correlation is derived from a channel model where the NLOS component is generated by of a ring of scatterers surrounding the receiver. A deterministic line-of-sight (LOS) path may exist between any pair of BS-user antenna elements. Various simulation parameters such as the angle spreads at the base station and the user, mean signal arrival directions, antenna array elements distance, and Doppler spread can be taken into account. The channel model also accounts for the other parameters such as the distance between the Base Station and the user and the radius of the ring of local scatterers surrounding the user. In this study, only the impact of transmit antenna element separations and the Ricean K-factor will be referred. A representative simulated 2×2 MIMO channel cross correlation function versus the user and the base station antennas spacing is shown in Figure 3-10. The parameter k characterizes the Angle of Arrivals (AOA) with a Von Mises distribution: it is isotropic if k=0, extremely non isotropic $k\rightarrow\infty$. The two particular cases correspond to a uniform distribution on of the range of $[0,2\pi]$ and to a Dirac delta, respectively. The parameter Δ is the angle spread at the BS and relates the distance between the BS and the user D and the radius of the ring of scatterers R as $\tan(\Delta)=R/D$. The angle Δ is generally small for macrocells in urban, suburban, and rural areas, most often less than 15°, and in some cases very small, less than 5°. Figure 3-10 shows a simulation of cross correlation function vs. transmit and receiver antenna separations with a K-factor of 4 dB. It shows that the minimum channel cross correlation of 0.7 is achieved with approximately 0.5 wavelengths with receiver antenna separation and about 18 wavelengths with transmit antennas separation.

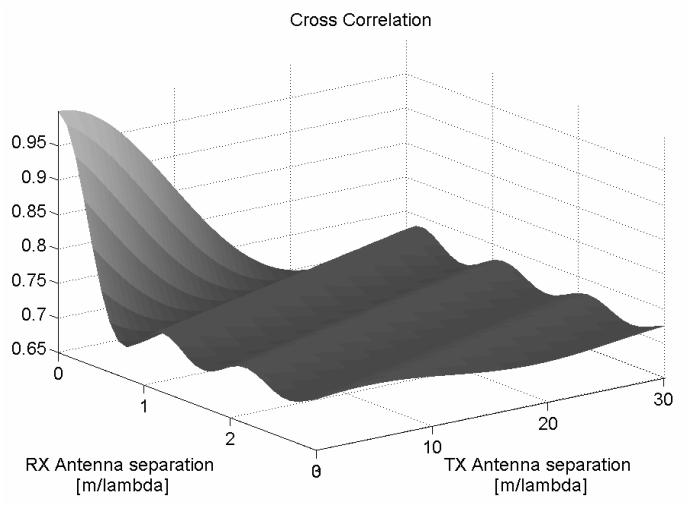

Figure 3-10: Simulation of transmit diversity cross correlation function vs. transmit and receiving antenna separations, K=4 dB, $k = 3°$, $\Delta = 2°$

The cross correlation is strictly related to the Ricean K-factor. Figure 3-11 shows a simulation of cross correlation function vs. transmit antenna separation and different Ricean K-factors. The trend is similar to the autocorrelation function presented in Figure 3-2. For about zero values of Ricean K-factor (NLOS), the cross correlation is less than 0.7 at about 7 wavelengths and it is almost zero at about 16 wavelengths. To get similar channel decorrelation with increasing values of the K-factor (LOS), higher antenna separations are required. For instance, for K=3, the cross correlation is less than 0.7 since about 20 wavelengths. Upper values of the K-factor would require higher antenna's separation for maintaining the same channel decorrelation, but it should be noted that diversity is a technique to aid the reception in environments with NLOS or at least with small values of the K-factor.

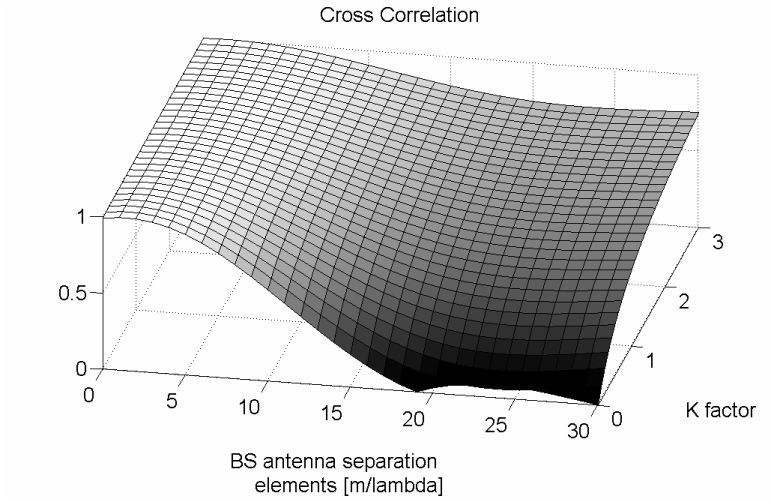

Figure 3-11: Simulation of transmit diversity cross correlation function vs. transmit antenna separation and the Ricean K-factor. $k = 3°$, $\Delta = 2°$

The cross correlation is greatly affected also by Δ. Figure 3-12 shows that the smaller is Δ, the higher are the transmit antenna separations required to achieve the same cross correlation.

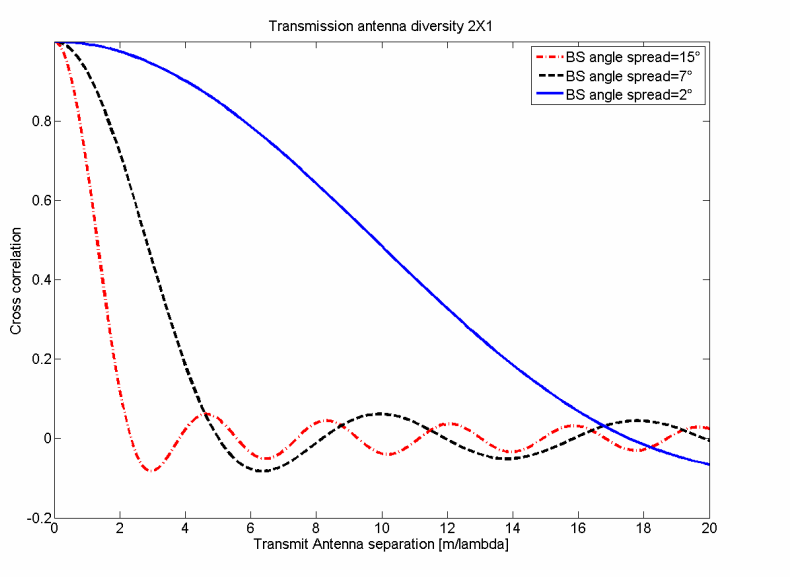

Figure 3-12: Simulation of transmit diversity cross correlation function vs. transmit antenna separation for different angle spreads.

In field trials presented in chapter 5, the transmit antennas array is placed on a structure of about 9.5 meters of width at the Brunel test site. Thus, at 730 MHz the wavelengths is 0.41 meters and the horizontal maximum separation between antennas is 23.1

wavelengths. According to the cross correlation model, this distance should be enough to decorrelate Rayleigh channels with Δ from 15° down to 2°, as proposed in [75]. However, practical combinations of the radius of the ring of scatters R and the base station-user distance D may result in $\Delta << 2°$ (for example, a small office very far from the transmitter). In these cases, 23.1 wavelengths of the antennas separation may not be enough. An additional transmit antenna can be employed to add 12 wavelengths of vertical separation. Combining together horizontal and vertical spacing, it is possible to reach around 27 wavelengths of separation between antennas. It is important to mention that the channel cross correlation model, the parameters values and the graphs are used only for general guideline and reference purposes.

To correlate the X_{iJ} elements of the channel matrix H_F presented in 3-6, the following method can be used

$$[X] = [R_{rx}]^{1/2} [H_{iid}] \left([R_{tx}]^{1/2} \right)^T \qquad 3\text{-}21$$

where R_{rx} and R_{tx} are the receive and transmit correlation matrices, respectively, and H_{iid} is a matrix of independent zero mean, unit variance, complex Gaussian random variables representing the channel, where

$$\begin{aligned} [R_{tx}] &= [C_{txij}] \\ [R_{rx}] &= [C_{rxij}] \end{aligned} \qquad 3\text{-}22$$

C_{txij} are the complex correlation coefficients between i^{th} and j^{th} transmitting antennas, and C_{rxij} are the complex correlation coefficients between i^{th} and j^{th} receiving antenna paths. An alternative approach uses the Kronecker product of the transmit and receive correlation matrices [76] (H_{iid} is an array in this case instead of matrix)

$$[X] = \{[R_{tx}] \otimes [R_{rx}]\}^{1/2} [H_{iid}] \qquad 3\text{-}23$$

The following is an example of 4 x 4 MIMO channel transmit and receive correlation matrix

$$R_{tx} = \begin{bmatrix} 1 & c_{tx12} & c_{tx13} & c_{tx14} \\ c_{tx21} & 1 & c_{tx23} & c_{tx24} \\ c_{tx31} & c_{tx32} & 1 & c_{tx34} \\ c_{tx41} & c_{tx42} & c_{tx43} & 1 \end{bmatrix}$$

$$R_{rx} = \begin{bmatrix} 1 & c_{rx12} & c_{rx13} & c_{rx14} \\ c_{rx21} & 1 & c_{rx23} & c_{rx24} \\ c_{rx31} & c_{rx32} & 1 & c_{rx34} \\ c_{rx41} & c_{rx42} & c_{rx43} & 1 \end{bmatrix}$$

The complex correlation coefficient calculation for each tap is based on the transmit and receive antennas separation [77]. Although the wireless channel emulator employed for the hardware simulation of chapter 4 uses a proprietary algorithms to generate a MIMO correlated channel, formulas (3-21) and (3-22) provide a reference a for a possible implementation.

3.7 Space-Time diversity codes

Earlier work on wireless communications focused on deploying an antenna array at only one end of the wireless link, usually at the receiver. However, for the highly-scattering environment, significant capacity gains are enabled when antenna arrays are used at transmit and receiver side. Tarokh and others first proposed the Space–time Block codes (STBC), consisting the transmission of multiple redundant copies of data to compensate for fading and channel noise and assuming that some of them may arrive at the receiver in a better state than others [18] [19]. STBC achieve significant error rate improvements over single-antenna systems. Their original scheme was based on trellis codes, but a simpler block codes based on two transmit antenna were developed by Siavash Alamouti [16] to develop STBC. Tarokh and others later developed an extension to any number of antennas [17]. Equation 3-25 shows a general form of the code matrix where $c_i(l)$ is the modulated complex symbol transmitted from the antenna i at the time index l. There are K time slots and N transmit antennas.

$$C = \begin{pmatrix} c_1(0) & c_1(1) & \dots & c_1(K-1) \\ c_2(0) & c_2(1) & \dots & c_2(K-1) \\ | & | & | & | \\ c_N(0) & c_N(1) & \dots & c_N(K-1) \end{pmatrix} \qquad 3\text{-}24$$

The code rate of an STBC measures how many symbols per time slot it transmits on average over the duration of one signal block. If a block encodes k symbols, the code-rate is

$$r = \frac{k}{K} \qquad 3\text{-}25$$

STBCs as originally introduced, and as usually studied, are orthogonal. This means that the STBC is designed such as the vectors representing any pair of columns taken from the coding matrix are orthogonal. This results in a simple, linear, optimal decoding at the receiver. A disadvantage is that all codes (except Alamouti) that satisfy this criterion do not have a reduced full-rate (code rate 1). In the case of STBC, the data stream to be transmitted is encoded in blocks, which are distributed among spaced antennas and across time. While it is necessary to have multiple transmit antennas, it is not necessary to have multiple receive antennas, although to do so improves performance specially if combined with Maximum Ratio Combining algorithm (MRC) techniques [78]. This process of receiving diverse copies of the data is known as diversity reception and is what was largely studied until Foschini's 1998 paper [79]. Alamouti is optimal for 1 receiver antenna, while for a 2 receiver antenna system optimal results are achieved by the Golden Code [80]. An example of achievable gain is provided in [81] where Alamouti code is applied to an OFDM 2×1 transmit diversity scheme over frequency selective fading channel (e.g. COST 207 [82] at Doppler shift of 10 Hz). The proposed two-branch OFDM transmitter diversity scheme provides about 12.5 dB of diversity gain at a bit error rate (BER) of $2\cdot10^{-4}$. Results are only 3 dB worse if compared with a classic MRC deploying a 1×2 schema. The 3 dB penalty is incurred because the simulations assume that each transmit antenna radiates half the energy in order to ensure the same total radiated power as with one transmit antenna.

3.8 DVB Compatible diversity codes

STBCs in the form described in the previous section are not suitable for extending to the existing systems, because will be non compatible with the standard. Therefore for standardized OFDM systems additional spatial diversity techniques can only be implemented, if these modifications keep the systems standard compatible. STBCs are not compliant to the current DVB standard i.e. DVB-T/H. The Cyclic Delay Diversity (CDD) [8] [24] [83] is complaint and is applicable to DVB-T/H without modifications to its existing physical layer mainly because its signal processing is performed on the baseband OFDM [84] symbol in time-domain. CDD can be efficiently realized by a phase rotation before OFDM, i.e., before the IFFT modulator block. In this case, the technique is called Phase Diversity (PD). The phase shift can be constant or continuously time varying. In the last case, this is referred as time-variant phase diversity [11]. Another standard compliant technique is Delay Diversity (DD). DD is simpler than CDD, because it merely consists of inserting delay between the two transmitted signal [85] and it does not need to be implemented within the DVB modulator. However, chapter 4 will show that this approach can lead to ISI impairment under certain channel conditions. Reference [86] proposes the DVB standard compliant Discontinuous Doppler Spread Diversity (DDoD), consisting of a small shift in frequency domain of the sub-carrier frequencies of each transmitted signal. CDD technique can be combined with the DDoD, that allows for respective reduction/removal of fading correlation in time and/or frequency domain, and therefore, optimizing diversity gains [87]. Finally, a simultaneous transmission on vertically and horizontally polarized antennas between which there are low levels of polarization rotation (polarization diversity) has been studied in [88]. This approach was proved to approximately double the capacity for DVB-T transmission in British Broadcasting Corporation (BBC) work presented in [89].

3.9 Software Simulation on CDD applied to DVB

References [8] [24] present software simulations on the impact of CDD diversity code when applied to a standard DVB-T/H system. Reference [8] investigates a 2Tx-1Rx antenna with CDD transmit diversity scheme applied to a DVB-T achieving diversity gain

over frequency selective fading channel (e.g. “Indoor Commercial, Channel B” and “Outdoor-Residential, High Antenna, Channel B” [70] at Doppler shift of 10 Hz and 50Hz, respectively). This diversity scheme provides a diversity gain at a bit error rate (BER) of $2 \cdot 10^{-4}$ of about 3.5 dB and 1.5 dB for indoor and outdoor channels, respectively. It was also observed that a cyclic delay $\delta > 1.5 \mu s$ resulted in no further improvements. Reference [24] extended the analysis to DVB-H networks. The CDD diversity scheme provides a diversity gain at a Bit Error Rate (BER) equal to $2 \cdot 10^{-4}$ of about 5.5 dB and 9 dB for Typical Urban and Bad Urban channels, respectively. [25] investigated the effects of the various channel cross correlations. Results shows that for a MISO systems with a channel cross correlation of C =0.2, the performance are slightly worst than the uncorrelated channels case. In particular, the degradation is about 0.1 dB for TU, 1.3 dB for RA and 0.9 dB for Indoor-B at BER of $2 \cdot 10^{-3}$. This BER value has been chosen as reference since the charts presented in [25] does not reach the $2 \cdot 10^{-4}$ condition. Finally, [27] estimate the gain by comparing the seconds containing MPEG packet lost after the Reed-Solomon decoder and the MPE-FEC error rate (corresponding respectively to the $ESR_{\%}$ and $MFER_{\%}$ detailed in chapter 4). The analysis is carried out for 2Tx-1Rx system with CDD, 1Tx-2Rx system with MRC, and 2Tx-2Rx system combining the CDD and MRC schema. Results show a diversity gain up to 4.9 dB for indoors when the $ESR_{\%}$ criterion is considered, that reduces to 1.7-2.5 dB when the MPE-FEC is included in the DVB-H decoding chain. Similarly, the 2.5-2.6 dB of gain measured in outdoor channel is reduced up to 0.8-1 dB because of the MPE-FEC effect. This gain reduction depends on the time interleaving feature of the MPE coding, providing the system with intrinsic time diversity capabilities. This issue will be detailed in chapter 5. Obviously, the MPE affects also the gain for 1Tx-2Rx and 2Tx-2Rx. Considering the 2Tx-2Rx system case, for instance, results show a diversity gain of 12.8-12.2 dB for indoor when the $ESR_{\%}$ criteria is considered, which is reduced to 7.8-8.5 dB when the effect of MPE-FEC is taken into account. To conclude, reference [27] also reports a system loss of 6 dB on Ricean channels compared to SISO if transmit DD is obtained. These results will be the basis for the studies performed in chapter 6. All the evaluation criteria will be detailed in chapter 4 and 5.

3.10 Laboratory/field trials on CDD applied to DVB

Reference [28] presents the results for a laboratory measurement campaign performed in parallel with the laboratory investigation presented in this thesis. The SISO, MISO, SIMO and MIMO configurations were first compared in DVB-T using TU6 channels in a laboratory environment and $ESR_{5\%}$ for the receiver quality criteria. With a cyclic delay of 1 μs between paths in MIMO and MISO modes the gains were measured for a 10 Hz Doppler shift. The MISO, SIMO and MIMO configurations provide a gain of 3 dB, 8 dB, and 9.7 dB, respectively. The MIMO configuration provides a gain of 1.7 dB if compared to SIMO case. Similar tests were performed adopting the *MFER* at 5% criteria. Results show the MISO, SIMO and MIMO configurations provide a gain of 1.7 dB, 6 dB, and 7.3 dB. The MIMO configuration provides a gain of 1.3 dB if compared to SIMO case. Laboratory tests also showed a gain reduction from 1.3 dB to 2.4 dB because of the MPE-FEC effects. In parallel with the field trials investigation related to this thesis, two other diversity DVB-T pilot testbed were deployed in Tamper (FI) and Metz (Fr) and they are described in [90][91]. Reference [92] reports a summary of the field trials performed in urban environment for rooftop fixed and mobile reception. For fixed Line Of Sight or Near Line Of Sight DVB-T reception with a rooftop antenna a degradation of 4dB was observed when transmit diversity was implemented. However, the urban mobile reception tests performed in Metz did not produce any significant MISO gain measured for both *ESR* at 5% and *MFER* at 5% criteria despite of the simulation and laboratory predictions. A possible explanation for this result will be detailed in chapter 5.

3.11 Summary tables

Table 3-6 provides a general overview of the investigation conducted and/or at the same time of this research thesis. Results focus on DVB standard compliant diversity. However, the Alamouti code applied to uncoded OFDM is also shown for comparison. The Alamouti code achieves for uncoded OFDM a diversity gain in TU COST 207 up to 12.5 dB. The table contains results related to the BER, Reed-Solomon codeword error rate after decoding of the outer Reed-Solomon Code (Post RS CER) [27], $ESR_{\%}$ and MPE-FEC Error Rate (MFER).

Table 3-6: Summary tables

Ref.	Method.	Criteria	System	Diversity	Chan. Or Envir.	F_D or Class recep.	Ch. Corr. or Ant. Spacing	Max. Gain (dB or %)
[81]	Soft. Simul.	BER at QEF	Uncod. OFDM	Alam.	TU COST 207	10 Hz	0%	12.5
[8]	Soft. Simul.	BER at QEF	DVB-T	CDD	Outdoor [70]	50 Hz	0%	1.5
					Indoor [70]	10 Hz	0%	3.5
[24]	Soft. Simul.	BER at QEF	DVB-H	CDD	TU COST 207	30 Hz	0%	5
					BU COST 207	50 Hz	0%	9
[25]	Soft. Simul.	BER= 2*10^-3	DVB-H	CDD	RA COST 207	30 Hz	0%, 20%, and 80%	8, 6.7, and 4.7
					Indoor [68]			6, 5.1, and 3.5
					TU COST 207			4.5, 4.4, and 3
[27]	Soft. Simul.	Post RS BER	DVB-T	CDD	Modified Indoor [70]	1 Hz	0%	5.1
				MRC				10
				CDD +MRC				12.8
		$MFER_{5\%}$	DVB-H	CDD				2.5
				MRC				7.5
				CDD+MRC				8.5
		Post RS BER	DVB-T	CDD	TU COST 207	50-10 Hz	0%	2.5-2.6
				MRC				7.9-7.8
				CDD +MRC				9.7-10.5
		$MFER_{5\%}$	DVB-H	CDD				0.8-1
				MRC				5.1-5.5
				CDD+MRC				5.8-6.7
[28]	Lab. test-bed	$ESR_{5\%}$	DVB-T	CDD	TU COST 207	10-50 Hz	0%	3
				MRC				8
				CDD +MRC				9.7
		$MFER_{5\%}$	DVB-H	CDD				1.7
				MRC				6
				CDD+MRC				7.3
[92]	Field Trials (Metz)	mean $ESR_{\%}$	DVB-T	CDD	Urban	Mobile	10 [lambda]	0
				MRC				4.5
				CDD+MRC				4.5
	Field Trials (TUT)	mean $ESR_{\%}$	DVB-T	CDD	Urban	Mobile	20 [lambda]	$ESR_{\%}$ reduction of 21%
		$ESR_{5\%}$		CDD	Indoor	Station ary	20 [lambda]	0-3

Table 3-7 shows a comparison of the diversity gain before and after the MPE-FEC decoder taken from reference [27]. MPE-FEC reduces the achievable gain in all the diversity configurations.

Table 3-7: Summary of results reported in [27]

		DVB-T gain compared to 1Tx-1Rx@10^-3			MPE-FEC Code Rate	DVB-H gain compared to 1Tx-1Rx@5%		
		2Tx-1Rx	1Tx-2Rx	2Tx-2Rx		2Tx-1Rx	1Tx-2Rx	2Tx-2Rx
JTC Indoor 1Hz [70]	QPSK, 3/4, 8k	4.5	9.7	12.2	3/4	1.7	6.9	7.8
JTC Mod. Indoor 10 Hz [70]	QPSK, 3/4, 2k	4.9			3/4	2.5		
JTC Mod. Indoor 1 Hz [70]	QPSK, 3/4, 2k	4.6	10	12.8	3/4	2.5	7.5	8.5
TU6 10 Hz	QPSK, 3/4, 2k	2.6	7.9	9.7	3/4	1	5.1	5.8
TU6 50 Hz	QPSK, 3/4, 2k	2.5	7.8	10.5	3/4	0.8	5.5	6.7

3.12 Summary

This section described the MIMO channel model used with DVB-T/H systems. The MIMO channel model consists of a combination of several SISO channels based on WSSUS channel. This channel model is fully determined by the echo delay due to multipath, and the Doppler shift due to the movement of objects in the channel. The amplitude of each delay echoes have Rayleigh or Ricean fading. Rayleigh fading is most applicable when there is no line of sight between the transmitter and receiver and Ricean fading if there is a line of sight. In Rayleigh fading, many objects scatter the radio signal in the channel model before it arrives at the receiver. Ricean fading is caused by partial line of sight signals. The signals arriving at the receiver is composed by two different parts, and at least one of the parts is time-varying and the other is fixed. A fading characterized by a Ricean distribution occurs when the direct path signal is much stronger

than the others. This delay profile for SISO channel based on COST 207 and JTC indoor channel model has been presented. Several types of outdoor channel models are described, including TU6, RA, and BU12. Several indoor channels have also been described, with particular reference to a JTC indoor channel modified profile. The modification consisted of adding two short delay echoes, representing the effects of a small office scatterers and introducing flat fading. This chapter also considered an equivalent baseband MIMO channel with M transmits antennas and N receiver antennas. First, the uncorrelated MIMO channel model was analyzed according to the individual SISO channel delay profile. Secondly, the correlation of transmitter and receiver antennas was considered in the correlated MIMO channel model. Moreover, a non-frequency channel cross correlation model has been described. The MIMO channel cross-correlation is related to the physical propagation parameters such as the transmitter/receiver antenna separation, the Ricean K-factor and the angle spread. This analysis fully justified the transmit antenna separation deployed for tests in chapter 5 and 6. Finally, this chapter presented a literature survey on general Space-Time diversity codes. Several DVB standard compatible diversity codes were discussed, with particular reference to the CDD applied to DVB. Furthermore, a section dedicated to diversity laboratory/field trials concludes the chapter. These results will be used as a reference for the experimental measurements presented in the next chapters.

4. Laboratory Measurement Campaign of DVB-T Signal with Transmit Delay Diversity

4.1 Introduction

This chapter describes the application of Delay Diversity (DD) and Maximum Ratio Combining (MRC) to spatial transmit/receive antenna diversity systems. The analysis is conducted by using actual receiver equipment in simulated laboratory conditions. The main objective is to confirm that diversity gains reported in the chapter 3 and that were predicted by mathematical modeling can be realized in realistic conditions using actual equipment. The hardware emulations provide additional information to the software simulations. First, it shows that the actual equipment can exploit the DD signal. For instance, while software simulations (e.g. [8] [24] [25]) assume perfect channel estimation, [93] [94] show that CDD can cause serious degradation in the performance of post-FFT processing such as channel estimation and integer frequency offset (IFO) estimation. As it will be explained later, while the BER-based software simulations evaluate the performance of the inner system of DVB-T system (e.g. up to the Viterbi decoder), the hardware simulation adopts metrics such as $ESR_{\%}$ which is closer to the realistic user experience. Finally, hardware emulations allow the test of diversity on commercial and state-of the art receiver implementations. The laboratory set-up includes a DVB modulator, a wireless channel emulator and two receivers from different manufacturers, namely: the Broadreach Systems Monitor Station and the Dibcom receiver. The Monitor Station is equipment developed by Broadreach Systems that comprises of a standard DVB receiver and additional processing to enable engineering data to be extracted. The Monitor Station acts in exactly the same way as a standard set-top box receiver. The Dibcom is a high performance DVB-T/H receiver, enabling the MRC reception and optimizing the mobile reception. A series of experiments were conducted to measure the dependence of transmit diversity gain against:

- Modulation scheme;
- Diversity Delay;
- Cross correlation coefficient;
- Doppler shift or speed of the receiver;

- Channel profile; indoors, outdoors etc.

This chapter first introduces a theoretical formulation of delay diversity applied to the DVB signals. Then, it describes the laboratory set-up for transmit diversity testing and evaluation, the measurement methodology, the channel models used for testing as well as the main system parameters and a summary of test cases. The measurement results and analyses of the different studied cases are presented. Finally, a section describing the MRC reception concludes the chapter.

4.2 Transmit Delay Diversity

DD consists of transmitting a main signal and its delayed replica through two or more antennas. Figure 4-1 shows the block diagram of N-transmit antennas applied to an OFDM system with DD. The OFDM modulated signals are transmitted using N antennas. The individual signals only differ in an antenna specific delay shift δ. After the insertion of the cyclic prefix or Guard Interval (GI), the delay δ is inserted. The functional blocks "UC" and "DC" stand for up-conversion and down-conversion, respectively, of the signals from the baseband into RF-band and vice versa.

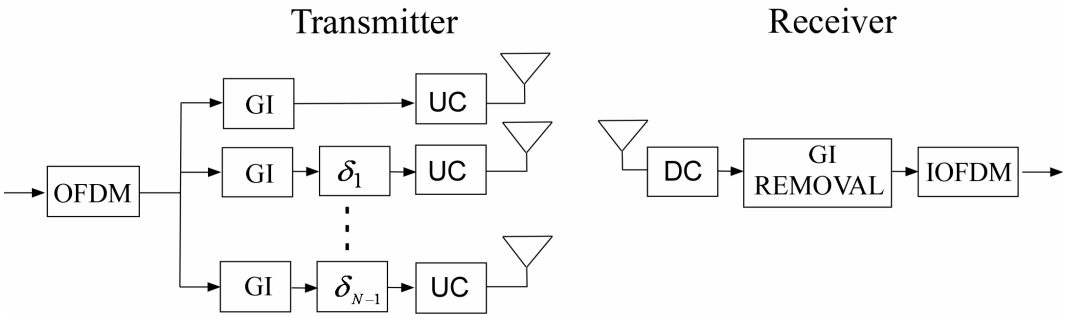

Figure 4-1. Transmit delay diversity applied to an OFDM system

DD can be applied to a standard DVB-T/H implementation because its signal processing is performed on the OFDM output symbols in the time-domain. Consider that the transmitted symbols are denoted by $s(t),\ t = 0,...K-1$ where K is the number of subcarriers. During transmission, these symbols are delayed between respective N transmit antennas. The symbols transmitted from i^{th} antenna at time t can be represented by:

$$s_i(t) = s_i(t-\delta_i)v(t-\delta_i) \qquad 4\text{-}1$$

where $v(x)$ is a mathematical function that sets zeros for negative time indices (see Appendix I), $i = 0,1,\ldots,N-1$, and δ_i is the delay introduced between the symbols. As shown in Figure 4-1, the cyclic prefix should be added before the delay operations. The delayed symbols can be recorded in a diagonal matrix as a codeword, C defined below:

$$C = \begin{pmatrix} s(0) & s(1) & \ldots & s(K-1) \\ 0 & s(0) & \ldots & s(K-2) \\ \ldots & \ldots & \ldots & \ldots \\ 0 & 0 & \ldots & s(K-N) \end{pmatrix}_{N\,x\,K} \qquad 4\text{-}2$$

From (1) and (2), it can be seen that i^{th} antenna is actually transmitting $s(0),s(1),\ldots,s(K-1)$ sequence that is delayed by δ_i. This can be then denoted as $0,\ldots,s(0),s(1),\ldots s(K-1-\delta_i)$. This system is equivalent to the transmission of the sequence $s(0),s(1),\ldots,s(K-1)$ over a propagation channel with one transmit antenna to receiver:

$$h^{e,t}(d) = \sum_{i=1}^{N} h_i^t(d-\delta_i)v(d-\delta_i) \qquad 4\text{-}3$$

where $h^{e,t}$ is the equivalent channel impulse response (CIR) at the receiver side, t denotes that CIR is in time domain, d denotes the index of delay in channel delay profile, and N denotes the number of transmitter antennas. Therefore the CIR can be described as:

$$h^{e,t} = \left[h^{e,t}(0),\ldots,h^{e,t}(K-1)\right] \qquad 4\text{-}4$$

In the frequency domain, the equivalent channel transfer function is expressed as:

$$H^e(k) = \sum_{i=1}^{N} e^{-j\frac{2\pi}{K}k\delta_i} H_i(k) \qquad 4\text{-}5$$

where according to [24], $H_i(k)$ denotes the channel frequency response of the transmission from the i^{th} transmit antenna to the receive antenna and δ_i is the delay of the i^{th} transmit antenna (there is no delay at first transmit antenna, $\delta_1 = 0$). Figure 4-2 shows the channel frequency response measured from a spectrum analyzer for a DVB-T system with and without DD. It is clear that DD has transformed the spatial diversity into frequency diversity; in other words, the Multiple Input Single Output (MISO) channel is

transformed into a single-input single-output (SISO) channel with increased frequency-selectivity. Therefore, the coherence bandwidth is decreased. Later in this chapter, experimental results show that a lower coherence bandwidth leads to a better error performance for coded OFDM systems in multipath environments.

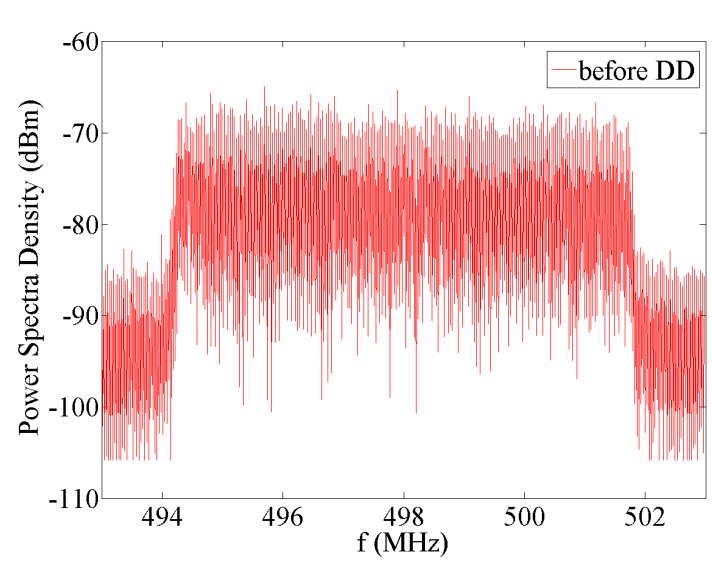

(a)

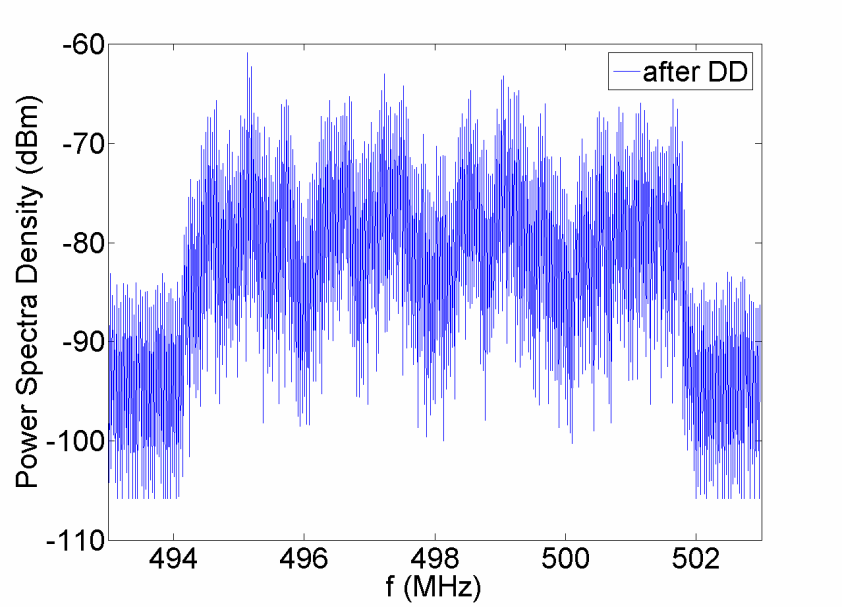

(b)

Figure 4-2. Power Spectra Density of signal at UHF 498 MHz before (a) and after DD (b)

Figure 4-3 shows an example of the delay diversity signal construction. As it was shown in chapter 1, no Intersymbol Interference (ISI) occurs if:

$$\delta_i \le N_g - \tau_{\max}, \quad i = 0,1....N-1 \qquad 4\text{-}6$$

If this condition stands, it can also be proven that DD is equivalent to other diversity techniques, e.g. Cyclic Delay Diversity (CDD) and Phase Delay (PD) [8] [24].

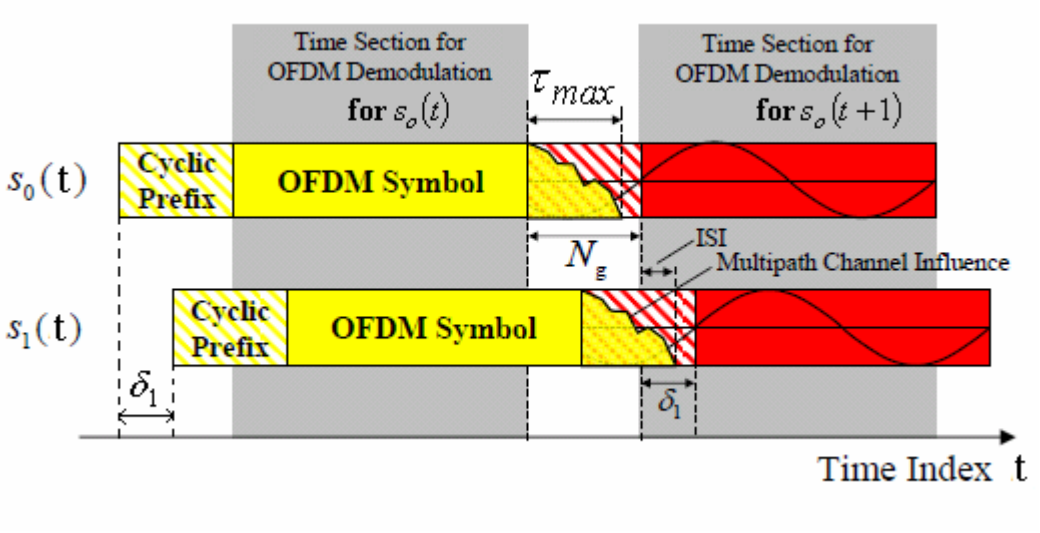

Figure 4-3: Delay Diversity signal construction [27]

To achieve any diversity affects (i.e. to obtain constructive and destructive interference within the OFDM signal bandwidth B), the delays δ_i (in samples) have to fulfill the relation:

$$\delta_i \ge \frac{1}{B \cdot T_s} \qquad 4\text{-}7$$

where T_s denotes the sampling time of the OFDM time domain signal. Results reported in [8] show that a delay of $\delta_i \ge 1.5\mu s$ derives no further improvement of diversity gain, defined as the offset between the C/N needed to achieve the same performances in single and multiple diversity antennas system. A theoretical upper bound for the DD performances is calculated in [25], where it is shown that maximum gain is achieved with an interleaver for OFDM symbols applied to the system. For a linear code C with minimum Hamming distance d_m, the optimal interleaver is an interleaver with permutes

the nonzero bits of all weight d_m codeword of C such that they are uniformly distributed within the length K block. In DVB system, a conventional "write in row read in column" block interleaver is used in combination with a convolutional code to improve the coding gain for the whole system. In [25], it was also shown that diversity gain is fully effective over uncorrelated channels. However, in reality, the respective signal paths between spatially separated antennas and the mobile receiver are likely to be correlated to a certain degree because of insufficient antenna separation at the transmitter and the lack of sufficient multipath in the channel. Table 4-1 shows the relationship between the channel correlation coefficient, c, and the transmitter antennas separation expressed in wavelength λ [75]. The degree of channel correlation as in $c = \{0, 0.25, 0.5, 0.75, 1\}$ corresponds to separation distances between two transmit antennas. We assume that spatial fading correlation occurs at the transmitter and thus the correlated signals appear at the receiver. In this case, the correlated channel is expressed as $h_2 = c \cdot h_1 + \sqrt{1-c^2}\, w$ where h_1 and h_2 are the two correlated fading channels, w is the Rayleigh fading factor and c is the correlation coefficient between h_1 and h_2. For $c = 0$, the two fading channels are fully uncorrelated while $c = 1$ represents a fully correlated case. The cross correlation between the two channels results in diversity loss and performance degradation of DD. Thus, it is apparent that DD cannot achieve the same diversity gain as obtained under the uncorrelated channel [25]. Therefore, the relationships linking the diversity gain, delays and the cross correlation of the channels are of high importance and are thus studied in this chapter through the laboratory setup described later in this chapter.

Table 4-1: Relationship between channel cross correlation and transmitter antennas separation [74]

Correlation between two transmitter antenna (c)	Distance between two transmitter antenna (λ)
1	0
0.75	6.5
0.50	9.7
0.25	13
0	17.5

4.3 Laboratory Set-Up for Transmit Delay Diversity Testing

This section describes the laboratory simulation set-up as depicted in Figure 4-4 and Figure 4-5. A test signal was generated by a standard DVB-T modulator, the output signal was then split into two paths and fed directly into a Spirent SR5500 radio channel emulator. Although the field trials set-up of Chapter 5 and 6 were set-up on channel 53 (730 MHz), the laboratory testing was conducted in the UHF band at channel 24 (498 MHz). This because the only band-pass noise filter available for the laboratory experiment (see later in the text) was tuned at that frequency. The Spirent SR5500 [95] is a two-path wireless channel emulator that simulates the characteristics of complex wideband radio channels, including time-varying multipath delay spread, fast and slow fading, path loss and variable amounts of correlation between the paths. The SR5500 allows the generation of arbitrary power delay profiles to emulate different channel scenarios (e.g. outdoor, indoor, and vehicular). Varying the correlation coefficient and the delay between the channels allows the investigation of the effect of diversity in laboratory channel conditions. The output signals were combined to simulate the signal at a single receive antenna. Additive White Gaussian Noise (AWGN) was generated by a variable noise source and added to the main signal to vary Carrier to Noise ratio at the receiver input. The nominal noise flatness of the noise generator was +/- 2 dB over 1 GHz bandwidth. Since the the main aim the receiver channel filter is to reject the image frequencies and the bandwidth can be possibly larger than 8 MHz, a band-pass filter was used to cut off the out-of-band noise, preventing any possible saturation of the receiver amplifier. Additional fixed attenuators were used to adjust the power to be within the dynamic range of a number of receiver devices such as the Rhode and Schwartz ETX DVB-T testing unit [96], the Dibcom DVB-T/H receiver [97] and the Broadreach monitoring station [98]. A splitter finally fed the faded signals into a spectrum analyzer and the three receivers. The results presented here are for the Broadreach monitor Station, which being based on a standard DVB set top box receiver provided performance most representative of general purpose DVB receivers. Few tests are performed also with the Dibcom receiver, to compare performances with a high performance receiver optimized for mobile reception.

Test results obtained with ETX where not presented because it showed results inaccuracy in low $ESR_{\%}$ range (e.g. multiple thresholds crossing, random errors, etc.).

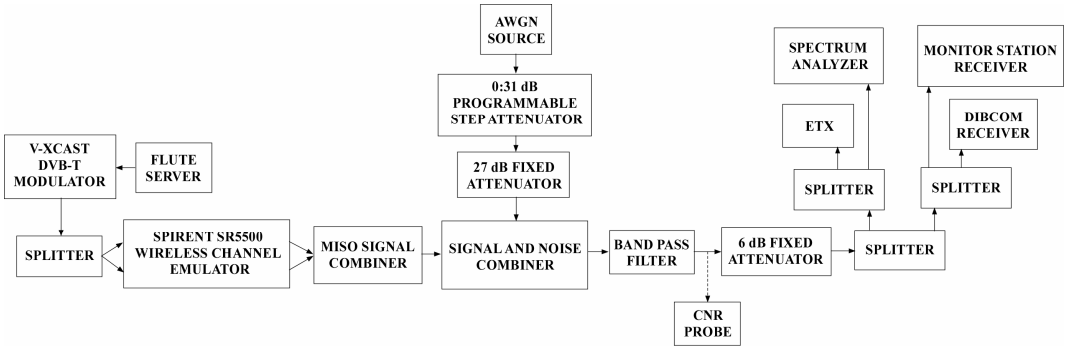

Figure 4-4. Block diagram's of transmit diversity laboratory test bench

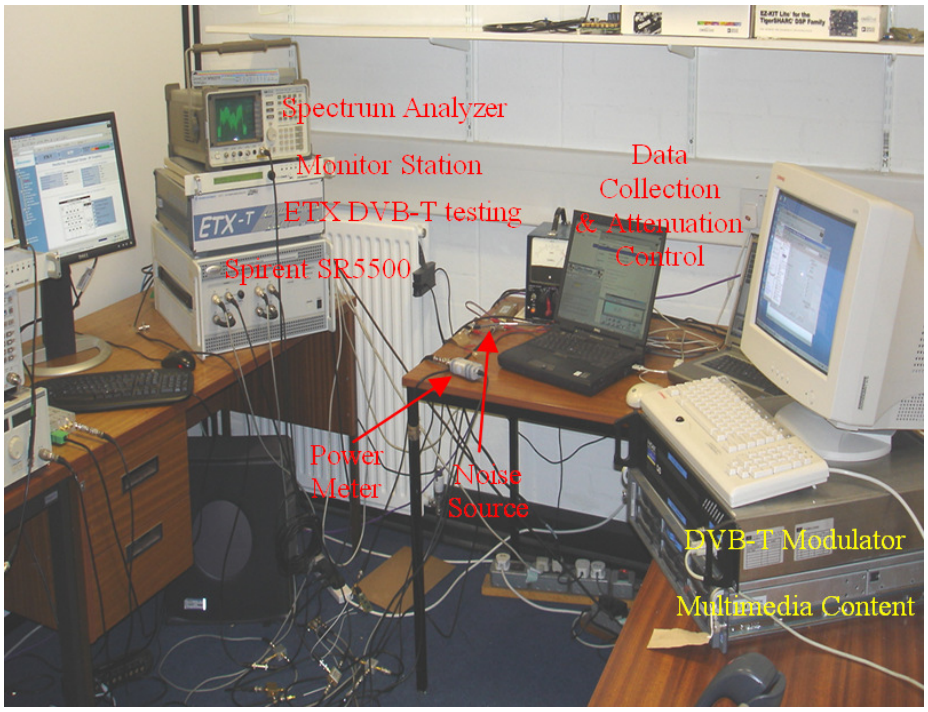

Figure 4-5. Laboratory test bench facilities

4.4 Measurement Methodology, channel models and main system parameters

4.4.1 Measurement Methodology

Testing was performed with 2 simulated transmit antennas. The delay value δ between the two signals was introduced by the Spirent channel emulator. In real world applications, the delay between signals would be introduced by a dedicated device or by using a specialized modulator designed specifically for transmit diversity. It is important to note that the overall transmitted power was normalized for all measurements, i.e. either 100% of the power was transmitted through a single antenna or 50% of the power was transmitted by each of 2 antennas. It was found to be impractical to base our measurements on the normally used BER metrics due to the bursty nature of the errors, and hence a criterion called $ESR_{\%}$ (Errored Seconds Ratio) was defined. An errored second occurs when the receiver counts at least one MPEG Transport Stream errored frame within a given second, e.g. an uncorrectable Reed-Solomon codeword. The $ESR_{\%}$ is the percentage of errored seconds observed during a defined integration period, this period being selected to be long enough to average effects of short term fading. It is defined as:

$$ESR_{\%} = \frac{ErroneusSeconds \times 100}{Numberof\ Measurement\ Seconds}$$

Generally, a duration of 20 minutes was found to be adequate for most scenarios and rendered a stable and accurate measure. The $ESR_{\%}$ was measured as a function of C/N at the receiver input so that we were able to measure the C/N at an arbitrary Threshold of Visibility (ToV) of 3%. (e.g. this is equivalent to 2 errored seconds every minute). This threshold has been estimated the early preparatory work presented [99]. However, some estimations of the ToV at 5% are also reported, in order to be consistent with the criteria appeared later in [100]. The two thresholds are denoted as $ESR_{3\%}$ and $ESR_{5\%}$.

To determine the $ESR_{\%}$, the signal power was kept at a constant level at least 20 dB above the receiver's noise floor, and the level of additive excess noise increased by changing the step attenuator, as recommended in [101]. The receiver characteristics are detailed in (Appendix II). The signal power and the noise level were measured after the Signal and

Noise combiner using a power meter. A simple calculation is used to map each $ESR_{\%}$ point to its corresponding C/N. The power meter had been set-up with 4096 points to establish the average, corresponding to 5 minutes of power integration in the time domain. The measurements' precision was estimated to be within 0.5 dB.

4.4.2 Channel Models

Tests were performed using 4 different simulated scenarios. These were the Indoor Modified "Commercial B" and COST 207 [82] outdoor environments: Rural Area (RA), Typical Urban (TU) and Bad Urban (BU) in UHF band. The Indoor Modified "Commercial B" is a derivation of the indoor channel delay profile specified by ITU-R in [70]. As mentioned in chapter 3, the standard scenario has been "modified" with the addition of 2 short delay taps (at 15 and 25 ns) to make the model more realistically represent reflections from nearby objects in an indoor scenario. The 2 additional taps have the effect of introducing significant "flat fading". Table 4-2 gives the Root Mean Square (RMS) delay spread σ and the associated approximate 90% coherence bandwidth of all profiles calculated according section 3.4. All the channels have Rayleigh fading. The power delay profiles are generated within the Spirent channel emulator and in the case of two transmit antenna testing, the amount of correlation between channels can be varied.

Table 4-2: RMS Delay Spread and 90% coherence bandwidth of channel model used for testing

	Indoor	RA	TU6	BU12
RMS Delay spread σ (μs)	0.1	0.1	1.1	2.5
90% Coherence bandwidth (MHz)	0.2	0.2	0.0182	0.003
Maximum Excess Delay* (μs)	0.52	0.7	0.45	10.0
*=values are estimated with reference to the last path with -15.0 dB of relative power				

4.4.3 DVB System Parameters

Basic transmission parameters are defined for an 8 MHz channel by the DVB-T standard

[2]. In the 2k mode (used in the UK), the OFDM symbol duration is $T_U = 224\mu s$ and the number of carriers is $K = 1705$. This yields a subcarriers spacing of $1/T_U = 4464\,Hz$ and a spacing between the spectrum band edge carriers of $(K-1)/T_U = 7.61\,MHz$. For the 8k mode (used in the rest of Europe), the basic parameters are $T_U = 896\mu s$ and $K = 6817$. In addition to these basic parameters, others that have to be defined are for modulation, guard interval length and channel coding. For Indoor, Typical Urban and Rural Area measurements, the guard interval lengths of $\tau_g = 1/32 \cdot 896\mu s = 28\mu s$ and $\tau_g = 1/32 \cdot 224\mu s = 7\mu s$ are both suitable because of the maximum channel delay is approximately $5\,\mu s$. Table 4-3 summarizes the transmission parameters used for tests. The Guard Interval is the same for all configurations for tests consistency.

Table 4-3: DVB-T systems parameters

Configuration Name	UK	QPSK UK	French
Code Rate	¾	¾	1/2
Signal Constellation	16-QAM	QPSK	64-QAM
DVB-T Mode	2k		8k
Hierarchy (α)	Non hierarchical		
Guard Interval	1/32		

4.5 Experimental Results

The system set-up was verified by performing a benchmark test, measuring the receiver's sensitivity in an AWGN channel and comparing it to that published in the DVB-T standard specifications [2]. Subsequently tests were performed as described in Table 4-4. The dependence of diversity gain against all variables was methodically measured, exploring the effect of varying channel correlation coefficient, diversity delay, and Doppler shift on different signal scenarios and in different broadcast modes. The simulation results reported in chapter 3 and in the literature suggest an achievable delay diversity gain of approximately 4 to 6 dB in RA and Indoor channels [25] [102], 3 dB to 5 dB in TU [25][24] and about 1.5 dB in larger delay spread outdoor channels [8]. The results presented in this section show that the predicted performance can be achieved with

actual equipment in simulated signal conditions.

Table 4-4: Transmit DD Test cases

Test case	Config.	$\delta = [1.5,...,0.25]$ (μs)	$C = [0.75,...,0]$	Channel	$Fd = [0,...,120]$ (Hz)	Purpose
A	UK, QPSK UK, French	N/A	N/A	AWGN	N/A	Benchmark with DVB-T specs
B	UK, French	All values	0.25	Indoor	1	Impact of different delay values
C	UK	1	All values	Indoor	1	Impact of different cross correlations
D	UK	All values	0.25	TU6	50	Impact of different delay values
E	UK, French	All values	0.25	Indoor, TU6	1, 50	Impact of different delay values
F	QPSK UK	1	0.25	TU6	All values	Impact of different Doppler frequencies
G	UK	1	0.25	Indoor, TU6, RA, BU12	1	Impact of different envir.

4.5.1 Benchmark Test of Experimental Equipment

This preliminary benchmarking measures the C/N for Quasi Error Free (QEF) operation as defined by the DVB-T specifications. The QEF operation is defined as a post-Viterbi Error Rate of 2 x 10^{-4} and this should occur at a C/N of 12.5 and 16.5 dB for the predefined UK and French modes respectively. Tests were performed for both Monitor Station and Dibcom receiver. Figure 4-6 shows measured BER versus C/N for these modes. In this situation it was possible to measure the Post Viterbi BER and C/N since an AWGN channel exhibits good stability against time. The sensitivity measured for each mode was within 1 dB of that published in the DVB specifications confirming the validity of the measurement setup and procedure.

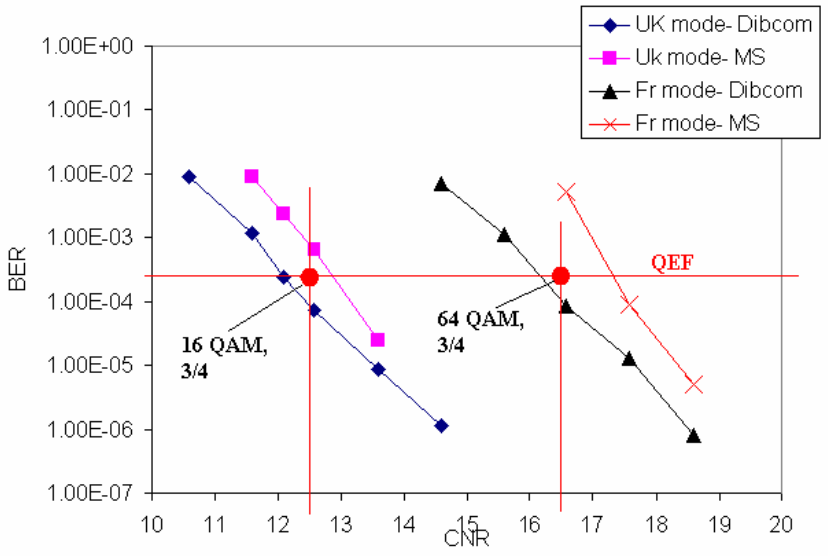

Figure 4-6. BER vs. C/N in AWGN channel, UK and French mode

For reference purposes, it is reported $ESR_{5\%}$ threshold for Portable Indoor (PI) and Portable Outdoor (PO) channel at 1.5 Hz Doppler shift [63].

Table 5: C/N (dB) for 5% ESR in PI & PO channel

Modulation	Code rate	PI	PO
16-QAM	3/4	20.5	22
64-QAM	3/4	25.3	27.5

The C/N performance figures are based on the state of the art receivers on the market added with a 2 dB margin.

4.5.2 Diversity Gain performance versus delay

This test case aims at evaluating the diversity gain achieved with different delay values in an indoor environment. The cross correlation between the channels was fixed at $c = 0.25$ and the Doppler shift was fixed at 1 Hz. Figure 4-7 and Figure 4-8 show $ESR_{\%}$ versus C/N for the indoor channel in the UK and French broadcast modes using the Monitor Station. The cross correlation value $c = 0.25$ corresponds to a distance between the two transmit antennas of about13 λ. This antenna separation can be reasonably achieved in practical UHF deployments. The reliability of this cross correlation channel model is discussed in Chapter 5, section 5.5.1.6. Single transmit antenna performances are included as a reference. Due to the low correlation coefficient between the channels, subcarriers experiencing a deep fade when transmitted from antenna '1' are unlikely to experience the same depth of fade when transmitted from antenna '2'. As mentioned in Section 4-2, DD increases channel selectivity and therefore decreases the likelihood of a deep fade occurring due to interference between the signals from the 2 antennas. Figure 4-7 shows results for DD Gain vs. Delay for UK broadcast mode and a simulated indoor channel. This shows that with a delay of 0.25 μs a gain of 0.7 dB at $ESR_{3\%}$ was achieved comparing with the single transmitter case. Furthermore as the delay value increased to 1.5 μs, the DD gain increased to 5.5 dB. Similarly for the French mode depicted in Figure 4-8, the delay value is 0.25 us, the DD gain is 3 dB at 3%. As the delay value increased from to 1.5 μs, the DD gain increased from to 7.2 dB. In conclusion, simulations have shown that for indoor scenarios, it can be expected to have a diversity gain exceeding 5 dB when the delay between the transmitted signals is above 1 μs.

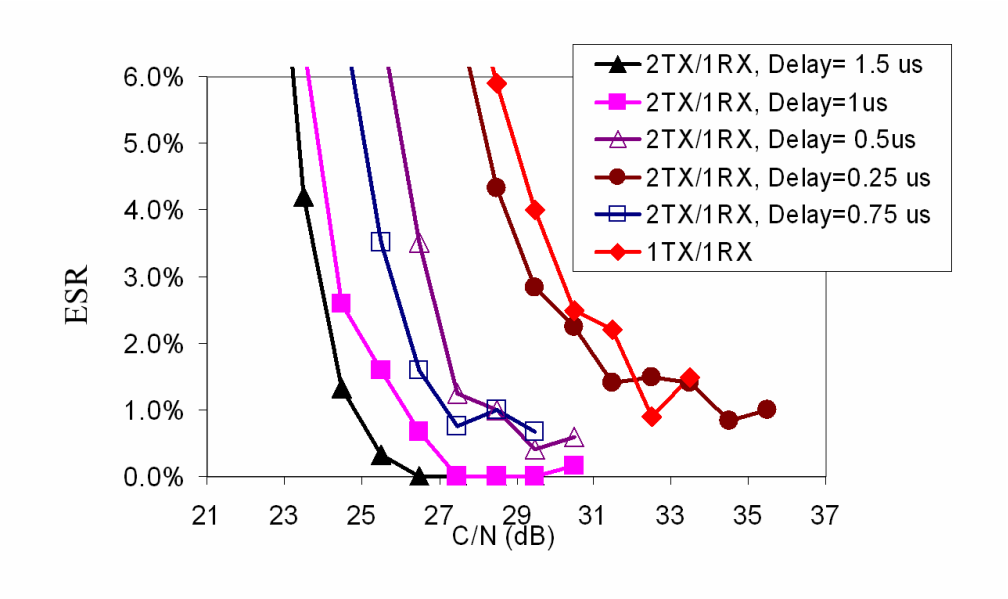

Figure 4-7. ESR$_{\%}$ vs. C/N for indoor channel, UK mode, $c = 0.25$, Fd=1 Hz, Monitor Station

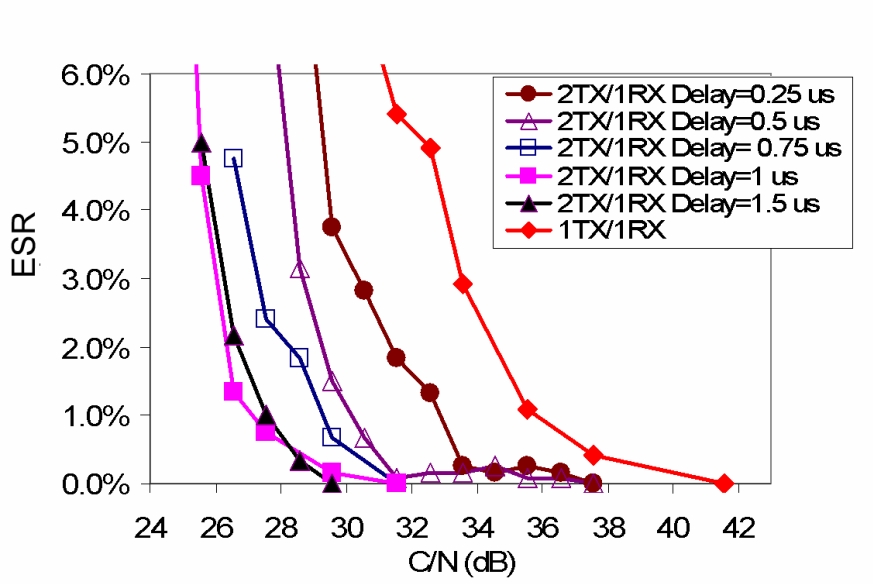

Figure 4-8: ESR$_{\%}$ vs. C/N for indoor channel, French mode, $c = 0.25$, Fd=1 Hz, Monitor Station

4.5.3 Delay Diversity Gain performance tests versus cross correlations

The purpose of this test case is to evaluate the relationship between the cross correlation coefficient between channels and the achievable diversity gain keeping the delay value and Doppler constants. This is extremely important to evaluate since the cross correlation

depends on the actual separation of antennas and their configuration in specific channel scenarios. Subsequently field trials will be largely concerned with determining the practical conditions that will produce decorrelated fading.

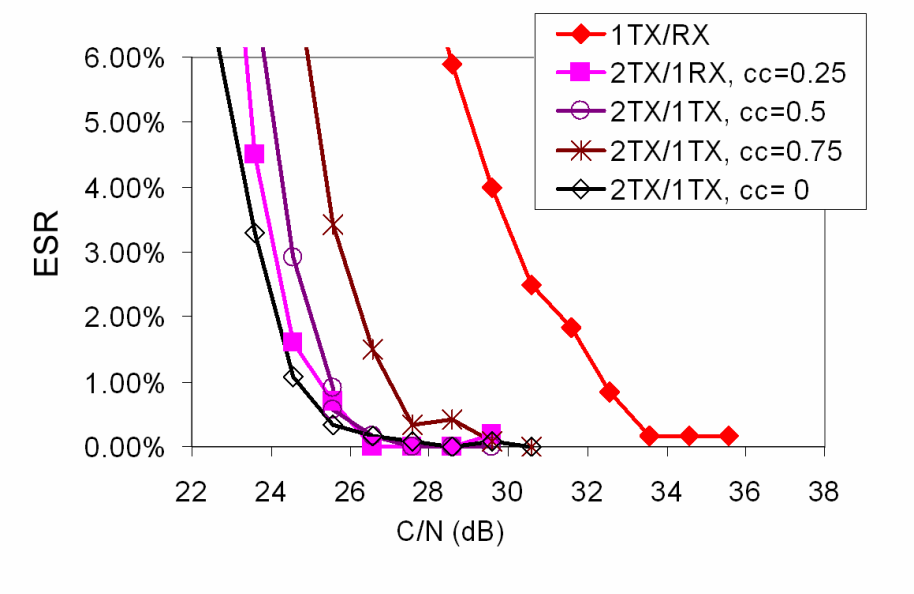

Figure 4-9. $ESR_{\%}$ vs. C/N for indoor channel, UK mode, $\delta = 1\mu s$, Fd=1 Hz, Monitor Station

The results shown in Figure 4-9 illustrate the relationship between correlation and diversity gain in the indoor channel with a delay value $\delta = 1\mu s$ and a Doppler frequency Fd= 1 Hz for the UK mode. These results show that when the cross correlation coefficient is less than 50%, a gain of approximately 4 dB can be achieved and the full gain of over 6.5 dB could be achieved with the theoretical 0% correlation.

4.5.4 Delay Diversity Gain Tests with a High Doppler Frequency

Figure 4-10 and Figure 4-11 illustrate the effectiveness of diversity in a typical urban (TU) environment at a high Doppler frequency of Fd= 50 Hz using the Monitor Station and the Dibcom receiver, respectively. For the Monitor Station experiment, it can be seen that in the SISO case, the $ESR_{\%}$ value cannot reach 0% even at high C/N ratio. The introduction of a transmit diversity signal with delay of $0.5\mu s$ or above provides 5 dB of diversity gain at an $ESR_{\%}$ of 3% and enables 0% error rate to be achieved.

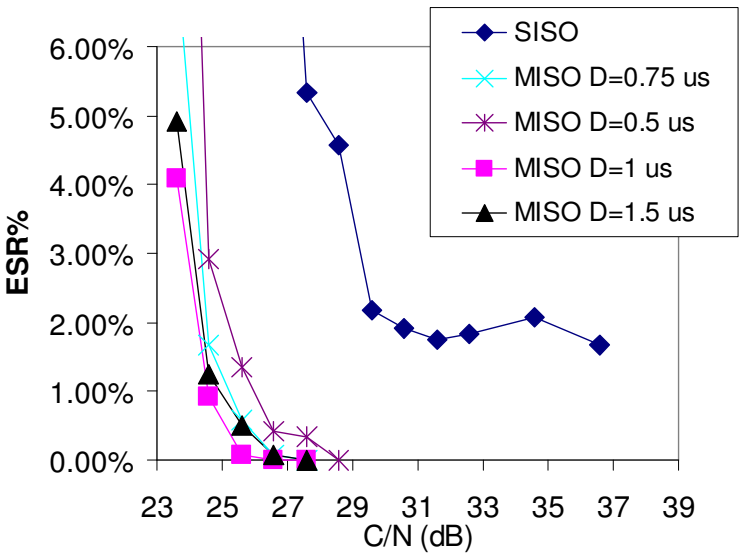

Figure 4-10. $ESR_{\%}$ vs. C/N for TU channel, UK mode, $c = 0.25$, Fd=50 Hz, Monitor Station

On the other hand, Figure 4-11 shows that the $ESR_{\%}$ value relative to the Dibcom receiver reaches 0% at high C/N=28.5 The introduction of a transmit diversity signal with delay of $1.5\mu s$ or above provides 3 dB of diversity gain at $ESR_{\%}$ of 3%.

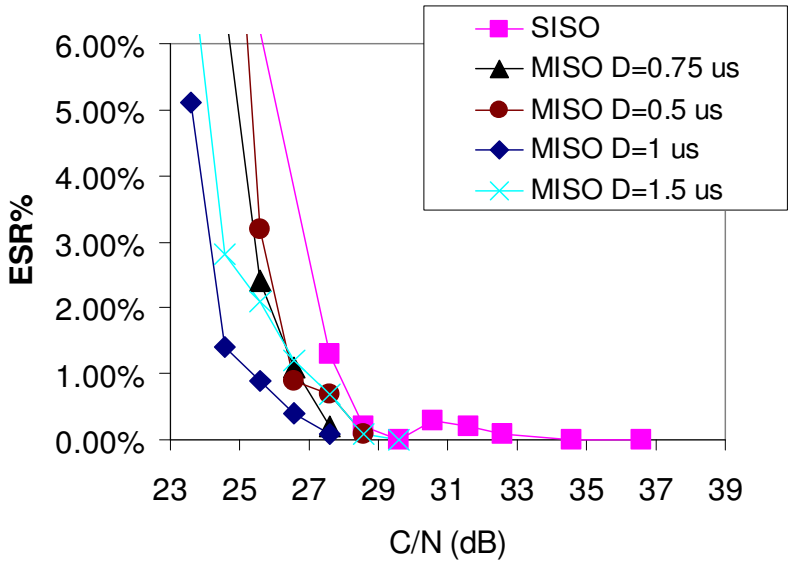

Figure 4-11: $ESR_{\%}$ vs. C/N for TU channel, UK mode, $c = 0.25$, Fd=50 Hz, Dibcom receiver

These results suggest that the SISO performances significantly depend on the receiver

implementation while the DD achieves the same performances in both receivers. This results in the same ToV for all receivers independently of the manufacturer, with significant advantages for network planning. Results show that DD can enable portable reception for standard DVB set top box.

4.5.5 Delay Diversity Gain Tests for different DVB-T modes, maximum Doppler Frequencies and environments

Figure 4-12 summarizes the diversity gain measured in a number of modes versus delay values. It can be seen that in flat fading environments like indoors, a diversity gain 7.5 dB for 8k modes or 6 dB for 2k mode can be achieved. The diversity gain is mainly affected by the increase in the delay value. The impact of the modulation or mode of transmission on the achieved diversity gain is not significant as expected from theoretical simulations reported in [8], a delay that is larger than 15 μs results in no further diversity gain improvement. It was shown in [25] that the achievable gain in the TU channel is 3 dB less for the Indoor channel case. This is mainly due to the different channel delay spreads. However, Figure 4-12 shows a maximum diversity gain in the TU case comparable with the indoor channel (an offset of about 1 dB at $\delta = 1.5\mu s$). The reason is mainly due to the Doppler frequency of the TU channel which is 50 Hz compared with 1 Hz for the indoor channel and TU6. In [8] a diversity gain of about 2 dB in TU6 with a low Doppler frequency of 10 Hz was predicted. This is confirmed by the tests of Figure 4-13 in different channels with a Doppler frequency of 1 Hz.

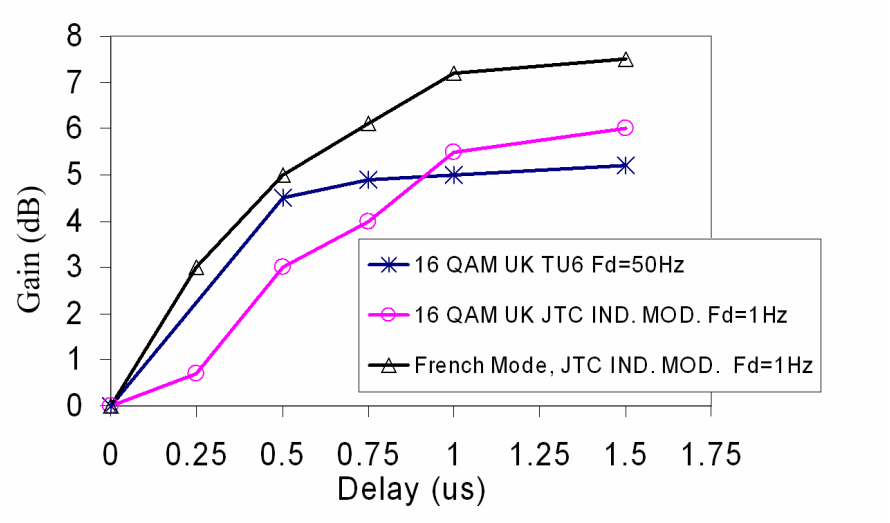

Figure 4-12. Delay Diversity Gain vs. Delay Code at $ESR_{3\%}$, $c = 0.25$, $\delta = 1\mu s$, MS receiver

4.5.6 Delay Diversity Gain for different maximum Doppler Frequencies

This case studies the impact of Doppler frequency on the achievable diversity gain. The effect of the Doppler frequency on diversity performances of the QPSK UK mode is shown in Figure 4-13. The QPSK is more likely to be adopted for fast mobile receiver applications. This operating mode allows the receiver to be more robust to faster channel variations associated with mobile reception hence providing an acceptable service quality [103]. Figure 4-13 shows that the SISO curve diverges from the MISO curve as the Doppler frequency increases. This results in 5 dB diversity gain at 50 Hz Doppler frequency in the MISO case. As the Doppler frequency increases further, the single transmitter curve reaches the failure point faster than the 2 Tx curve. From Figure 4-13 it can be observed that for $Fd \geq 120$ Hz, the receiver cannot track fast channel variations even in the diversity case, resulting in the failure of signal demodulation even with very high C/N levels. For low Doppler frequencies (~1 Hz) as in a quasi-static channel, a diversity gain of approximately 3 dB was achieved.

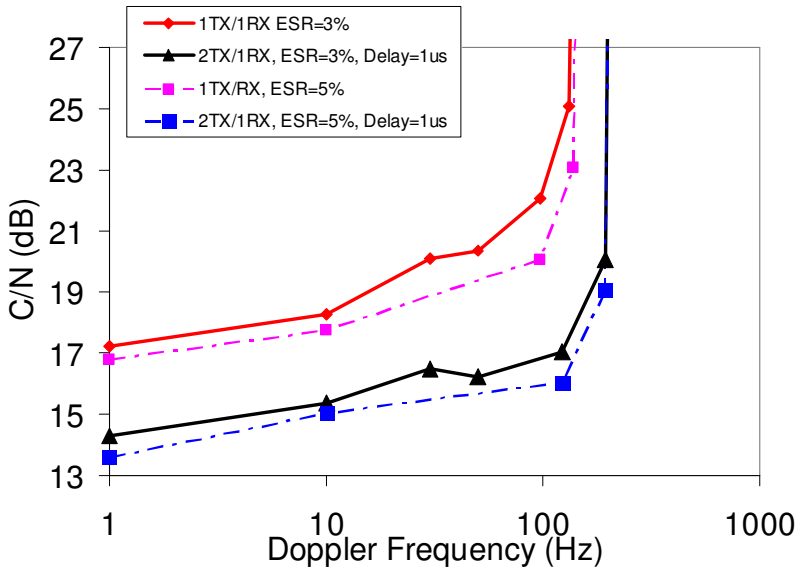

Figure 4-13. C/N at TOV vs. Doppler Frequency, TU, QPSK UK mode, $ESR_{3\%}$ and $ESR_{5\%}$, $c = 0.25$, $\delta = 1\mu s$, MS receiver

Fig. 4-14 shows the variation of $ESR_{\%}$ versus Doppler frequency at a fixed C/N for Monitor Station and Dibcom receiver. With a single transmitter the $ESR_{\%}$ exceeds the 3% TOV at a low Doppler frequency of around 4 Hz, whereas in the 2 transmitter case, the $ESR_{\%}$ value does not exceed the 3% threshold until a Doppler of 105 Hz is reached. For this particular receiver implementation, a Doppler shift of about 105 Hz introduces sufficient Inter-carrier interference (ICI) to inhibit the receiver operation.

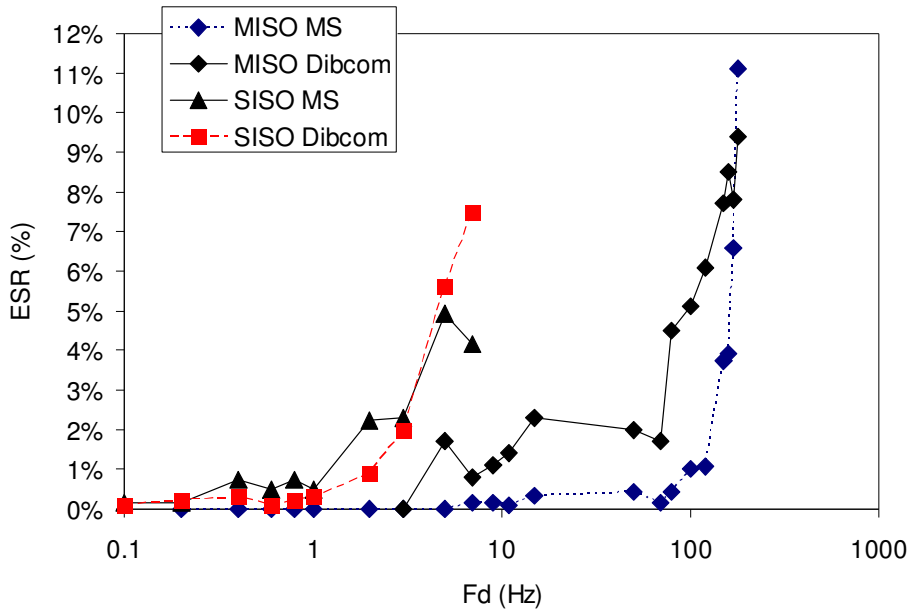

Fig. 4-14. $ESR_{\%}$ vs. Doppler Frequency at C/N=18.06 dB, TU, 4 QAM UK mode, $c = 0.25$, $\delta = 1\mu s$, Monitor Station and Dibcom receiver.

4.5.7 Delay Diversity Tests for different environments

In this test case, the transmit delay diversity gain is evaluated in several environments with different power delay profiles and delay spread values. Figure 4-15 shows the achieved diversity gain in four channels namely BU12, TU6, RA and indoor. All other parameters are kept constant; the cross correlation coefficient is 0.25, the delay value between the channels of the two antennas is 1 μs and the Doppler frequency is 1 Hz in the UK mode.

As expected, channels with large delay spread values lead to smaller diversity gains since there is a low probability of experiencing flat fades. It should be noted that in the case of RA and Indoor channel, the coherence bandwidth is significantly higher than the TU and BU coherence bandwidth. Consequently, a higher number of subcarriers can fall in flat deep fades simultaneously, resulting in a highly demanding channel for the DVB signal. In this situation the greatest diversity gain has been measured showing the potential of transmit diversity with low delay spreads. It is concluded that the diversity gain is approximately proportional to the inverse of the channel delay spread value. The gain for the RA and Indoor channel is very similar since they both share the same RMS DS.

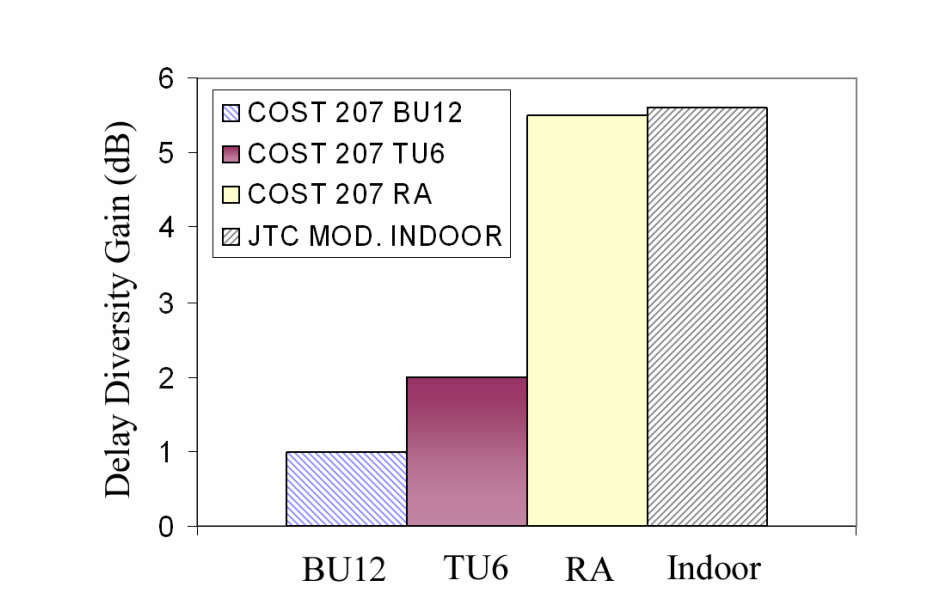

Figure 4-15. Diversity Gain for different Power Delay Profiles, UK mode, $c = 0.25$, $\delta = 1\mu s$, Fd=1 Hz.

4.5.8 Comparison with MRC receiver diversity

The target of this section is to compare the performance of transmit delay diversity with conventional receive diversity with Maximum Ratio Combining (MRC). Figure 4-16 shows the block diagrams of an OFDM receiver with MRC. The signals of M receiver branches are linearly combined in order to maximize the SNR [36]. This requires that the CIR (Channel Impulse Response) of each branch is known. The combining operations are performed at subcarrier level after the DFT operation.

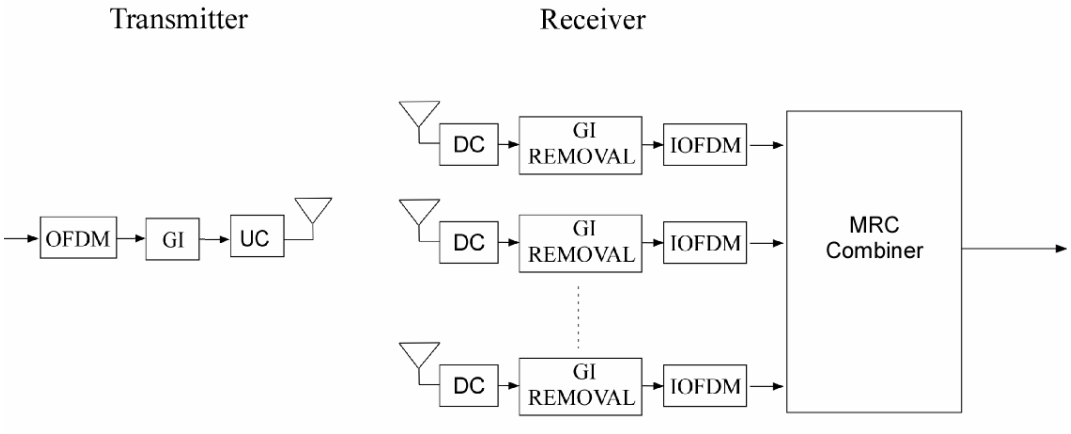

Figure 4-16: Block diagram of the OFDM receiver with MRC

The Dibcom dual diversity receiver is used with the Spirent channel emulator in a SIMO (Single Input Multiple Output) configuration. Figure 4-17: shows of the diagram of the receiver diversity MRC laboratory test bench. The system is partially derived from the transmit diversity set-up described previously in this chapter. For simplicity, this set-up employed the built-in channel emulator functionalities to generate the adjustable powers of uncorrelated AWG noises (e.g. N_1 and N_2) to be added to two diversity signals (e.g. C_1 and C_2). The C/N can be easily regulated by the channel emulator user interface.

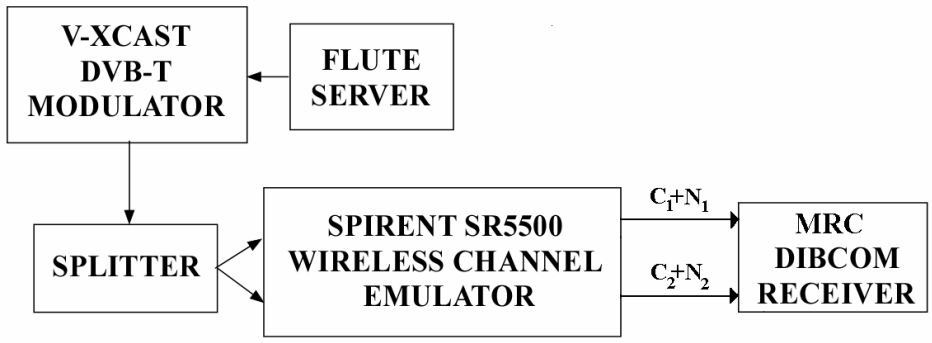

Figure 4-17: Block diagram's of receiver diversity MRC laboratory test bench

The transmission mode selected is QPSK targeting DVB-T high speed mobile and handheld applications. The selected environment for the tests is TU6 and the transmit delay diversity value is 1 μs. Tests were conducted for low and high Doppler values for different channel cross correlations. Since these measurements were expected to be used

for commercial purposes, the diversity gain was evaluated with the most used $ESR_{5\%}$ criteria (instead of the $ESR_{3\%}$). Figure 4-18 shows, for the UK DVB-T mode (2k QPSK 3/4 ½), the C/N vs. Frequency Doppler with a correlation factor between the two input paths varying continuously from 0 to 1 in Typical Urban channel.

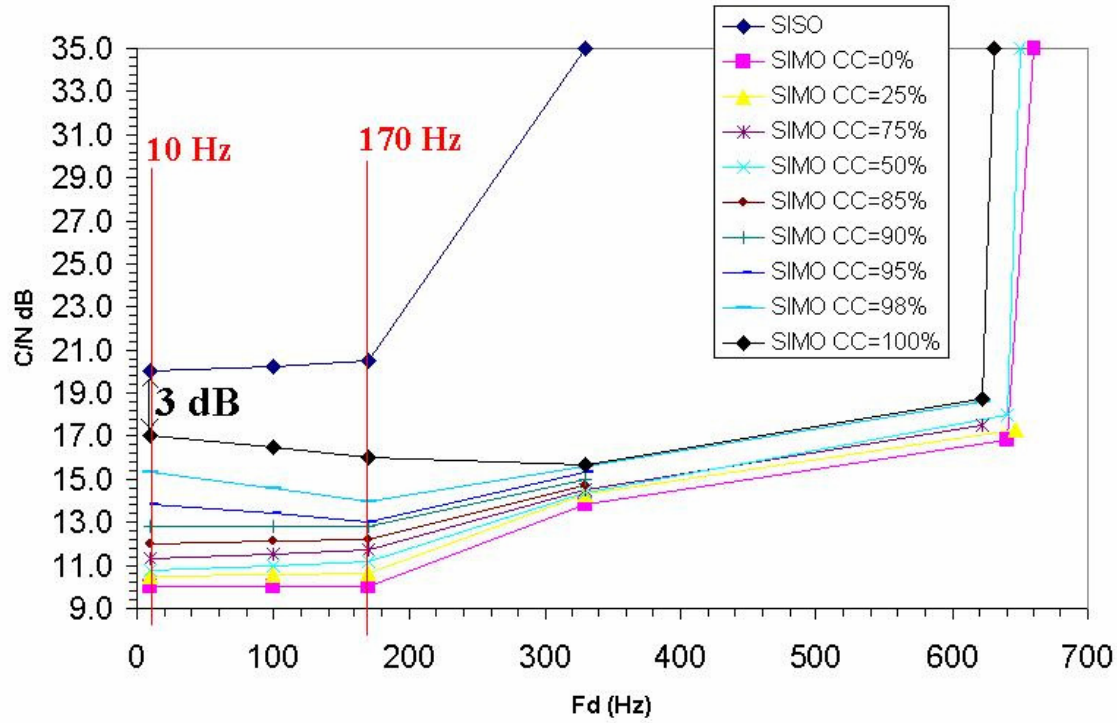

Figure 4-18: Measured impact of paths correlation on SIMO / SISO Diversity Gain

The SIMO performance curves appear accurate up to the frequency of about 170 Hz. Above this frequency, values are not considered because the curves are not accurate since they cross each other. The SIMO / SISO Diversity Gain vs. the correlation factor is plotted on Figure 4-19 for two specific frequencies: 10 Hz and 170 Hz. As expected, the maximum SIMO Diversity gain (e.g. ~10 dB) is obtained for $c = 0$ and the minimum gain of 3 dB for $c = 1$. This minimum 3 dB value can be easily explained: for $c = 0$ the signals C1 and C2 are perfectly correlated (e.g. C=C1=C2), while the Gaussian noises at each receiver input (e.g. N1 and N2) are still de-correlated; consequently the carrier to noise figures (C/N1) and (C/N2) are de-correlated. It is concluded that similar to the transmit diversity cases reported above, the receive diversity gain increases with the cross correlation value between the channels and decreases for high and low Doppler. On the

other hand, the Doppler frequency does not affect the receiver diversity gain as the transmit diversity does. This can be explained noting that the increased selectivity of the transmit DD channel can make more robust the channel estimation for high Doppler shift, while the MRC channel estimation techniques do not exploits the selectivity of the channels.

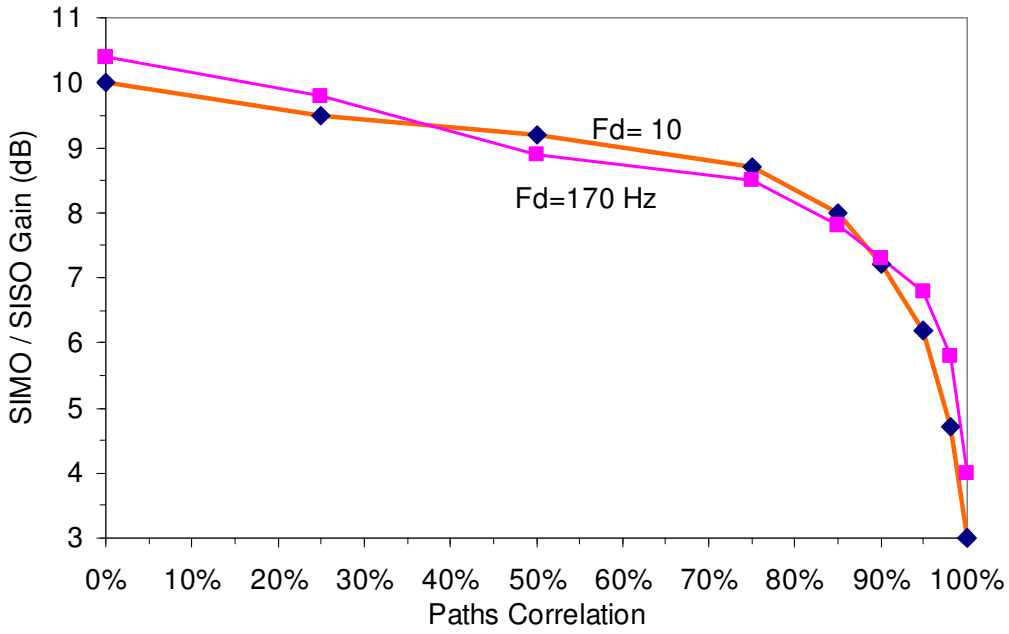

Figure 4-19:Dibcom SIMO Receive Diversity Gain for different Channel Cross Correlations (2K, QPSK ¾, 1/32) for a TU6 Channel at low and high Doppler.

Thus, the receive diversity gain is higher than transmit diversity gain especially at low Doppler frequencies at the cost of increased receiver complexity as shown in Table 4-6. This results can be compared with the approximate 8 dB gain estimated in simulations presented in Table 3-6 and Table 3-7.

Table 4-6: Comparison of Transmit and Receive Diversity Gains

Doppler Frequency (Hz)	MS MISO Gain (dB)	Dibcom SIMO Gain (dB)
10	2.5	9.5
170	7	9.8

4.6 Conclusions

In this chapter, the simulated performance of transmit delay diversity has been reported for DVB-T systems. Measurement results confirm that transmit delay diversity (DD) achieves significant diversity gain for de-correlated channels. Diversity gain increases as delay between the transmitted signals increases until there is maximum decorrelation between all received channels. In practice, measurements suggest that a delay value of 1 μs should be sufficient to achieve fairly sub-optimal diversity gain. Diversity gains of up to 7.5 dB should be achievable for indoor scenarios with a low delay spread and for outdoor scenarios with a longer delay spread diversity gains of up to 5 dB should be achievable. The key factor affecting success of diversity is cross correlation of the channels and measurements have shown that scenarios with a relatively short delay spread can still deliver high diversity gain with relatively high degree of cross correlation at 50%.

For mobile reception, DD significantly improves receiver performance until the impact of Doppler on inter symbol interference becomes unacceptably high for a particular receiver's implementation. The DD impact for mobile reception has been shown for two different receiver implementations. In mobile reception, the SISO performances are significantly different depending on the receiver implementation while the DD performances are the same and optimal for both receivers. This would result in the same ToV for all receivers independently of the manufacturer, with significant advantages for network planning designers. Moreover, DD technology can enable portable reception for standard DVB set top box technology, saving the receiver design costs of developing sophisticated channel estimation algorithms optimized for high speed reception.

It has also been confirmed though laboratory measurements that the gain predicted from previous theoretical simulations can be realized or exceeded using actual equipment in realistic propagation conditions. It was shown that the diversity gain obtained from MRC receive diversity is higher than transmit diversity gains especially at low Doppler at the cost of expensive processing at the receiver. The gap between MISO and SIMO gains reduce considerably as the Doppler frequency increases. However, the transmit delay diversity can be used to improve significantly the quality of the signal in DVB-T/H broadcast networks in inaccessible environments and for high speed the receiver

situations, thus reducing the need of diversity receivers. In the next chapter, field tests will be performed to verify these conclusions in real world environments and to show how coverage area of a DVB transmitter can be increased by using diversity. It is envisaged that these results should also be applicable for other OFDM broadcast systems.

5. Measurement Campaign on Transmit Delay Diversity for Mobile DVB-T/H Systems

5.1 Introduction

This chapter describes work carried out to quantify the advantages that can be achieved if Transmit Delay Diversity is applied to systems employing the DVB standard. The techniques that were investigated are applied to standard receiver equipment without modification. An extensive and carefully planned field trial was performed to validate predictions from theoretical modeling of chapter 3 and laboratory simulations of chapter 4. The transmissions were performed in the 730 MHz frequency band with a DVB-T/H transmitter and an EIRP of 20 dBW. The impact of the transmit antenna separation and the MPE-FEC was also investigated. It is shown that transmit delay diversity significantly improves the quality of reception in fast fading mobile broadcasting applications. This generic understanding can then be applied to other OFDM standards. The outline of this chapter is as follows. The experimental network deployed for the field tests is first described. The different investigated scenarios for mobile reception and the parameters used to analyze the performance are discussed. Finally, the results for DVB-T and DVB-H network experiments conclude the chapter.

5.2 Experimental Network

The experimental network is presented in this section. First the transmitter set-up is described, then, the receiver set-up. The transmitter and receiver calibration is also detailed.

5.2.1 Transmitter

The transmitter was located at Brunel University in Uxbridge, in the west outskirts of London, 1.2 km east of Uxbridge. The measurement area is relatively flat and representative of a typical sub-urban area. The field trial used two power amplifiers, rated at 100W, feeding a linear array of directive antennas. In the tests we compared quality of reception in the measurement area when either all power was transmitted from a single

antenna (Single Input Single Output) or half power from each of 2 separate antennas (Multiple Input Multiple Output). The EIRP was 20 dBW for both the single transmitter and dual transmitter (MISO) configurations on channel 53 which has a central frequency of 730 MHz and bandwidth of 8 MHz. A linear array of directive antennas was installed on top of one of the University buildings (named Tower D), pointing toward the east. The antennas are horizontally polarized panels with a gain of 12 dB, a half-power beam-width of 53° degrees in the H plane and 24° degree in the V plane. The antennas radiation pattern is presented in [91]. A maximum number of two antennas (out of five) were active at any time. The horizontal spatial separations between active antennas could be selected from 7 to 20 wavelengths. A vertical separation of 5 wavelengths can be optionally selected as shown in Figure 5-1. Table 5-1 summarizes the main technical characteristics of the transmission.

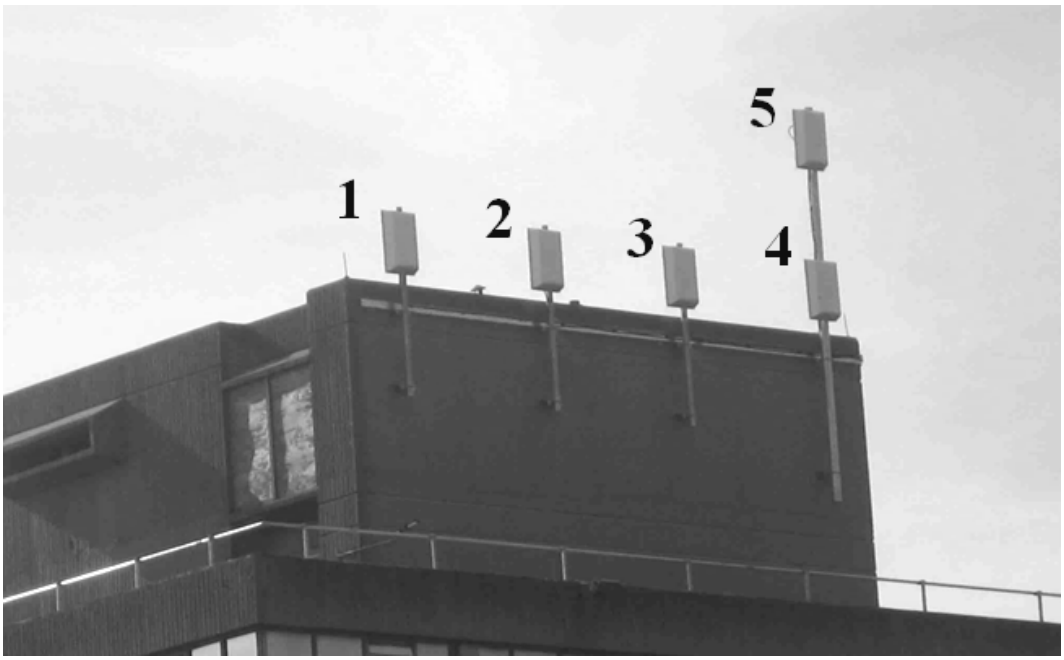

Figure 5-1: Brunel University's Diversity Antenna Array

Table 5-1: Technical Characteristics of The Transmission

Transmitter Centre	Uxbridge
Broadcaster	Brunel University
Coordinates	51.532367N; 0.473218W Decimal Degrees (DD)
Frequency	730 MHz
Bandwidth	8 MHz
EIRP	20 dBW
Antenna	Directive/Horizontal Polarized
Antenna(s) gain	12 dB
Antennas separations	7, 14, 20λ horizontal or 20λ horizontal and 5λ vertical.
Total feeders loss	6.8 dB (6.6 dB + 0.2 dB)
Height of the antenna above the ground	25 m

Figure 5-2 shows the schematic of the transmit system. The transport stream comprised Pseudo Random Binary Sequence (PRBS) packets for field measurements; the system is also capable of delivering multimedia content, encoded into MPEG-2 Transport Stream (TS) packets and transmitting it over the network for demonstration purposes. In case of DVB-H tests, sample video streams described in Table 5-10 were transmitted. A standard DVB-T Modulator was used to feed IF signals directly into the Broadreach Diversity Unit (custom made) [104], introducing a 1.1 μs relative delay between the two transmitted signals. The Diversity Unit has been designed to aid research into transmit diversity for DVB-T and DVB-H. The unit digitizes the input signal and passes it to a Digital Signal Processor (DSP). This DSP allows the signal to be split into two, each signal being processed by a number of digital filter stages before being passed to two independent upconverter/modulator devices. The low power transmitter (LPT) up converts the signal to 730 MHz. The signal is then amplified and filtered. The Amplifier A and amplifier B have

similar performance. The total feeder loss was 6.8 dB and the switch matrix connecting the amplifier B with one of the diversity antennas had a loss of 0.2 dB.

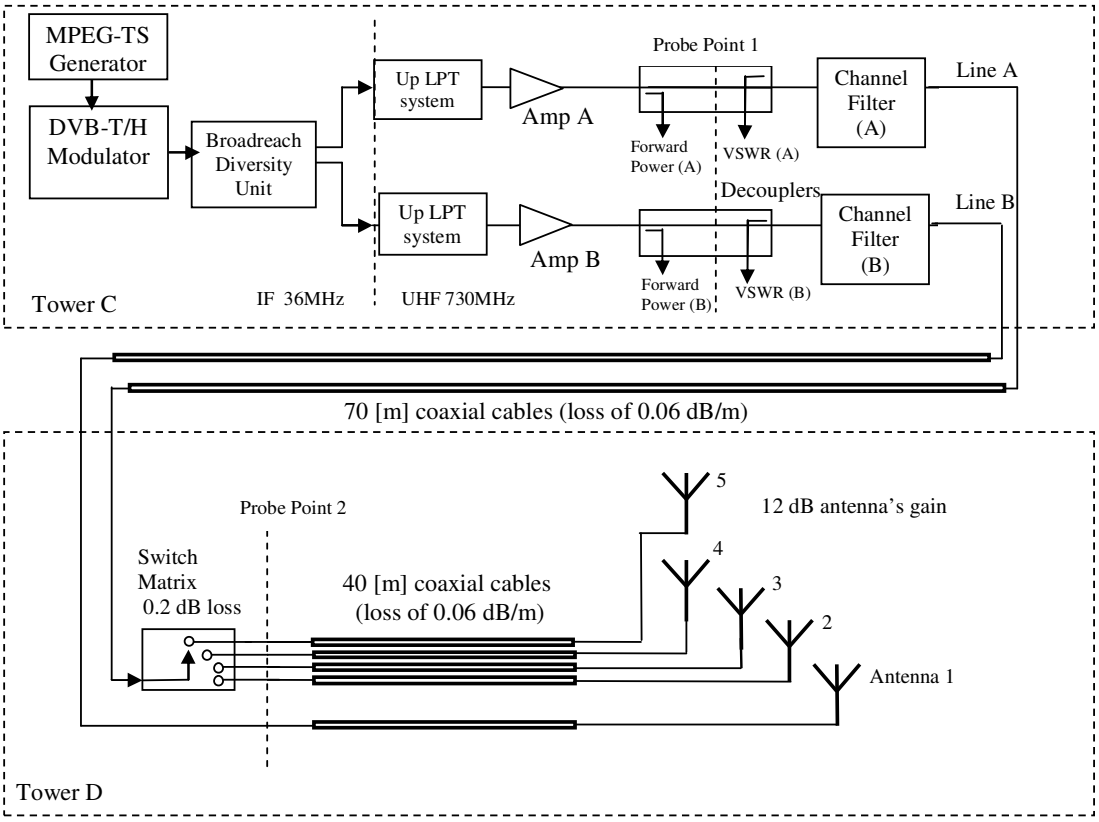

Figure 5-2: The RF diversity transmit system

Signal quality was tested at several stages in the transmit chain to ensure it was acceptable. The relative levels of the spectrum shoulders are fully compliant with the RF signal spectrum mask of DVB-T standard [92] [101]. The two amplifiers did not introduce any significant non-linear effects when operating with a SISO configuration (e.g. at full power). The power transfer system was calibrated and the power levels were carefully measured, adjusted and monitored during the measurements using a power measurement device with calibration traceable to national standards [105] [92]. The average MER at each point of the transmitted chain was estimated to be above 30 dB by using the EXT. In the MISO case each antenna transmitted half of the EIRP of the SISO case. The signal quality at full output power was comparable for both transmitters. A preliminary set of driving measurements was performed on a radial route to test the average received signal

strength indication (RSSI), carrier to noise ratio (C/R) and reception quality. Results are presented in [105].

5.2.2 Receivers

Mobile reception was measured using a purpose developed DVB-T receiver from Broadreach Systems [98]. This receiver allowed measurement of uncorrectable Reed-Solomon blocks, carrier to noise ratio (C/N), the Received Signal Strength Indication (RSSI) and delay spread were all tagged with GPS position, time and speed. The equipment was thoroughly calibrated and tested in chapter 4 laboratory simulations and in Appendix II, so that its performance compared to theoretical predictions was understood. From these measurements we would be able to derive the impact of diversity on other standard OFDM based broadcast standards. Mobile reception was measured using a car equipped with the Broadreach DVB-T receiver. Figure 5-3 illustrates the integrated system used to record seconds in which uncorrectable Reed-Solomon blocks are observed and from whom the $ESR_{\%}$ is calculated. The C/N and RSSI are also measured together with location coordinates acquired using a global position system (GPS) receiver.

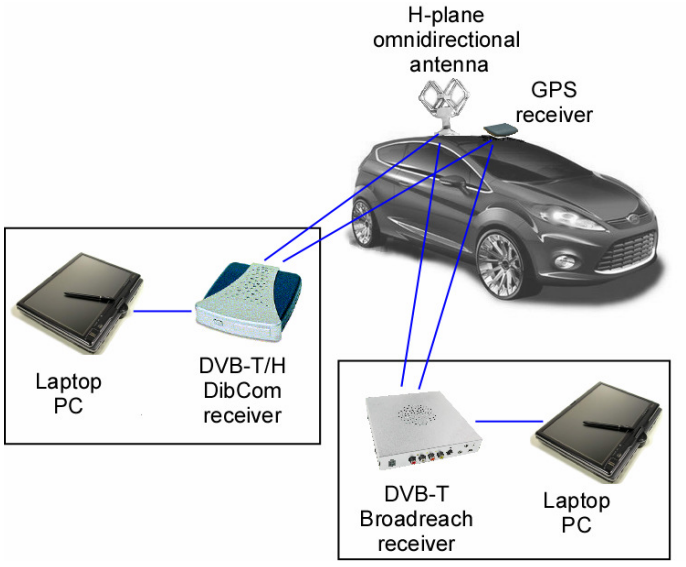

Figure 5-3: The car experimental set-up

After the initial measurement campaign using the MS receiver, a second campaign was performed using a proprietary DVB-H receiver from Dibcom [97]. This campaign enabled

to check that the DVB-T measurements could be correlated with DVB-H performance in accordance with theoretical predictions. A locked DVB-H receiver can receive DVB-H frames, which are either correct or incorrect. Incorrect tables can (sometimes) be corrected by the Multi-Protocol Encapsulation Forward Error Correction (MPE-FEC) code. The DVB-H receiver was supplied with a tool which logs parameters such as Carrier to Noise Ratio (C/N), Frame Error Rate (FER), and Multi-Protocol Encapsulation FER (MFER). MFER is the ratio of the number of residual erroneous frames (e.g. not recoverable) and the number of received frames. FER is the ratio of the number of erroneous frames before MPE-FEC correction and the number of received frames [4]. Location and speed are recorded with a GPS device. The signal was received using an omnidirectional horizontally polarized antenna, installed on the rooftop of the test vehicle. The antenna radiation pattern is presented in [91].

5.3 Area classification and selection

The area in which the measurements were conducted was classified into six different environments (Figure 5-4 and Figure 5-5). The experimental receiving conditions can be associated to a class C reception [4] where the characteristics of those environments are:

- "University Campus" (A Zone) includes high buildings, offices, and residential halls. The typical heights of these buildings are 30 m and the area includes several trees. Several locations are in LOS with the transmitter antenna array.
- "Sub-urban" (B Zone) can be described as a low density sub-urban area, with a significant presence of trees and vegetation. Residential streets within this zone are typically 10 meters wide.
- "Playground fields" (C zone) include typically football or tennis playgrounds, without a significant presence of buildings or trees.
- "Tree areas" (D zone) is of the same type as the playground fields' zone, but with a significant presence of trees.
- "Wide roads" (E zone) are 19.7 meters wide roads, 2 lanes each way, holding moderate traffic and surrounded by 2 floor residential houses. The speeds on these roads varied significantly with many accelerations and decelerations due to the variable traffic level,

- "Medium roads" (F zone) are 11.5 meters wide roads with 1 lane each way. They hold light traffic, but the speeds varied significantly.

Table 5-2: Description of zones

Class	Scenario	Zone	Description
C	Car, 20 km/h	A	high buildings, offices, and residential halls
C	Car, 20 km/h	B	low density sub-urban area, with a significant presence of trees and vegetation
C	Car, 20 km/h	C	Sport playgrounds
C	Car, 20 km/h	D	playgrounds with trees
C	Car, 48.2 km/h	E	Roads with two lanes each way
C	Car, 48.2 km/h	F	Roads with one lane each way

Figure 5-4 and Figure 5-5 show the two selected routes which covered mainly sub-urban zones and included wide and medium roads in all directions reaching marginal areas of Brunel's service coverage. Route A was in the main direction of the transmit power, it is approximately 13.2 km. The maximum range covered by Route B was 1.72 km. It should be mentioned that the measurements were repeated two or three times on the same routes. In total more than 500 km of mobile measurements were recorded. Route B was in the main direction of the transmit power along the zone E and it was selected to ensure similar propagation features and a more constant speed during the tests.

Figure 5-4: Route A and area classification

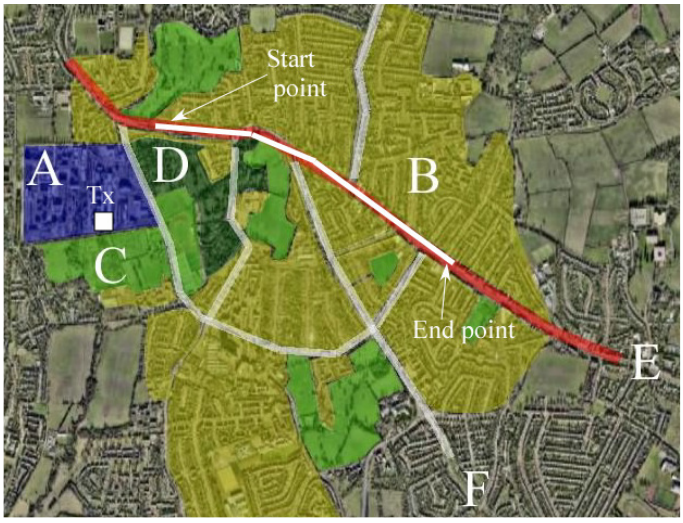

Figure 5-5: Route B and area classification

5.4 Parameters used to analyze performance

This section defines the parameters used to analyze the performance of the DVB-T/H systems. First, DVB-T and DVB-H parameters are explained. Next, transmission quality and signal quality parameters are described. Finally, the diversity gain is explained.

- DVB-T parameters

$ESR_{\%}$ denotes the percentage of the time when seconds are marked as erroneous. As defined in chapter 4, an erroneous second consists of a second containing at least one faulty TS-MPEG packet. The degradation point is set to 5% value and it is denoted as $ESR_{5\%}$ [100].

- DVB-H parameters

$FER_{\%}$ is defined as the ratio between the number of the erroneous frames and the total number of frames. A frame is marked erroneous if any TS packet within the frame is erroneous.

$$FER_{\%} = \frac{Number\ of\ Erroneus\ MPE\ Frames \times 100}{Total\ Number\ of\ Frames} \qquad 5\text{-}1$$

The degradation point is set to 5% value and it is denoted as $FER_{5\%}$

$MFER_{\%}$ is the ratio between the number of erroneous frames after the MPE-FEC correction and the total number of frames.

$$MFER_{\%} = \frac{Number\ of\ Erroneus\ Frames \times 100}{Total\ Number\ of\ Frames} \qquad 5\text{-}2$$

The degradation point is set to 5% value and it is denoted as $MFER_{5\%}$.

- DVB-T/H gain

$\Delta_{\{ESR_{\%},FER_{\%},MFER_{\%}\}}$ compares directly the SISO with the MISO performances. For instance, $\Delta_{ESR_{\%}}$ is defined as:

$$\Delta_{ESR_{\%}} = ESR_{\%SISO} - ESR_{\%MISO} \qquad 5\text{-}3$$

$\Delta^{R}_{\{ESR\%,FER\%,MFER\%\}}$ compares $\Delta_{\{ESR_{\%},FER_{\%},MFER_{\%}\}}$ with $\Delta_{ESR_{\%}}$ SISO performances and it is an adimensional parameter. For instance, $\Delta^{R}_{ESR\%,}$ is defined as:

$$\Delta^{R}_{ESR_{\%}} = \frac{\Delta_{ESR_{\%}} \times 100}{ESR_{\%SISO}} \qquad 5\text{-}4$$

5.5 Results

This section presents the results of the field trials. First the reception channel features are described, and then, the DVB-T results are shown, and finally the DVB-H results are presented.

5.5.1 DVB-T Tests

DVB-T tests are performed along route A. The time required for driving along the route was approximately 30 minutes. The diversity gain was estimated by comparing SISO and MISO driving tests performed sequentially to ensure analogous traffic conditions for the two measurements. Weather conditions were sunny or partly cloudy and background traffic was generally light/medium. Typical speeds were in the range of 0 to 48.2 km/h, with an average of 30 km/h. The measurements taken when the receiver was stationary were removed from the data presented here to eliminate the effects of random stops due to traffic lights on the total reception statistics. The tests results presented here were obtained when employing the broadcast conditions described in Table 5-3. A 20 λ horizontal antenna separation was adopted for the tests because it yielded the optimal gain among the possible MISO configurations (as shown in section 5.5.7).

Table 5-3: DVB-T system parameters

Configuration Name	SISO	MISO
Code Rate	3/4	
Signal Constellation	QPSK	
DVB-T Mode	2K	
Hierarchy (α)	Non hierarchical	
Guard Interval	1/32	
Bitrate (Mbit/s)	9.05	
EIRP (dBW)	20	17 (ant. 1) +17 (ant. 4)
Antenna separation (λ)	-	20
Diversity Delay (μs)	-	1.1

5.5.1.1 Channel estimation and features

This section describes the methodology and the processing employed to derive the channel features from measurements and a channel model to characterize the propagation scenario. The resulting models represent an outdoor mobile channel for SISO and MISO DVB networks. In chapter 4 it was shown how the transmit DD gain is related to the

propagation channel and to its parameters, particularly to root mean square delay spread (RMS DS). The Broadreach receiver was used which was capable of capturing channel Impulse Responses (IRs) consisting of 77 sample taps, equally spaced in 74 ns bins. The IRs were measured every 1 second and stored in a text log file. In this analysis we have chosen an appropriate power threshold to reduce noise. After studying the measurement data, it was concluded that 30 dB is an appropriate value for the dynamic range of the impulse responses. This means that signals which are 30 dB below the strongest power level are considered as noise and they are removed. This threshold is also consistent with other published works [106]. Path loss and shadowing effects were removed by normalizing the peak power of each impulse response to 0 dB. For each IR, the first tap with maximum power (0 dB) was chosen as reference starting point and the last tap with power exceeding the -30 dB threshold was chosen as last value. A cross correlation based algorithm aligns all the IRs for the PDP estimation. The IRs with a correlation lower than 0.5 if compared with the adjacent IRs and IRs taken were the receiver was not locked were discarded. Finally, it was estimated the sample mean of IRs taps relative to same temporal bin index, yielding an average power delay profile (PDP). A typical number of 1000 IRs are used. Figure 5-6 and Figure 5-7 shows the PDP over the route A for SISO and MISO configuration. The second cluster of echoes generated by the second diversity antenna starts at about 1.1μs. It should be noted that the average peak power of the second cluster is very similar to the peak power of the first cluster (0.2 dB below the first cluster peak), providing a qualitative confirmation of the equal average power radiated from the two transmit antennas.

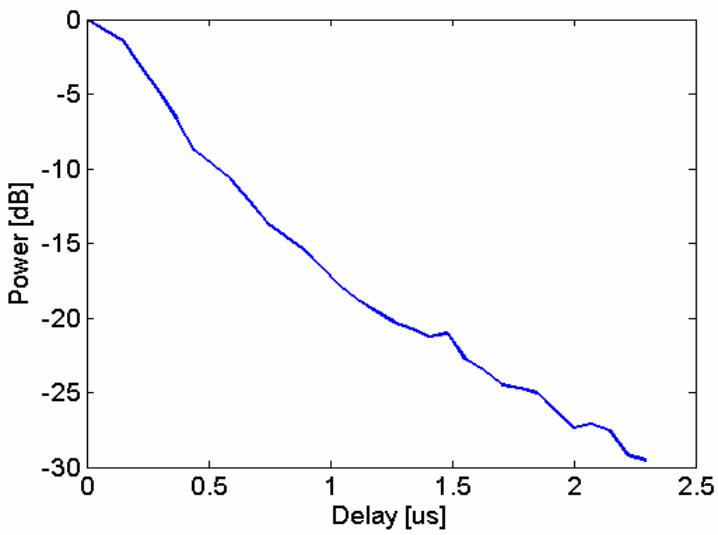

Figure 5-6: SISO Power delay profile (one transmitter on)

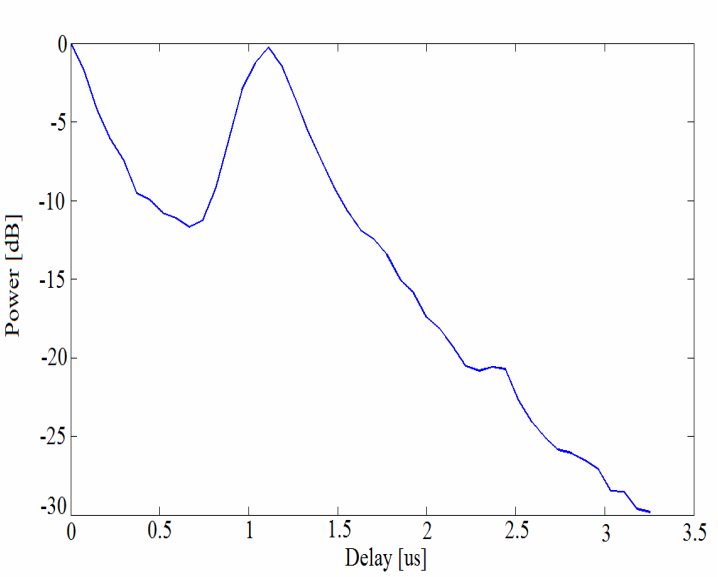

Figure 5-7: SISO Power delay profile (two transmitters on)

The exact delay and power values of the taps for the SISO and MISO models are given in Table 5-4. The reasons to select 30 taps were chosen to unify the two models and to find a compromise between accuracy and complexity of the channel models (both models report taps up to -20 dB).

Table 5-4: SISO and MISO Power Delay profile models

	SISO		MISO	
Tap number	Delay [us]	PDP [dB]	Delay [us]	PDP [dB]
1	0	0	0	0
2	0.074	-0.7241	0.074	-1.7034
3	0.148	-1.4543	0.148	-4.2461
4	0.222	-3.1905	0.222	-6.0922
5	0.296	-4.884	0.296	-7.422
6	0.37	-6.681	0.37	-9.5097
7	0.444	-8.8145	0.444	-9.9696
8	0.518	-9.7766	0.518	-10.814
9	0.592	-10.7437	0.592	-11.1196
10	0.666	-12.1528	0.666	-11.6747
11	0.74	-13.6207	0.74	-11.2774
12	0.814	-14.5347	0.814	-9.2107
13	0.888	-15.4076	0.888	-6.0881
14	0.962	-16.633	0.962	-2.9419
15	1.036	-17.7788	1.036	-1.2973
16	1.11	-18.754	1.11	-0.2677
17	1.184	-19.5251	1.184	-1.4322
18	1.258	-20.2344	1.258	-3.4771
19	1.332	-20.7333	1.332	-5.6211
20	1.406	-21.281	1.406	-7.4495
21	1.48	-21.0452	1.48	-9.2293
22	1.554	-22.7703	1.554	-10.7099
23	1.628	-23.4688	1.628	-11.9041
24	1.702	-24.4763	1.702	-12.4475
25	1.776	-24.7265	1.776	-13.4619
26	1.85	-25.0029	1.85	-15.0239
27	1.924	-26.2287	1.924	-15.8563
28	1.998	-27.3866	1.998	-17.4379
29	2.072	-27.0867	2.072	-18.1479
30	2.146	-27.5059	2.146	-19.269

Further three parameters were also analyzed from the acquired data: total excess delay, the RMS DS, and the number of taps. The total excess delay by definition is the difference in delay between the first and the last of the received taps. The RMS DS is calculated as detailed in formula 3-14. The number of taps is the taps within the total excess delay. Table 5-5 shows the average parameters of the SISO and MISO channel models. The second transmitter affects the values of the RMS DS and the number of the taps, by approximately doubling as expected. Moreover, the excess delay is increased to about 1.04 μs.

Table 5-5: Channel parameters

	SISO	MISO
Number of IRs used in the estimation	998	1018
RMS DS (us)	0.21	0.59
Excess Delay (us)	2.2	3.2
Number of taps	32	45

Comparisons of the SISO channel model with previous published work shows good agreement. A mobile DVB channel profile with a single transmitter published in [106] is very close to the PDP shown in Table 5-4 where estimated RMS DS and Excess Delay are 0.25μs and 2.21μs, respectively. These values match well with the SISO channel parameters proposed in Table 5-5.

5.5.1.2 DD over different days

Figure 5-8 shows the $ESR_{\%}$ for the entire route for SISO and MISO configuration. The measurements were taken during different days. In each case, multiple measurements were conducted during the same day. The MISO performances were compared with the SISO performances for antenna 1.

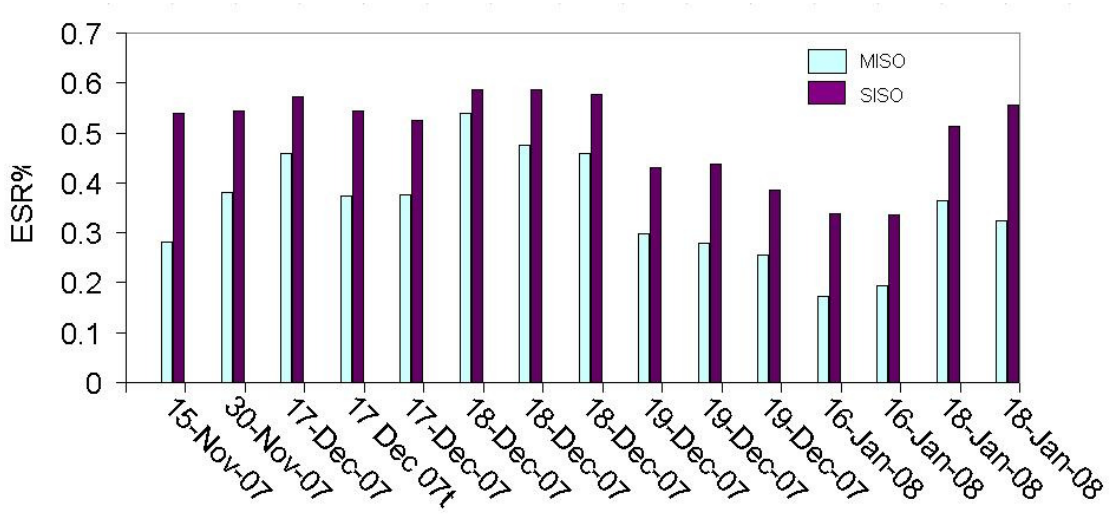

Figure 5-8: $ESR_{\%}$ of all experiments

Table 5-6 shows the sample mean and variance of $\Delta_{ESR_{\%}}$ and $\Delta^{R}_{ESR\%,}$ for all the tests presented in Figure 5-8. Moreover, a 95% confidence interval (CI) derived from Student's t-distribution is also presented [107]. The t-student distribution is usually adopted to calculate the confidence interval when the sample size is small. The sample mean of $\Delta_{ESR_{\%}}$ is about 14.7% with a sample variance of 33.4% and a 95% CI lower and upper bound equal to 12.6% and 16.77%, respectively. The $\Delta_{ESR_{\%}}$ values out of this interval are probably due to significant variations of the traffic conditions for the measurements compared. Impulsive noise due to car engine ignition systems also should be considered [4]. It was noted that the MISO performances are always better than SISO.

The sample mean of $\Delta^{R}_{ESR_{\%},}$ is about 0.31 with a sample variance of 0.017 and a 95% CI lower and upper bound equal to 0.27 and 0.36, respectively. The two SISO and MISO 95% CI intervals do not overlap, suggesting that there is less than 5% of possibility for MISO $ESR_{\%}$ to reach values as high as SISO $ESR_{\%}$.

Table 5-6: Sample mean and variance of the gain measurements and confidence intervals derived from Student's t-distribution

	$ESR_{\%}$ Sample Mean	$ESR_{\%}$ Sample Variance	Number of samples	t-student Degree of freedom	t-student Value (95%)	95% CI Lower bound	95% CI Upper bound
SISO	48.42	81.50	23	22	1.717	45.19	51.65
MISO	33.71	130.15	23	22	1.717	29.63	37.80
$\Delta_{ESR\%}$	14.71	33.44	23	22	1.717	12.63	16.77
Δ_R	0.317	0.017	23	22	1.717	0.270	0.36

5.5.1.3 EIRP and $ESR_{5\%}$ gain estimation

This section defines and estimates the EIRP and $ESR_{5\%}$ diversity gain from the measured data. This calculation is useful to estimate the practical reduction of the transmitted power (directly related to the EIRP) in a BS diversity system while keeping the same average performances of a SISO system transmitting at full power. The averaged Probability of Erroneous Second (PES) can be defined as

$$\overline{PES}(\Gamma) = \int_0^\infty p(\Gamma,\gamma) PES^{\gamma} d\gamma \qquad 5\text{-}5$$

where γ is the instantaneous value of the RSSI, Γ is the EIRP, $p(\Gamma,\gamma)$ is the probability density function (p.d.f.) of the RSSI and PES^{γ} is the probability of erroneous second estimated at γ. It is worthwhile to mention that $p(\Gamma,\gamma)$ is a function of Γ and it can be assumed to have a Rayleigh fading distribution in NLOS situation [28]. In practical measurements, $p(\Gamma,\gamma)$ also involves long term fading terms such as log-normal, shadowing, etc. In our practical analysis, the a priori theoretical quantities are replaced with the normalized number of occurrences (relative frequencies) coming from discrete measured data. Equation 5-6 can be rewritten as:

$$\overline{ESR_{\%}}(\Gamma) = \sum_{i=0}^{\infty} p_{\gamma_i}(\Gamma) ESR_{\%}^{\gamma_i} \Delta_i \qquad 5\text{-}6$$

where Δ_i is the RSSI measurement quantization step, $ESR_{\%}^{\gamma_i}$ is the errored second ratio measured at γ_i (e.g. the relative frequency of erroneous seconds at γ_i) and $p_{\gamma_i}(\Gamma)$ is the relative frequency of the γ_i. The EIRP gain can be defined as:

$$\Delta_{ERP} = \Gamma_{SISO} - \Gamma_{MISO} \quad for\ \overline{ESR_{\%}}(\Gamma_{SISO}) \approx \overline{ESR_{\%}}(\Gamma_{MISO}) \qquad 5\text{-}7$$

Figure 5-9 shows the empirically estimated Δ_{ERP} along the route A. The procedure is detailed as follows:

i. The $ESR_{\%}$ for SISO transmission was measured.
ii. The $ESR_{\%}$ for MISO transmission was measured. The EIRP is the same as the SISO case.
iii. The EIRP for MISO was reduced in steps of 1 dB until the observed $ESR_{\%}$ was equivalent to the SISO $ESR_{\%}$ case.
iv. The Δ_{ERP} is the reduction of MISO EIRP required to achieve MISO $ESR_{\%}$ equivalent to the SISO $ESR_{\%}$.

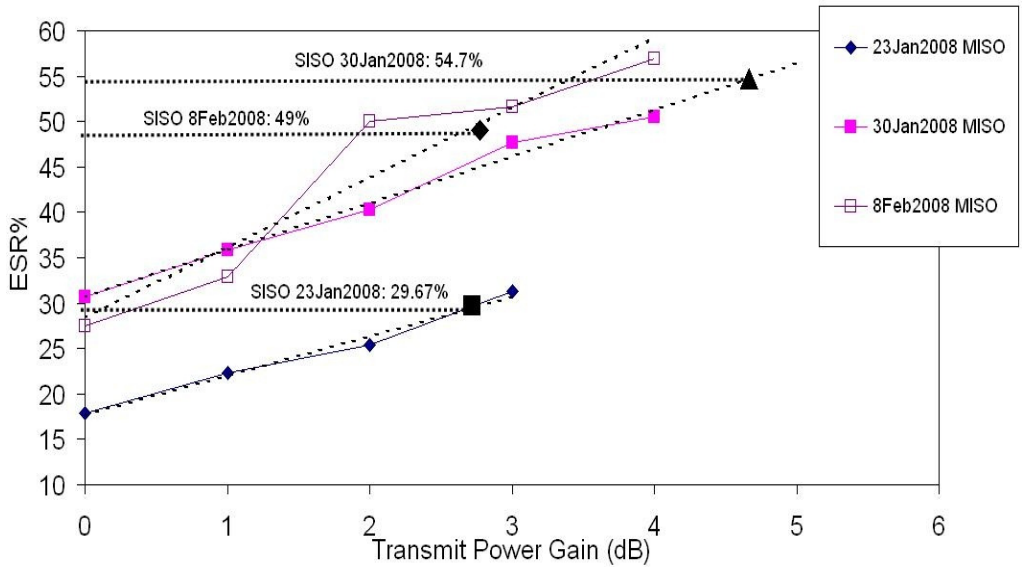

Figure 5-9: Transmit power gain vs. $ESR_{\%}$

The test was performed on three different days. The accuracy in setting the power is estimated to be ±0.2 dB. Numerical results are also reported in Table 5-7. In two cases the results show a gain of 2.7, 2.8 dB an in another case, the result show a gain higher than 4 dB. The small values of $\overline{ESR}(\Gamma)$ for SISO and MISO 23 January case are probably due to very different traffic conditions. A linear regression was used for this case and 4.6 dB was estimated. As mentioned before, Δ_{ERP} provides an estimation of the power to be increased in a SISO transmitter to get the same *average* performances of MISO network.
It should be mentioned that values presented in Table 5-7 differs from reference network planning thresholds [4], with $ESR_{\%}$ ranging from 30% to 5%. It is of interest to estimate the diversity gain at a particular value of the $ESR_{\%}$ (e.g. $ESR_{5\%}$).

Table 5-7: Δ_{ERP} estimated during three different days

	$\overline{ESR}(\Gamma)$ (SISO)	$\overline{ESR}(\Gamma)$ (MISO)	$\overline{ESR}(\Gamma)$ (MISO) Γ -1 dB	$\overline{ESR}(\Gamma)$ (MISO) Γ -2 dB	$\overline{ESR}(\Gamma)$ (MISO) Γ -3 dB	$\overline{ESR}(\Gamma)$ (MISO) Γ -4 dB	$\Delta_{ESR\%}$	Δ_R	Δ_{ERP} (dB)
23-Jan-08	29.7	17.8	22.3	25.3	31.3	35.0	11.9	0.4	2.7
30-Jan-08	54.7	30.7	35.8	40.3	47.7	50.5	24	0.43	>4
08-Feb-08	49.0	27.5	32.9	50.0	51.7	56.8	21.5	0.43	2.8

The $ESR_{5\%}$ for different values of RSSI was estimated using all data presented in section 5.5.1.2. The RSSI value is obtained from the receiver and is computed directly from the automatic gain controls (AGC) outputs. Approximately $2.5x10^6$ data measurement seconds are used for the processing. Figure 5-10 shows the SISO and MISO $ESR_{\%}$ against the RSSI values. Per each RSSI point, at least 100 seconds are considered to calculate the $ESR_{\%}$. Each $ESR_{\%}$ point is calculated taking data from a 3 dB interval. The curves show a diversity gain at $ESR_{5\%}$ of about 4 dB.

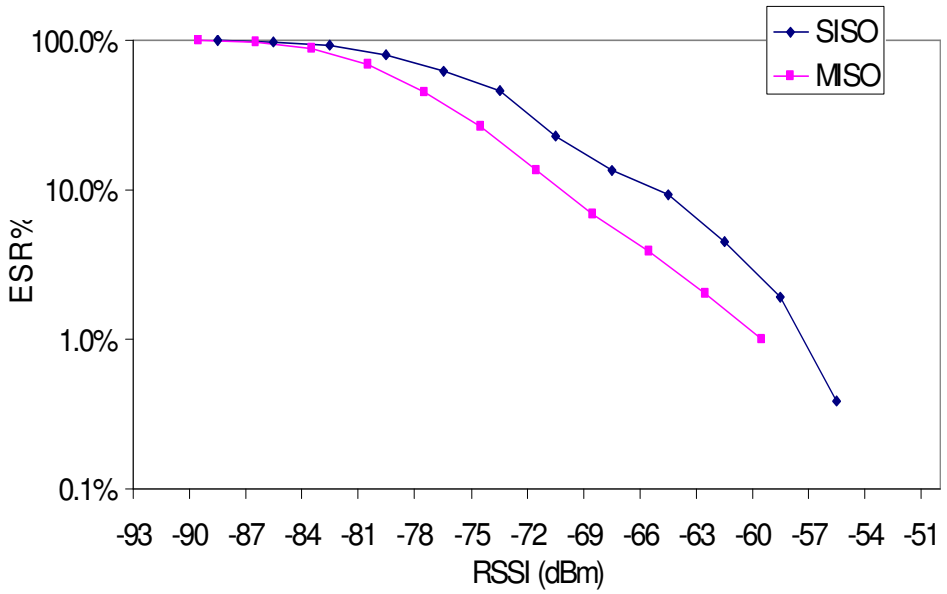

Figure 5-10: SISO and MISO $ESR_{\%}$ vs. RSSI

It is possible to compute the SISO and MISO coverage percentage from the same set of data. Reminding the space=time×speed relationship and assuming a constant receiver speed over the measurement track, the track sections with no coverage is equal to the measurement time with no reception (the speed factor in the formula is normalized when the ratio is calculated). This “linear” coverage metric can be interpreted as the reception limit at the borders of an area of interest. Thus, the $ESR_{\%}$ shown in Figure 5-10 can also be used to estimate the coverage percentages. A similar approach can also be found in [108]. Thus per each value of SISO coverage a corresponding value of MISO coverage can be mapped for the same RSSI. Figure 5-11 shows that a coverage of network planning reference 95% and 70% (e.g. "good" and "acceptable" reception, respectively) [4] with MISO transmitter corresponds to 88% and 50% coverage respectively with SISO.

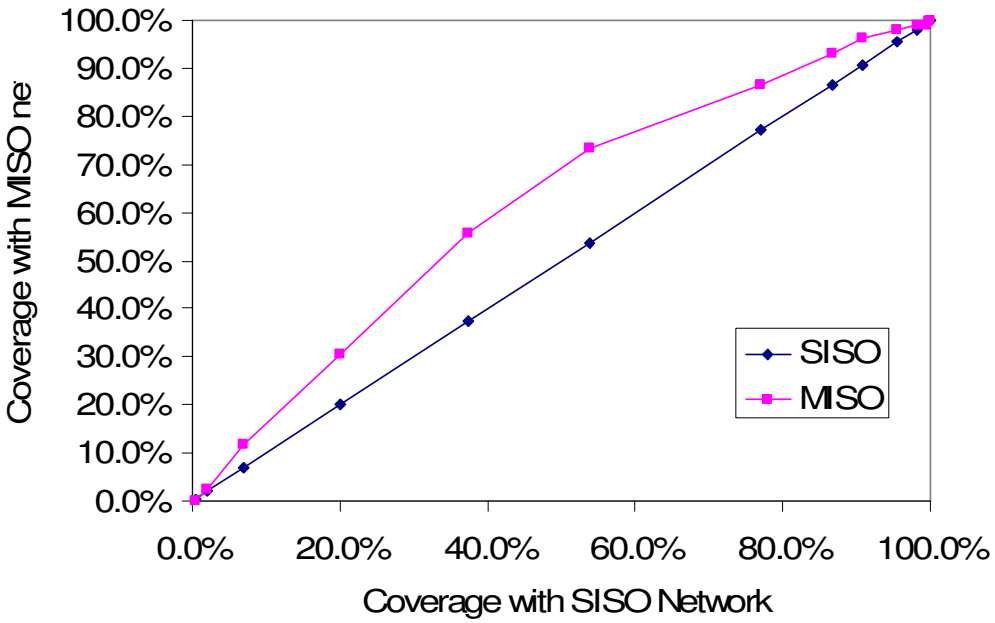

Figure 5-11: MISO vs. SISO coverage

Figure 5-12 shows the typical RSSI distribution along Route A. The RSSI is divided into three 15 dB sets, marked with different colors. The blue marks correspond to the highest RSSI level (-48.5 dBm ≥ RSSI ≥ -63.5 dBm). It is unlikely to observe an appreciable gain within this region: in fact Figure 5-11 shows a SISO $ESR_{\%}$<5%. The yellow marks correspond to a medium RSSI level (-63.5 dBm > RSSI ≥ -78.5 dBm). Figure 5-11 shows that MISO $ESR_{\%}$ is lower than SISO $ESR_{\%}$, so a reduction of erroneous seconds is expected. Finally, the red marks correspond to a low RSSI level (-78.5 dBm > RSSI ≥ -93.5 dBm). In this RSSI region both SISO and MISO $ESR_{\%}$ curves converge to an $ESR_{\%}$=100%, indicating no improvement.

Figure 5-12: RSSI profile along the Route A for SISO configuration. (RSSI 15 dB steps)

Figure 5-13 and Figure 5-14 shows the errored and error free seconds along Route A for SISO and MISO reception, respectively. The circles in Figure 5-14 highlight the zones of the route A where the errored second reduction is more evident. These zones correspond approximately to the RSSI region between -63.5 dBm and -78.5 dBm (Figure 5-12).

Figure 5-13: Errored and errors free seconds vs. geographical position for SISO reception along Route A

Figure 5-14: Errored and error free seconds vs. geographical position for MISO reception along Route A. It the reduction of errored seconds (marked as red squares) is clear if the zone within the white circles are compared with Figure 5-13

5.5.1.4 Capacity improvement estimation

Measurements have also been conducted to explore how transmit Diversity might be used to enhance system throughput capability. SISO and MISO $ESR_{\%}$ was compared at 3 different code rates of 1/2, 2/3, and 3/4. The tests were repeated over 4 different days. Figure 5-15 shows that during all tests, MISO $ESR_{\%}$ with a code rate of 3/4 always outperform SISO $ESR_{\%}$ with a code rate of 2/3. Since code rates of 2/3 and 3/4 correspond to 8.04 and 9.05 Mbps bitrate [2], the measurements suggest that a minimum improvement of 1 Mbps data rate can be achieved. Values for MISO 2/3 are higher than values for SISO 1/2 except for the 25/01/2008 case. Table 5-8 shows the detailed measured $ESR_{\%}$ values. From these measurements the throughput of a SISO network with a code rate 2/3 can be achieved with the same or better reception quality by using a MISO network with a code rate 3/4. Reference [63] shows that at least 2.1 dB additional EIRP is required to achieve the same $ESR_{5\%}$ when the modulation changes from QPSK 2/3 to 3/4 in a portable outdoor (PO) channel. The 4 dB gain estimated at $ESR_{5\%}$ in Section 5.5.1.3 ensures that QPSK 3/4 with MISO will outperform QPSK 2/3 with SISO. These results also indicate that a SFN network can be planned for mobile reception (up to approximately 50 km/h) using a QPSK ¾ modulation with diversity having the same or better reception quality of QPSK 2/3. Since this comparison was performed with the average values of $ESR_{\%}$, the $ESR_{\%}$ are too high for network planning purposes. An additional number of tests would help to perform the gain estimation at $ESR_{5\%}$ reference threshold as performed in Figure 5-10.

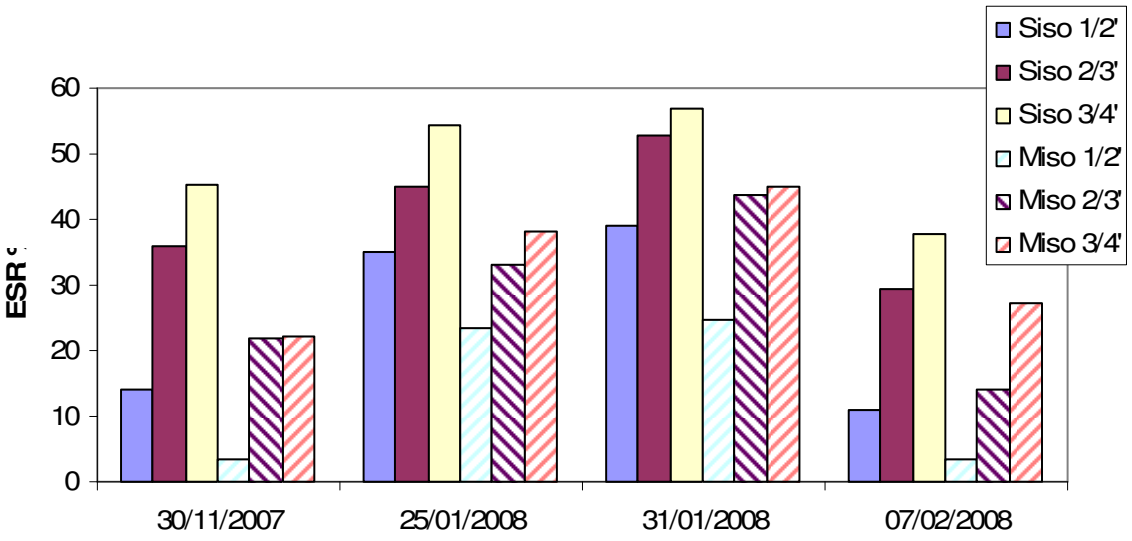

Figure 5-15: SISO bitrates compared with MISO for different code rate. The Guard Interval is 1/32 and the modulation is QPSK

Table 5-8: SISO and MISO $ESR_{\%}$ with different codes rates

	SISO $ESR_{\%}$			MISO $ESR_{\%}$			Bitrate Gain (Mbit/s)
	1/2'	2/3'	3/4'	1/2'	2/3'	3/4'	
30/11/2007	14.05	35.83	45.23	3.44	21.82	22.05	1.01 (2/3 SISO-3/4 MISO)
25/01/2008	35.0	44.91	54.40	23.41	33.20	37.98	1.01 (2/3 SISO-3/4 MISO)
31/01/2008	39.05	52.79	56.78	24.73	43.78	45.062	1.01 (2/3 SISO-3/4 MISO)
07/02/2008	10.94	29.34	37.78	3.47	14.10	27.33	1.01 (2/3 SISO-3/4 MISO)
Bitrate (Mbps)	6.03	8.04	9.05	6.03	8.04	9.05	

5.5.1.5 Comparison with published work

Table 5-9 shows the SISO RMS DS calculated for the COST 207 TU6 and RA channel models and compares this to the RMS DS estimated in Table 5-5. It can be seen that the measured RMS DS is 0.24 μs and falls between the TU6 and RA channel RMS DS figures [62]. The second part of Table 5-9 compares the diversity gain measured in a simulated environment for Doppler Frequency of 1Hz and 50Hz in TU6 and 1 Hz in RA. The channel cross-correlation is 0.25. No data for RA frequency higher than 1 Hz were available at the time of writing this chapter. The laboratory measurements conducted in chapter 4 were compared with the field trials. The average maximum Doppler shift of driving tests was 20 Hz while the minimum and the maximum Doppler shifts were 4.4Hz and 32.3Hz, respectively. It can be seen that the estimated diversity gain is within the expected range of 2-5.0 dB for TU6 thus validating our measured 4 dB of gain at 20 Hz for $ESR_{5\%}$.

Table 5-9: Delay Spread and transmit power gain

SISO channel RMS DS (μs)			Gain at $ESR_{5\%}$ (dB)			
COST 207		Estimated in 5.3	COST 207			Estimated in 5.4
TU6	RA		TU6, Max FD= 1 Hz	TU6, Max FD= 50 Hz	RA, Max FD=1Hz	Typical Max FD= 20.2 Hz
1	0.1	0.24	2.0	5.0	5.2	4

5.5.1.6 Antenna separation

The spatial separation of transmit antennas is required to achieve a sufficient de-correlation of fading between channels. From chapter 3, modeling predicts that a minimum separation of approximately 10 times the carrier frequency wavelength is required for a typical urban transmitter. In chapter 4 and [25], it was shown that diversity gain is fully effective over uncorrelated channels. However, in reality, the respective

signal paths between spatially separated antennas and the mobile receiver are likely to be correlated to a certain degree because of insufficient antenna separation at the transmitter and the lack of sufficient multipath in the channel. In LOS or near LOS conditions, the respective signal paths between spatially separated antennas and the mobile receiver are likely to be correlated to a certain degree because of insufficient multipath in the channel. These results in a diversity loss and methods of overcoming this are also being researched [109]. Under this perspective it is also worthwhile to investigate the relation between the antenna horizontal and vertical spatial separation and the MISO performances. The $ESR_{\%}$ has been measured along the standard test route and effect on MISO gain measured as a function of antenna distance. The test was repeated on consecutive days. Figure 5-16 shows the test performed in two different days. The results were near identical and it was decided not to conduct further tests. The results suggest that among the tests conducted the optimal antenna separation corresponds to MISO with antenna 1 and 4 (horizontal 20λ). A smaller horizontal separation would increase the channel correlation and thus degrade the performances. However, it is envisaged that a larger antenna separation would not necessary improve the performances since the fact that [75] suggests that a decorrelated channel should be already achieved with 20λ antenna separation. These results can be used as an indirect proof of the cross correlation channel model predictions. However, in order to fully proof the reliability of this model, the channel cross correlation can be estimated from CIRs using the same measurement set-up. A vertical plus horizontal antenna separation has been also tested in order to increase the spatial separation and reduce the 2 transmitter channel correlations. However, the antenna at a higher position led to a higher K-factor at the receiver thus reducing the transmit diversity gain [109]. With 20λ horizontal separation we generally observe good diversity gain since reception from these antennas exhibits a lower K-factor (e.g. the receiver is in a NLOS situation during most of the drive). The results suggest that high elevation transmitter antenna would tend to reduce the diversity gain because of the increased K- factor value. It should be mentioned that the broadcasting antennas with such horizontal separations can be deployed easily on existing buildings. However, since there are limitations in terms maximum transmitted power, the deployment of such systems seems feasible only on dedicated structures such as broadcasting towers, where the vertical separation can be more easily achieved. Thus, it seems worthy to investigated the diversity system

performances with antenna elements with only vertical separation (e.g. in this thesis set-up, antenna 4 and 5).

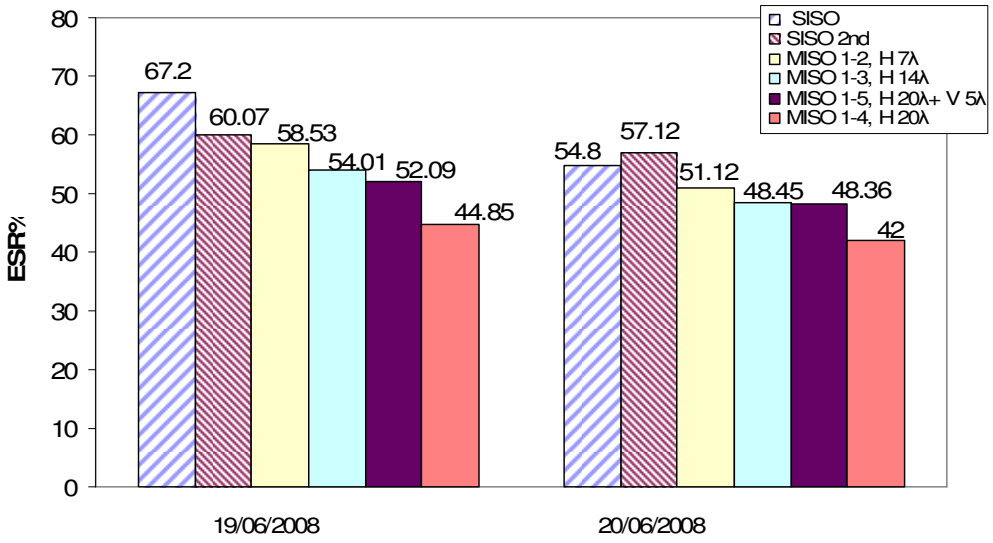

Figure 5-16: $ESR_{\%}$ for different antenna separations

5.5.2 DVB-H Tests

As mentioned in the introduction, the DD transmit diversity can also be applied to several OFDM standards. In this section, a sample application to DVB-H is presented. Previous work based on software simulations presents the impact of diversity at the bit error rate (BER) level (e.g. after the Viterbi decoder) [8] [24] [25] while [27] shows the DD gain taking into account also the impact of the MPE-FEC encoding. A comparison of the measured performances against the reference simulation is presented later in this chapter. Since the test condition cannot match exactly the simulation set up (e.g. the same propagation channel properties, the constant Doppler, the same channel estimation algorithm, etc.) the reference simulation can be used as general guidelines.

5.5.2.1 Performance over different days and different routes

The transmitter set-up is the same as the previous DVB-T investigation, except for the fact that here the DVB-H transport stream (TS) with video content is transmitted instead of PRBS. Table 5-10 shows the four MPE streams contained in the DVB-H (TS) and related to four different packets identification numbers (PIDs):

Table 5-10: Description of the content TS adopted for the DVB-H tests

PIDs	MPE-FEC	Frame rows	Content
4097	7/8	512	ESG
4098	7/8	1024	Star Wreck Trailer
4099	7/8	256	Light and Life

In DVB-H forward error correction is defined separately for each MPE stream. In these tests the FER and the MFER of the PID 4099 was monitored. The transmission parameters are summarized in Table 5-11. The in-depth interleaver option was not used. The padding and the time-slicing was created and optimized automatically

Table 5-11: Set up adopted for the DVB-H tests

Constellation	4 QPSK
Sub-Carriers	2K, 8K
Guard Interval	1/32
Bandwidth	8 MHz
MPE-FEC Rate	7/8
Frame rows	256
Code Rate	3/4
Transmit Antenna Separation	20 λ

The DVB-H receiver implements proprietary channel estimation algorithms especially designed for high speed mobility [97]. This optimization has been shown in chapter 4 to improve the SISO performance and leaves unchanged MISO performance, resulting in a smaller diversity gain at the Reed-Solomon decoder level (e.g. $ESR_{\%}$) in urban environment compared to the standard DVB-T receiver. The MPE-FEC extension is required to combat deep and long shadowing encountered in some mobile channels. According to results presented in this section, the DD transmit diversity gain is more obvious when the MPE-FEC is not taken into account, since this already partly exploits time diversity by introducing a virtual time-interleaving. The implementation of MPE-FEC is not compulsory in the DVB-H receiver, since an MPE-FEC incapable (but MPE capable) receiver will be able to receive the data stream in a fully backwards-compatible

way. This, together with MFER%, FER% also was measured. The MPE FEC requires a parity overhead from 12.5% to 50% of the total bit rate and it is worthwhile to investigate in which situations the DD can help to improve the capacity. The DVB-H receiver can monitor one MPE stream at time, by logging the C/N, and the DVB-H parameters every second. Measurements were made along route A and B. An external 12 dB attenuator has been added at the receiver for both SISO and MISO experiments. This attenuator is needed to significantly increase the number of frame errors after the MPE-FEC without reducing the EIRP at the transmitter. Results for route A are illustrated in Figure 5-17 and Table 5-12.

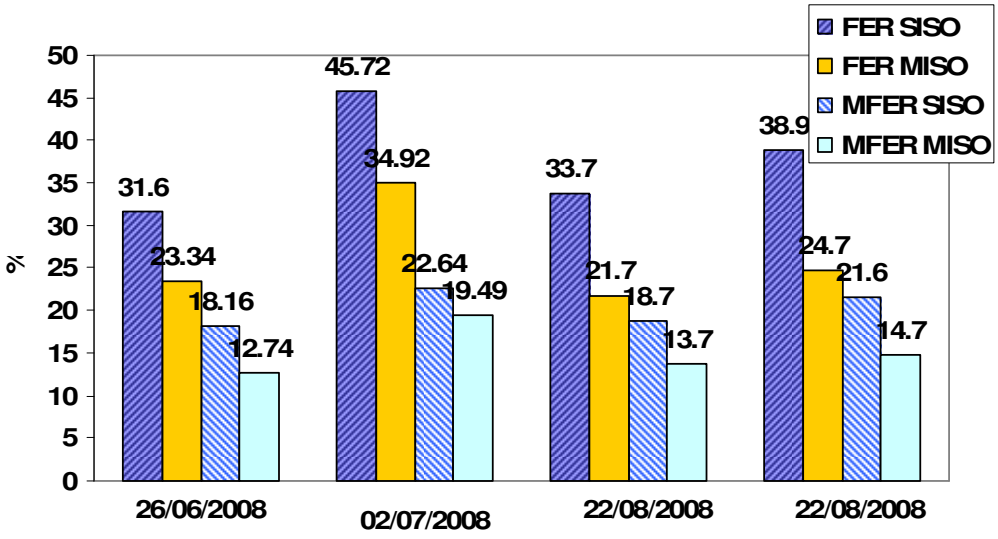

Figure 5-17: FER and MFER for DVB-H for route A

Table 5-12: FER and MFER Summary for DVB-H for route A. The transmission mode was 2K and 12 dB of external attenuators were added at he receiver.

Date	FER				MFER			
	$FER_{\%}$ SISO	$FER_{\%}$ MISO	$\Delta_{FER\%}$	$\Delta^{R}_{FER\%}$	$MFER_{\%}$ SISO	$MFER_{\%}$ MISO	$\Delta_{MFER\%}$	$\Delta^{R}_{MFER\%,}$
26/06/08	31.6	23.3	8.3	0.26	18.2	12.7	5.5	0.29
02/07/08	45.7	34.9	10.8	0.23	22.6	19.5	3.1	0.134
22/08/08	33.7	21.7	12	0.35	18.7	13.7	5	0.27
22/08/08	38.9	24.7	14.2	0.36	21.6	14.7	6.9	0.32

The experiment was repeated on four different days to ensure repeatability. From Table 5-12 it can be calculated that $\Delta_{FER\%}$ and $\Delta^{R}_{FER\%}$ were on average 8.03% and 30.42, while $\Delta_{MFER\%}$ and $\Delta^{R}_{MFER\%,}$ were on average 5.12% and 25.57. It can be seen from these results that generally the diversity gain observed before MPE-FEC is higher than after MPE-FEC. MFER% is lower than FER% because the MPE-FEC decreases the C/N demand by 5 dB to 8 dB [63]. The resulting MFER% and FER% measured corresponding to each C/N value is plotted in Figure 5-18. In order to have more data at different levels of C/N, additional measurements were made with at 0 dB and 6 dB attenuators fitted to the receiver's antenna input.

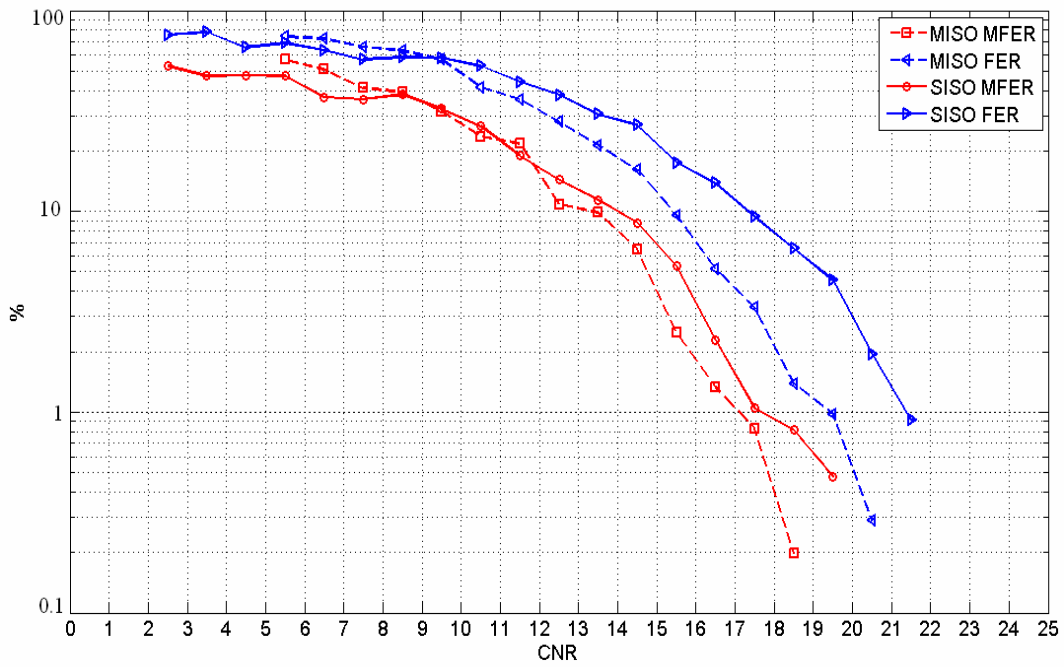

Figure 5-18: MISO and SISO MFER and FER on Route A

Each $FER_{\%}$ and $MFER_{\%}$ point are calculated by taking into account at least 100 tables as recommended in [4]. Data per each point are collected within 1 dB C/N intervals. This interval is chosen to have a trade-off between accuracy and smoothness of curves. Unlike the DVB-T receiver, DVB-H receiver does not provide the RSSI level; thus, the C/N calculated using the proprietary algorithm was of about 2.5 dB and 1 dB of gain measured for $FER_{5\%}$ and $MFER_{5\%}$, respectively. The $MFER_{5\%}$ curves do not show a smooth trend probably because of the small number of points. Reference [28] shows $ESR_{5\%}$ and $MFER_{5\%}$ diversity gain with the Dibcom receiver in TU6 uncorrelated channel at FD=50 Hz of about 3 dB and 1.7 dB, respectively. The actual performance figures with $FER_{5\%}$ are expected to be similar with what would be achieved using $ESR_{5\%}$ criterion to the transport stream directly [4]. Further results presented in [102] show an $ESR_{5\%}$ gain of about 2.5 dB. The Dibcom receiver shows an $ESR_{5\%}$ diversity of about 2 dB smaller of the gain measured with Broadreach receiver under the same test conditions and showed in Table 5-9. As mentioned before, it is envisaged that the gain reduction is due the Dibcom's chipset implementation, enhancing the SISO high mobility reception (chapter 4). However, Figure 4-10 and Figure 4-11 show that the C/N threshold for MISO $ESR_{5\%}$ was the same for both Dibcom and Broadreach receivers. Thus, it can be assumed for network

planning design that, when MISO diversity is applied, the $ESR_{5\%}$ C/N thresholds are better than SISO, independent of the chipset implementation and the same for all receivers. It is reasonable to assume that the approximate 0.5 dB of gain reduction compared to gain observed in the laboratory tests is due to different tests conditions. (e.g. a small amount of channel cross correlation, impulsive noise instead of AWGN, etc.). Table 5-13 shows the test repeated along the Route B with the transmission mode of 2K. The 95% CI lower and upper bounds are also calculated for SISO and MISO. The CI intervals do not overlap in either the FER or MFER cases.

Table 5-13: FER (a) and MFER (b) summary for DVB-H for fast route The transmission mode is 2K

	Sample Mean	Sample Variance	Number of samples	t-student Degree of freedom	t-student value (95%)	95% CI Lower bound	95% CI Upper bound
SISO $FER_{\%}$	29.6	9.18	6	5	2.015	27.17	32.15
MISO $FER_{\%}$	20.06	4.83	6	5	2.015	18.25	21.87
$\Delta_{FER\%}$	9.6	14.54	6	5	2.015	6.46	12.733
$\Delta^{R}_{FER\%}$	0.31	0.01	6	5	2.015	0.23	0.40

(a)

	Sample Mean	Sample Variance	Number of samples	t-student Degree of freedom	t-student value (95%)	95% CI Lower bound	95% CI Upper bound
SISO $MFER_{\%}$	12.53	1.74	6	5	2.01	11.4	13.62
MISO $MFER_{\%}$	9.83	4.47	6	5	2.01	8.09	11.57
$\Delta_{MFER\%}$	2.7	2.1	6	5	2.01	1.50	3.89
$\Delta^{R}_{MFER\%,}$	0.21	0.01	6	5	2.01	0.12	0.31

(b)

Figure 5-19 and Figure 5-20 shows the errored and errors free seconds along the Route A for SISO and MISO reception, respectively. The circles in Figure 5-20 highlight the zones of the route A where the errored second reduction is more evident.

Figure 5-19: Uncorrectable (red marks) and corrected received tables (green marks) tables for SISO reception along Route B.

Figure 5-20: Uncorrectable (red marks) and corrected received tables (green marks) tables for MISO reception along Route B.

Table 5-14 shows the same test repeated using 8K mode. The $FER_{\%}$ SISO upper bound CI and MISO lower bound CI overlaps only for about 0.5%. It is still reasonable to assume that the two SISO and MISO configurations lead to statistically different results. In the

case of $MFER_{\%}$ measurements, a certain amount of gain is still observed but because of the variability of results and the small amount of gain, it cannot be proven that results are significantly different when diversity is adopted. It is interesting to note that 8K set-up is providing better average performances than 2K set-up for the same route, while 2K and 8K yield the same performances for low Doppler shift region. This can be explained by noting that 8K is more resistant than 2K to impulse noise produced by car engine ignition systems [4].

Table 5-14: FER (a) and MFER (b) Summary for DVB-H for fast route. The transmission mode is 8K

	Sample Mean	Sample Variance	Number of samples	t-student Degree of freedom	t-student value (95%)	95% CI Low bound	95% CI Upper bound
SISO FER%	21.07	12.68	6	5	2.01	18.14	24.00
MISO FER%	15.74	12.87	6	5	2.01	12.79	18.69
$\Delta_{ESR\%}$	5.33	19.77	6	5	2.01	1.67	8.99
$\Delta^{R}_{ESR\%}$	0.24	0.02	6	5	2.01	0.09	0.38

(a)

	Sample Mean	Sample Variance	Number of samples	t-student Degree of freedom	t-student value (95%)	95% CI Lower bound	95% CI Upper bound
SISO MFER%	9.55	3.58	6	5	2.015	7.99	11.11
MISO MFER%	7.84	3.71	6	5	2.015	6.25	9.42
$\Delta_{MFER\%}$	1.71	2.51	6	5	2.015	0.40	3.01
$\Delta^{R}_{MFER\%,}$	0.17	0.027	6	5	2.015	0.04	0.31

(b)

5.6 Conclusions

The results presented in this chapter show that DD transmit diversity is effective when applied to a standard DVB-T/H system and that performance predicted by software laboratory simulations can be realized in real world situations. DVB-T experiment results showed that, when driving in a sub-urban area, the number of errored seconds observed is greatly reduced and instances of acceptable reception are significantly increased. The diversity gain in terms of EIRP and $ESR_{5\%}$ has been measured and found to generally agree with theoretical predictions. The coverage was improved of about 7% and 20% for the network planning reference coverage of 95% and 70%, respectively. It has been shown that transmit Diversity can be used to provide a data bitrate improvement of 1 Mbps. Finally, highest gain was achieved by adopting a 20λ of horizontal separation between transmit antennas. An additional 5λ of vertical separation reduced the gain as the Ricean K-factor figure increased. Wherever it was possible, the tests were repeated to provide the 95% confidence interval of the estimated figure. Dibcom's DVB-H experiment results shows approximately 2.5 dB and 1 dB of gain measured for $FER_{5\%}$ and $MFER_{5\%}$, respectively. The $FER_{5\%}$ gain is significantly smaller than the $ESR_{5\%}$ measured with Broadreach receiver because of the chipset implementation has already been optimized for high mobility reception. The $MFER_{5\%}$ gain is reduced compared to $FER_{5\%}$ because of time

interleaving effects of the MPE-FEC encoding. The DVB-H gain has also been measured for 8K FFT size. The measurement presented in the next chapter will explore the effectiveness of transmit diversity for indoor reception and evaluating the impact on radio network design. Resulting DVB broadcast networks could have fewer transmitter sites, lower EIRP or support higher data bitrates due to the increased performance and thus would be more cost-effective. This chapter has also shown through practical measurements that the technique of transmit diversity can be applied to DVB standard systems to improve reception in difficult to reach areas without impacting the standard or increasing complexity of receivers. The effect of transmit diversity is to improve quality of reception, by illuminating difficult non-Line of Sight situations rather than affecting overall range. Now that this technique has been shown to be viable, more complex implementations can be investigated that would improve the effectiveness and deliver higher gains.

6. Signal Profiling Techniques for Fixed Indoor, Rooftop, and Driving Tests

6.1 Introduction

Although transmit DD can provide a gain in NLOS situations, it can introduce degradation in LOS situation. When the Ricean K-factor component of the channel is significantly high, the channel performs similar to an AWGN channel where the performance degrades due to DD that artificially increases the fading. This phenomena degrades the rooftop reception and it can make unattractive the adoption of DD techniques for broadcasting where both NLOS and LOS scenarios needs to be considered. However, some techniques to mitigate the negative impact of transmit DD are investigated in [27]. One of the main contributions of this chapter is the practical analysis of the effectiveness of these new techniques. This chapter first provides the theoretical guidelines to predict the impacts of transmit DD on LOS and NLOS reception and the techniques employed to reduce the degradation performance in LOS while aiming to keep the same gain in NLOS reception. The test sites and the two experimental measurement set-ups are described. Then, the impact of DD loss mitigation techniques for LOS and NLOS stationary reception is presented. Results on the impact of these mitigation techniques for mobile experiments conclude the chapter.

6.2 Theoretical guidelines

In Chapter 3 it is showed that to achieve transmit diversity gain, the signals from different antenna elements should be sufficiently uncorrelated, e.g. at least less than a correlation of 0.7. Figure 4-9 shows a sub-optimal gain is obtained with a cross correlation of 0.25. The decorrelation of the channels can be achieved by deploying the two transmit antennas with sufficient spatial separation. A diversity gain is expected to be observed in NLOS situations assuming that the observed signals have uncorrelated or quasi-uncorrelated fading.

In LOS or near LOS conditions, the respective signal paths between spatially separated antennas and the mobile receiver are likely to be correlated to a certain degree because of insufficient scattering in the channel. The transmit diversity techniques are effective in the NLOS situations where the K-factor is small valued. In real word, if the K-factor is significantly high the channel is subsequently highly correlated and the performance gets worse than SISO. This is because the correlated signal replica creates deconstructive fades at the receiver, resulting in a diversity loss. Figure 6-1 shows the average power profile at the receiver side for SISO and MISO transmission on a reference AWGN channel. In the MISO case, it is possible to see the deconstructive interference fades.

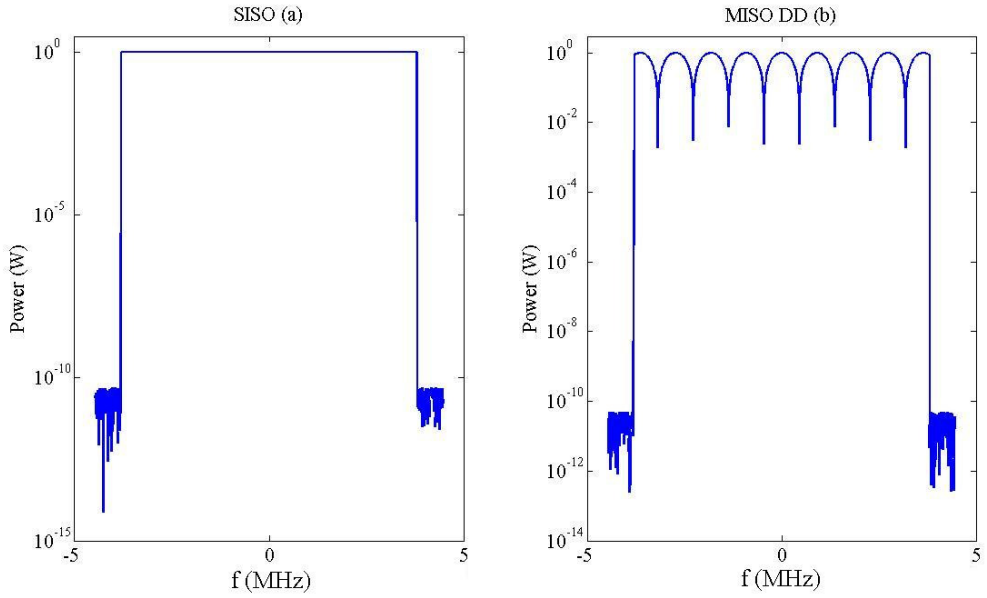

Figure 6-1: Average power profile for the SISO (a) and MISO DD (b) on AWGN channel case for 2k mode

To mitigate the diversity loss, some techniques have been developed in previous research work. For instance, [110] observes that the NLOS gain for a two branch system is the highest in the case of both branches having equal power. Even for the case with power differences of 6 dB between both branches, the NLOS gain was still appreciable versus the single Rayleigh scenario. Starting from this principle, it is envisaged that unbalancing the two diversity signal powers will mitigate the degradation in LOS reception while keeping a significant gain in NLOS [27]. Figure 6-2 shows the effect show the gain versus the Ricean K-factor for 2 transmitters with cyclic delays of $\delta = 1.09\,\mu s$. The gain is evaluated by comparing the SNR performances for 2 CDD transmitter with 1 transmitter at Quasi

Error Free (QEF) condition (e.g. BER = 2×10^{-4}), for 2k mode, 16-QAM modulation and an inner code rate of 3/4. The guard interval length is 1/32. The Doppler spectrum of the Rayleigh (non-LOS) components is uniform with a bandwidth of 0.1% of the subcarrier spacing (e.g. 4.464 Hz) and thus negligible in terms of intercarrier interference. At the receiver, a perfect channel estimation is assumed. In Rayleigh fading channels, DD provides additional propagation paths, which increases the available diversity gain. The Ricean K-factor is defined according to [2] for the static reception:

$$K = 10Log\frac{|h|^2}{\sum_{n=1}^{D}|h_n|^2} \qquad 6\text{-}1$$

where $|h|^2$ is the power of the constant LOS path at zero delay, and $|h_n|^2$ is the average path power of Rayleigh propagation path n, and D is the total number of echoes. For the analysis in Figure 6-2, the average path is chosen according to the JTC indoor channel model [70]. In pure LOS condition (e.g. AWGN channel), there are no time-variant multipath components. Thus, the diversity additional path transforms the AWGN channel into a static frequency selective one, which degrades the system performance. A power offset factor ΔP defining the power offset between the two transmitted signals was introduced. The total Effective Isotropic Radiated Power (EIRP) remains the same as the SISO case. In Figure 6-2, the curves relative to $\Delta P = 0$ corresponds to the standard MISO with CDD (e.g. with no signal shaping profile) and yields an SNR loss of 6 dB for the AWGN channel. If the offset ΔP is increased (e.g. the two signals are unbalanced), the diversity loss is reduced. The higher is ΔP the lower is the diversity loss. An offset $\Delta P = 6\ dB$ reduces to loss up to 1.8 dB, but it slightly degrades the gain in NLOS reception. The case $\Delta P \to \infty$ corresponds to the SISO configuration.

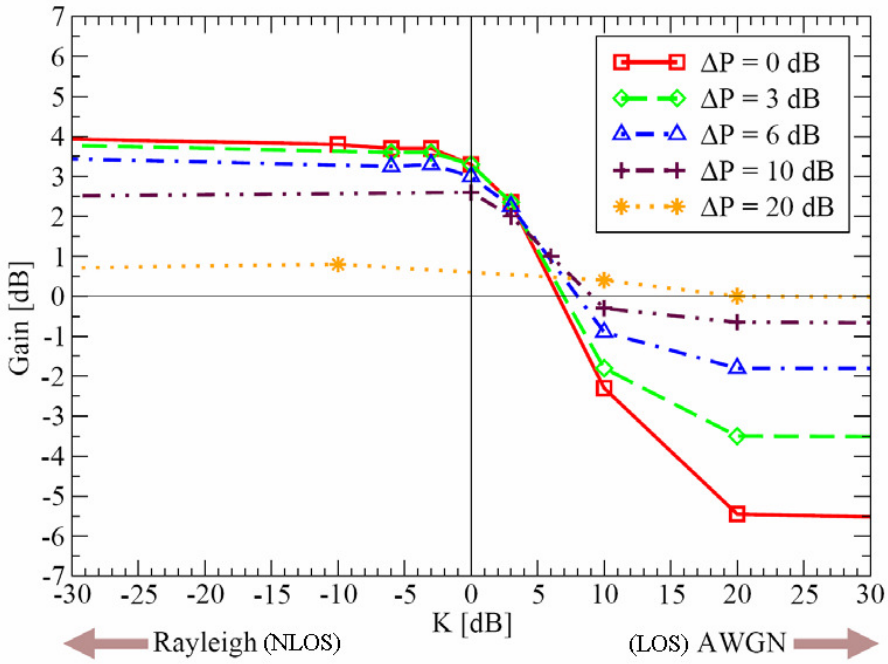

Figure 6-2: Gain at BER = 2×10^{-4} vs. Ricean K-factor [27]

Reference [27] proposes two signal profiling techniques namely, Amplitude Weighting (AW) and Spectrum Shaping (SS) profiling. Based on the Figure 6-2, 6 dB is considered a fairly good offset. In AW profiling, the power transmitted from each transmit antenna is deliberately unbalanced. Figure 6-2 shows that a $\Delta P = 6$ dB weighting factor between the two transmitted signals is expected to provide the best trade-off among LOS degradation reduction and NLOS gain. It can be seen from Figure 6-2 that a 6 dB weighting reduces the degradation (compared to SISO) at high K-factor from -5.5 dB to -1.8 dB while reducing the NLOS of about 0.5 dB. A modification to the AW profiling is the SS profiling, an amplitude profile that varies across the signal spectrum is applied. The intention is to achieve a power profile with 6 dB difference among subcarriers transmitted from each antenna. This technique produces characteristic "hills" and "valley" profiles along the signal spectrums. In this way, the interference can be minimized in high K-factor situations but the same average power can be maintained in each channel for optimal low K-factor performance. In real word test beds, the two signal profiling will be performed by the Diversity Unit described at Chapter 5, with a 16 tap filter. Figure 6-3 shows a schematic of the transmitted signal. Figure 6-3-a shows the SISO profile, assuming a 0 dB power. Figure 6-3-b shows the two MISO DD signal, flat and with a power of -3 dB to maintain the same total transmitted power of SISO (e.g. 0 dB). In

Figure 6-3-c the two diversity signals are 6 dB unbalanced, having the 80% and the 20% of SISO EIRP. In Figure 6-3-d the two diversity signals have a maximum of 6 dB difference in power level among carriers transmitted from each antenna.

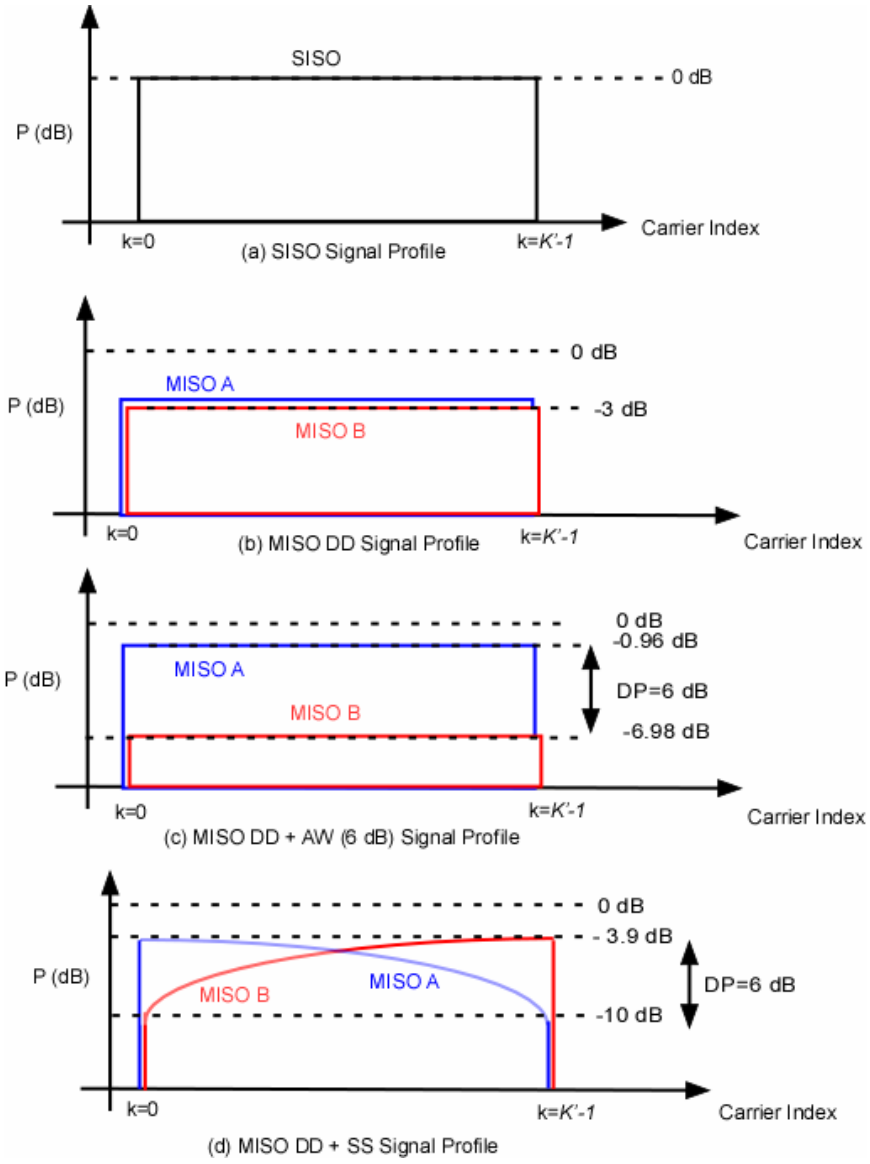

Figure 6-3: Signal Spectrum Profile comparison

It is worthwhile to mention that the gains presented in Figure 6-2 are estimated by comparing the Bit Error Rate at QEF condition for a particular indoor channel model with relatively small Doppler shift. However, results presented in this chapter are estimated by

using the $ESR_{5\%}$ as defined in formula 5-1 and the $\Delta^{R}_{ESR\%,}$ for driving as defined in formula 5-5. Results presented in Figure 6-2 will be used as general reference guidelines.

6.3 Methodology

This section describes the measurements methodology to justify the experimental network set up for stationary measurements. The delay between transmitted signals would be introduced by a device designed specifically for transmit diversity. The main idea is to estimate the $ESR_{\%}$ criterion for SISO and MISO received signals and to compare the $ESR_{5\%}$ thresholds defined in Chapter 4 and 5. Generally an integration time of 2 minutes per each $ESR_{\%}$ estimation was found to be adequate for most scenarios and rendered a stable and accurate measure. The Monitor Station (MS) was incorporated with a programmable step attenuator, enabling the operator to define the *measurement sweep* parameter. To determine the $ESR_{\%}$, the signal power was gradually reduced by increasing the attenuation of the receiver input attenuator value until the $ESR_{5\%}$ threshold was exceeded. The step attenuator range is from 0 dB to 30 dB. A *measurement point* was defined as the $ESR_{\%}$ for a given input attenuation and an integration time of 2 minutes. A *measurement sweep* was defined as a collection of *measurement points* relative to an ascending ordered input attenuations, with a defined initial, step size, and final attenuation. The receiver was located in a fixed position (e.g. stationary reception condition). Although a stationary channel is obviously typical for the rooftop reception, it is also believed that a stationary channel is a likely scenario for indoor digital TV. The channel can be time variant since the scatterers around the receiver are non-stationary. The time variability of the channel can depend on people, cars moving and foliage moved by the wind in the case of areas with trees in between the transmitter and the receiver. The vegetation impact is more effective during summer, when trees have full foliage [111].

Two experimental network set-ups were tested, namely the *operator based* and the *remote controlled* test. The first approach consists of receiver performing measurements in different test sites with an operator at the receiver side to perform manually the tests. This methodology provides flexibility in terms of the deployment of receiver equipment, and it is suitable for performing a number of tests in several locations with decorrelated test

conditions and thus provides more representative results [112]. A remote controlled network was also deployed to collect a larger amount of data compared to the operator based set-up, but from a smaller number of test sites.

6.4 Experimental Network Set-Up

This section describes the operator based and the remote controlled set-up. The operator based set-up is simply composed of a receiver antenna and a Monitor Station (MS) connected to a laptop. For rooftop type experiments, the omnidirectional antenna was replaced with an 11 dBi directional antenna [113]. According the type of test, the antenna can be mounted on a tripod, placed on a trolley or on a table/cabinet. Figure 6-4 shows the design of the remote controlled set-up. The scheme is an extension to the operator based set-up, and is designed to automatically conduct the tests over a long period of time using several receivers at the same time. The receivers were deployed within the Brunel University Network, e.g. within the range of radio coverage in the sites characterized previously in Chapter 5 by the short-term trials. Each MS embedded two DVB receivers and two receiving antennas can be connected per each MS. Each Monitor Station had a serial number and MAC address and was located in a specific environment which is identified with Ethernet Port number and is assigned a fixed IP address. Because the IP network is private, there is no need to spare the address range. Therefore Class C addresses have been used to define every IP sub-net. The receivers are connected to the IP network to send the measurement reports periodically to the Control, Monitor and Process Applications (CMPA), which is a set of Matlab based routines, designed to manage one or more Monitor Station(s).

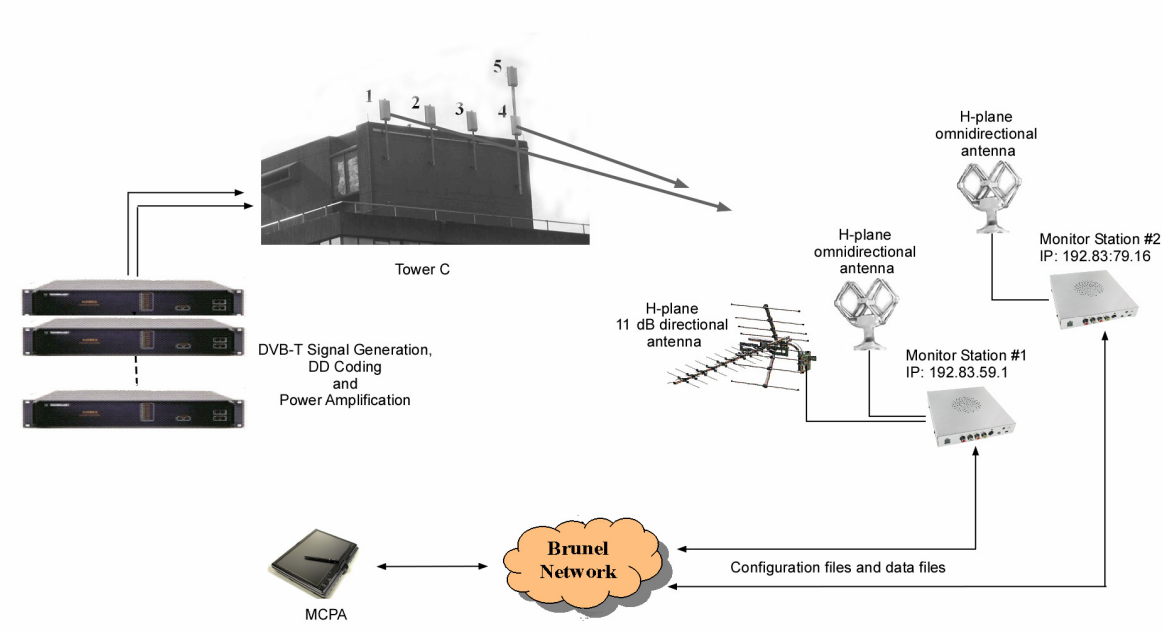

Figure 6-4: The layout of the remote controlled network

The CMPA also performs some post-processing tasks. Per each experiment, three main stages are defined:

1) The operator initiates the experiments through this system by sending a measurement configuration file via File Transfer Protocol (FTP) to each registered Monitor Station. The configuration file defines all measurements parameters, including *measurement sweep* parameters. Once the MS station receives the configuration file, it starts to perform a measurement *sweep*.
2) The CMPA constantly monitors the progress of the measurement sweep per each MS. Each *measurement point* performed by the MS is temporally stored in a single file in the MS memory. Once the number of *measured points* reaches a defined number, a summary file is produced and all the *measurement point* files are downloaded by the CMPA into a PC storage memory.
3) Data are then stored and classified for post-processing by associating a text file reporting with the serial number of the MS and the creation time. This feature is used to separate data taken during office hours. If an error occurred, the CMPA sends another configuration file to the MS to start

another *measurement sweep*.

The number of repetitions is defined in advance by the operator and it depends on the kind of experiment performed. The CMPA enables the operator to remotely follow up the measurement progress and perform post-processing functions while data are collected and optionally update the *measurement sweep* parameters to centre the *measurement sweep* around the $ESR_{5\%}$ and thus minimize the number of measurements points. The experiment can be performed with no interruption for several days, allowing collection of statistically reliable data. Measurement sweeps with multiples $ESR_{\%}$ can be removed from the data. Optionally, data taken when people were moving around the receiver can also be removed from the whole set of data by excluding measurements taken during office hours.

6.5 Test Site Description

This section describes the four sites where measurements were performed. Three sites were chosen within the Brunel's University Campus to be connected to the remote controlled network. The Horseden Hill site is 10.2 km distance from the transmitter and an operator based approach was employed.

6.5.1 Test sites within Brunel's Campus (short range)

Table 6-1 shows the main characteristic of the sites chosen for the remote controlled tests, while Figure 6-5 shows on a geographical map the position of the transmitter and the receivers. All the receivers within the Brunel campus are within a range of 1 Km. The green zone shows the areas between transmitter and receiver with a significant concentration of trees. The green and red markers indicate LOS and NLOS reception points, respectively. The pro-active office is located within the A Zone, while the sport Pavilion office and rooftop receivers are located within the zone B described in Chapter 5.

Table 6-1: Test sites within Brunel's Campus classification

	Coordinates [Decimal Degrees (DD)]	Distance from Tx. [m]	Recep-tion	Ant. Type	Coax. Cable att. [0.25 dB/m]	Exter-nal att. (dB)	Room Dim. [m]
Pro-Active office in Sports Centre	51°31'56.41''N; 0°28'12.69'' W	298	Office Indoor NLOS	Omni H plane	0.125 [for 0.5 m]	0	10×10
Sports Pavilion Office	51°31'44.66''N; 0°28'48.61'' W	698	Office Indoor NLOS	Omni H plane	0.125 [for 0.5 m]	0	1.8×3.5
Sports Pavilion Rooftop	51°31'44.66''N; 0°28'48.61'' W	698	Rooftop LOS	10 dB Directional H plane	2.25 [for 9 m]	20	N.A.

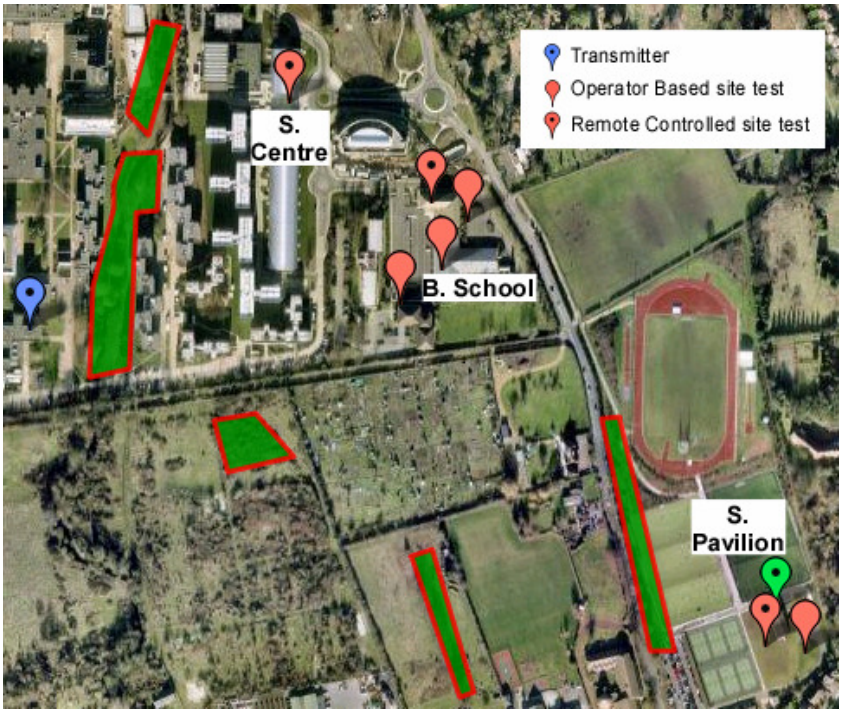

Figure 6-5: Locations of transmitter and identified environments

(b)

(c)

Figure 6-6 shows the reception sites relative to remote controlled set-up, namely (a) the Sport Centre Office, (b) the Sport Pavilion Rooftop antenna and (c) the Sport pavilion indoor office. The circle indicates the position of the receiving antenna The test sites are briefly detailed below.

Pro-Active Office in Sports Centre: The room is approximately 10×10 m. The antenna was placed on a cabinet at 1.90 meters from the ground, beside the wall. There are large windows on the south side.

Sport Pavilion Office: The room is approximately 1.80×3.5 m. The antenna was placed on a cabinet at 1.50 centimeters from the ground, beside the wall. There is a small window on the west side. The circle indicates the position of the receiving antenna.

Sport Pavilion Rooftop: The antenna was placed on the building rooftop at 5 meters from the ground, pointing towards the transmitter site (west direction).

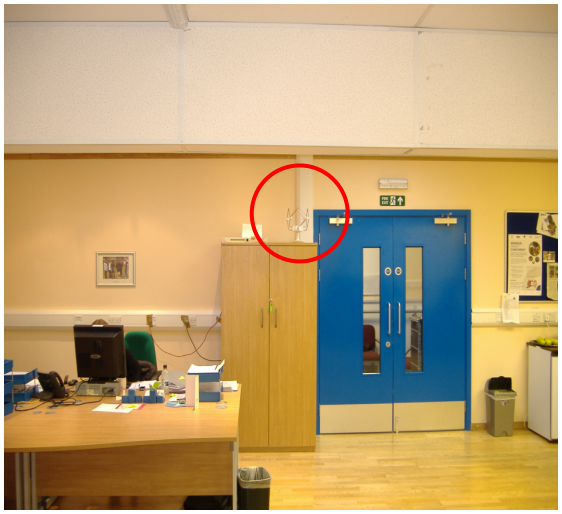

(a)

(b)

(c)

Figure 6-6: Sport Centre office indoor reception (a), Sport pavilion Rooftop antenna (b) and Sport pavilion indoor office reception (c)

6.5.3 Horseden Hill site (long range)

A test site for these measurements was selected on a hill some distance away from the transmitter. The hill was at a height that would provide similar performance to a rooftop mounted antenna. The distance was over 10 km from the transmitter, compared to the maximum range for driving measurements of between 1 and 2 km relative to Chapter 5. The reception equipment also included a Global Position System (GPS) receiver. The antenna is connected to the receiver with a 2 meter long coaxial cable, adding an attenuation of 0.5 dB. The receiver includes a programmable step attenuator. As detailed in Chapter 5, the attenuator is needed to gradually increase the number of errored seconds without reducing the EIRP at the transmitter. A link budget calculation derived by radio planning tools [114] is used it to check whether Horseden Hill could receive enough power for LOS reception or not. The propagation tools model implements the Longley-Ricean model (ITM) [115] [116] in point to point mode. Prediction takes into account the geomap data height elevation available in the net [117]. These tools will determine consistently if a radio link is line of sight or not. In case of LOS, a 2-ray calculation model will be used to estimate the reception, while in case of an obstructed path, the ITM model is applied. To determine a line of sight the clearance of the Fresnel zone is determined. Statistical and environmental parameters are used with the terrain profile in calculating path loss. A stationary unit mode was selected. The software's Mode of Variability also

defines three parameters: percentage of time, percentage of locations and percentage of situations. Time variability accounts for variations of hourly median values of attenuation due to, for example, slow changes in atmospheric refraction or in the intensity of atmospheric turbulence. Time variability describes the effects of these changes over time. The time variability for the calculation is expressed as a percentage from 0.1% to 99.9%. This value gives the fraction of time during which actual received field strength is expected to be equal to or higher than the hourly median field computed by the program. Location variability accounts for variations in long-term statistics that occur from path to path due to, for example, differences in the terrain profiles or environmental differences between the paths. The location variability for the calculation is expressed as a percentage from 0.1% to 99.9%. This value gives the fraction of locations where actual received field strength is expected to be equal to or higher than the median field computed by the program. Finally the situation variability provides a confidence margin including all other unknown parameters not taken into account of the prediction software. From these values, the simulation tool calculates a value called Statistics Loss in dB. For 99% of time, 70% of locations and 70% of situations the value of Statistics Loss is 9.5 dB. Forest and urban areas do not produce significant losses. Horizontal polarization was employed in this analysis. The variation in height between transmitter and receiver (e.g. the Terrain Elevation variation) was 33.4 m. The LOS should be defined as percentage of 1st Fresnel zone obscured. As rule of thumb, if path clearance is less than 0.5 of Fresnel zone then diffraction occurs and the radio wave propagation behave as if it is not in “free space”. For instance, WiMAX define LOS as 0.6 of Fresnel zone has to be clear [118]. From geomap data, the radio planning tool estimated that the propagation mode line was line of sight with minimum clearance of 0.1 Fresnel Zone at 1.9 Km from the transmitter. Thus, it expected an additional attenuation to the free space path loss. The main characteristics of the reception site are summarized in Table 6-2.

Table 6-2: Details of Horseden reception

Transmitter Data	Receiver Data
Brunel University	Horseden Hill
Location: 51º31’54”N 0º28’45”W	Location: 51º32’52.8”N 0º19’40.7”W (GPS position)

EIRP=50 dBm	Directional antenna
Directional antenna (12 dBi)	Antenna Gain = 11 dBi
Coaxial Cable attenuation =0.5 dB	
Carrier Frequency = 730 MHz	
Distance = 10.2 Km	
Terrain Elevation variation = 33.4m (variation in height between transmitter and receiver)	
Propagation mode line of sight, with minimum clearance of 0.1 of the First Fresnel Zone at 1.9 Km	

Figure 6-7 shows the Horseden Hill test site on a geographical map, while Figure 6-8 shows the altitude map using geomap data taken from internet. Figure 6-9 shows the receiver antenna and the test site at the top of hill.

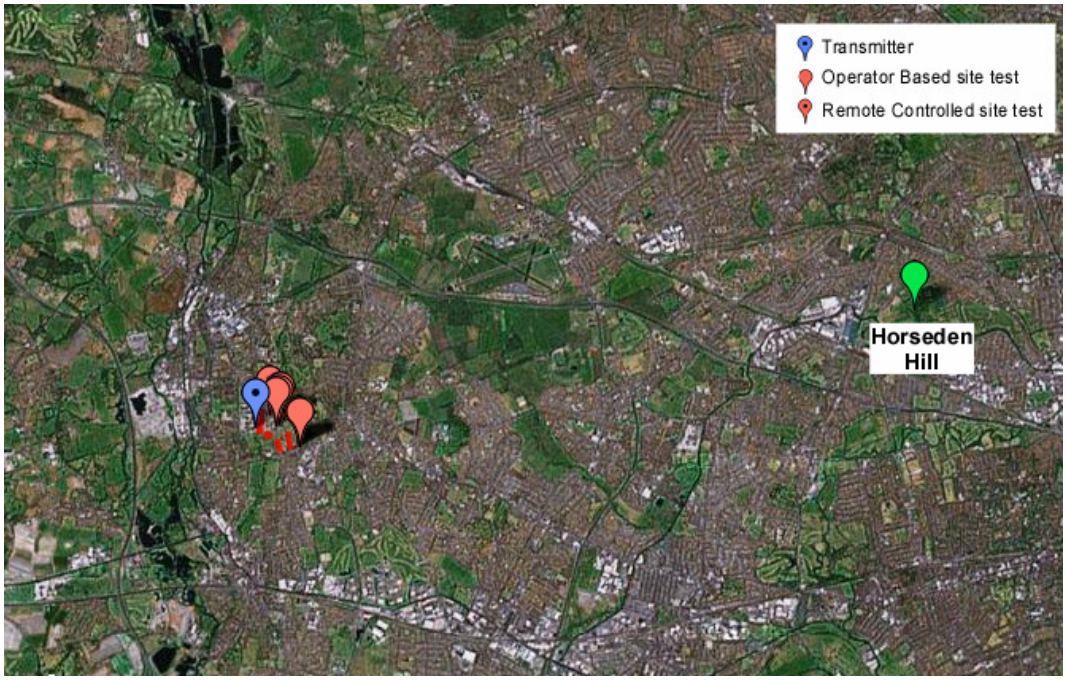

Figure 6-7: Horseden Hill Test Site

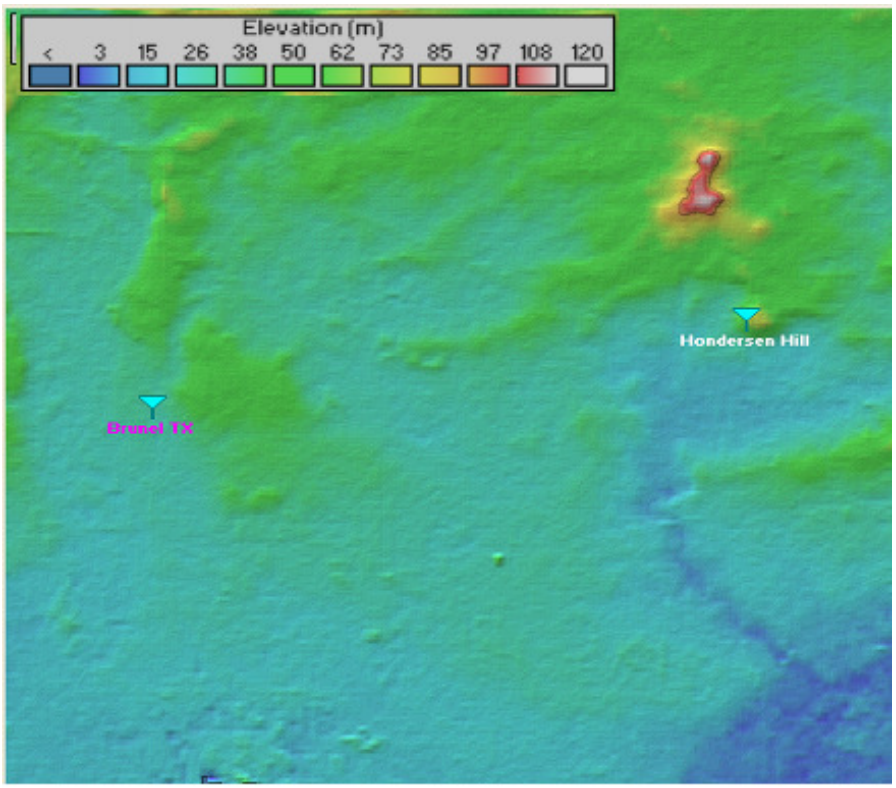

Figure 6-8: Horseden Hill altitude map

Figure 6-9: Horseden LOS antenna Reception

The Effective Isotropically Radiated Power (EIRP) describes performance of a transmitting system:

$$EIRP(dBm) = P_T + G_T - L_L^T \quad 6\text{-}2$$

where P_T is the transmit power, G_T is the transmit antenna gain, and L_L^T is the transmitter cable loss. From Chapter 5, $EIRP = 50\,dBm$, $L_L = 7\,dB$, $G_T = 12\ dBi$ yielding $P_T = 45\ dBm$. The system gain G_S [119], is defined as total gain of the radio system without considering antennas/cables, e.g.:

$$G_S(dB) = P_T - Th_R, \quad 6\text{-}3$$

where Th_R is the receiver threshold relative to the MS. Th_R values are estimated as Quasi Error Free (QEF) condition on a Gaussian channel. Th_R are -93.4 dBm and -88.4 dBm for a transmission with a code rate equal to ¾ and a modulation of QPSK and 16 QAM, respectively. The thresholds are estimated experimentally in Appendix II and they are confirmed by MBRAI specifications presented in [63]. The total propagation loss L_T is defined as:

$$L_T(dB) = L_{FS} + L_O + L_U + L_F + L_S \quad 6\text{-}4$$

where L_{FS} is the free space loss, L_O is the attenuation factor due to the physical obstruction of the hill, L_U is the attenuation factor due the urban building impact, L_F is the loss due to the trees attenuation, and L_S is the static loss.

The Fade Margin M_F defines the extra signal power added to a link to ensure it continues working if it suffers from signal propagation effects:

$$M_F(dB) = G_S + (G_T + G_R) - L_T - (L_L^T + L_L^R) \quad 6\text{-}5$$

where G_R and L_L^R are the receiver antenna gain and cable loss, respectively. Finally, the received power level is:

$$P_{RX} = P_T + (G_T + G_R) - L_T - (L_L^T + L_L^R) \quad 6\text{-}6$$

The link budget prediction is shown in Table 6-3. The link budget prediction shows that it can be expected a fade margin of 17.1 dB for QPSK and of 12.1 dB for 16 QAM. The estimated received power is –75.8 dBm. It can be concluded that the receiver at Horseden hill should have enough fade margin to estimate the $ESR_{5\%}$ threshold.

Table 6-3: Link Budget Prediction for Brunel Rooftop Measurements

Propagation Model	
Longley-Rice	
Link Loss	
L_{FS}	109.8 dB
L_O	17.0 dB
L_U	0 dB
L_F	0 dB
L_S	9.5 dB
L_T	136.3 dB
$EIRP$	50 dBm
P_T	45 dBm
G_R	11 dBi
L_L^T	7 dB
L_L^R	0.5 dB
System Gain QPSK, 3/4	
Th_R	-93.4 dBm
G_S	138.4 dB
System Gain 16QAM, 3/4	
Th_R	-88.4 dBm
G_S	133.4 dB
Receive Margin	
M_F for QPSK, 3/4	17.6 dB

M_F for 16 QAM, 3/4	12.6 dB
Estimated Received Power for both modulations	
-75.8 dBm	

6.6 Measurement Results

This section details data analysis of the measurement results. It first shows the estimation of the channel parameters. Then, the $ESR_{5\%}$ estimation of the Horseden Hill, Rooftop and Office reception sites are presented and the diversity gain was calculated by comparing the fade margin. The fade margin is calculated using the $ESR_{5\%}$ threshold compared with the external attenuation values, since the CNR and RSSI values are estimated by the receiver and they might not have the same reliability in terms of accuracy and linearity. Finally, the impact of spectrum profile for the driving tests is presented.

6.6.1 Channel Model

Table 6-4 shows the parameters of interest of the propagation channels, where RMS Delay Spread, excess delay, number of taps, number of impulses responses (IR) defined in Chapter 5 are reported. The IR was normalized with the peak power. Consistently with Chapter 5, the first tap reaching the 0 dB thresholds was chosen as a reference starting point and the last tap with power exceeding the -30 dB threshold was chosen as the last value. The taps within the two thresholds are considered for the channel modelling. To increase the accuracy, IR data are taken from *measurements with* smallest attenuation and with $ESR_{\%}$ <5%. A cross correlation based algorithm aligns all the IRs for the PDP estimation. Table 6-4 shows the estimated channel parameters. A RMS Delay Spread from 0.2 μs to 0.46 μs characterizes the Sport Pavilion and Sport Centre offices SISO reception. These values are significantly larger than the RMS DS expected for an Indoor channel, e.g. 0.1 μs as shown in Table 4-2. Although this discrepancy can be attributed to different indoor scenarios, the different power threshold used for the RMS DS calculation can also affect the results (e.g. -30 dB and -21.7 dB for the Sport Pavilion and the JTC Indoor channel, respectively). A RMS Delay Spread of about 0.1 μs characterizes the

Rooftop Sport Pavilion and Horseden SISO LOS reception. These small RMS DS values are expected since the LOS channel with a directive antenna obviously does not have a rich multipath content.

Table 6-4: Channels parameters

	RMS DS (us)	Excess Delay (us)	Number of taps	Number of IRs used in the estimation
SISO A Sport Pavilion Office	0.26	2.9	29	1200
SISO B Sport Pavilion Office	0.3	2.7	25	840
MISO Sport Pavilion Office	0.63	2.7	36	1200
SISO A Sport Centre Office	0.25	1.5	23	1100
SISO B Sport Centre Office	0.46	1.5	23	5040
MISO DD Sport Centre Office	0.63	2.8	34	8040
SISO A Horseden Hill	0.14	1.7	25	480
SISO B Horseden Hill	0.13	1.9	27	837
MISO Horseden Hill	0.6	2.9	41	720
SISO A Sport Pavilion Rooftop	0.1	0.8	10	600
SISO B Sport Pavilion Rooftop	0.1	0.6	13	600
MISO Sport Pavilion Rooftop	0.57	2.07	29	600

Figure 6-10 and Figure 6-12 shows sample Averaged IRs with several transmit configurations for the Horseden Hill and for the Sport Centre office tests.

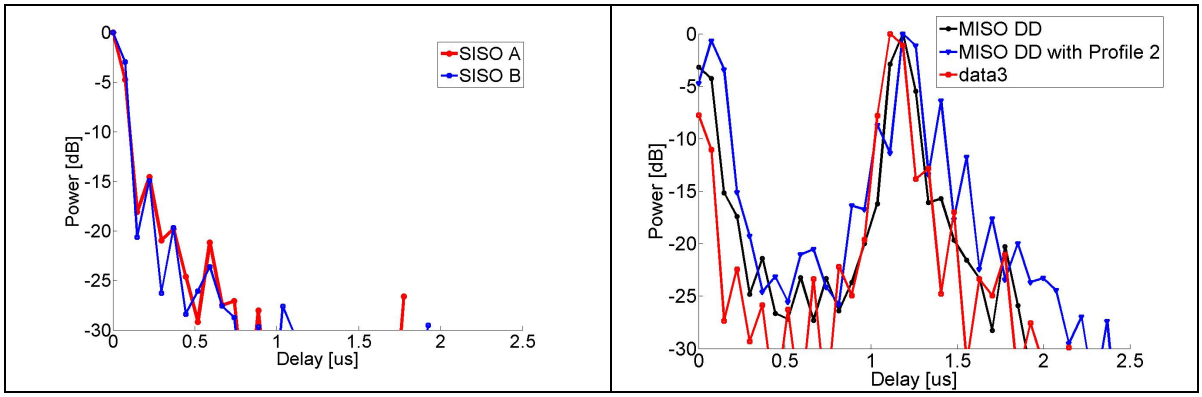

Figure 6-10: Averaged IR of the Horseden Hill for SISO A and SISO B (a), MISO DD+ SS, MISO DD+ AW 6dB, and MISO DD (b)

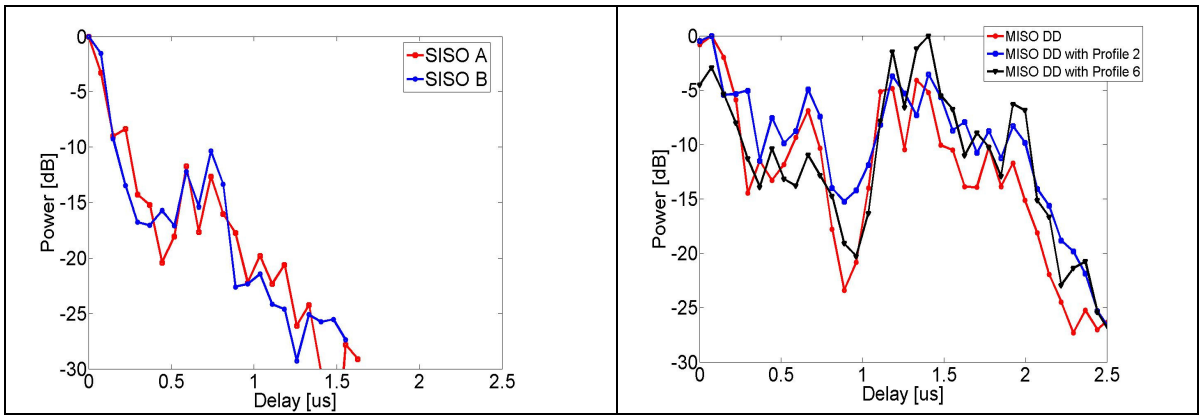

Figure 6-11: Averaged IR of the Sport Centre office for SISO A (a), SISO B, MISO DD with Profile SS, MISO DD with Profile AW 6dB, and MISO DD (b)

6.6.2 Rooftop LOS Horseden Hill Measurements

The median measured receiver power with 0 dB attenuation among all the tests was about -75.1 dBm, while the prediction from Table 6-3 was -75.8 dBm. The estimated receiver fade margin $\tilde{M}_F$ corresponds to the excess attenuation needed to degrade the SISO performances up to the $ESR_{5\%}$ visibility threshold, namely $Att_{5\%}$. Figure 6-12 shows the $ESR_{\%}$ scan vs. input attenuation for LOS reception for SISO and different MISO spectrum profiles for 16 QAM constellation. To exceed the visibility threshold, it was required an excess attenuation of about 12.5 dB for 16 QAM and 20.5 dB for QPSK. These results are compared with the 12.6 dB and 17.6 dB provided by the planning tool in the previous section for 16 QAM and QPSK, respectively. Figure 6-12 shows also that a degradation of the fade margin at $ESR_{5\%}$ is about 5.5 dB can be expected when normal transmit DD is applied. This degradation can be effectively reduced up to 1.5 dB by applying the spectrum shaping mitigation techniques. In any case, there is still a high fade margin and the application of diversity has not affected the reception. Figure 6-13 confirms the results for QPSK constellation. Results were produced with the operator based set-up.

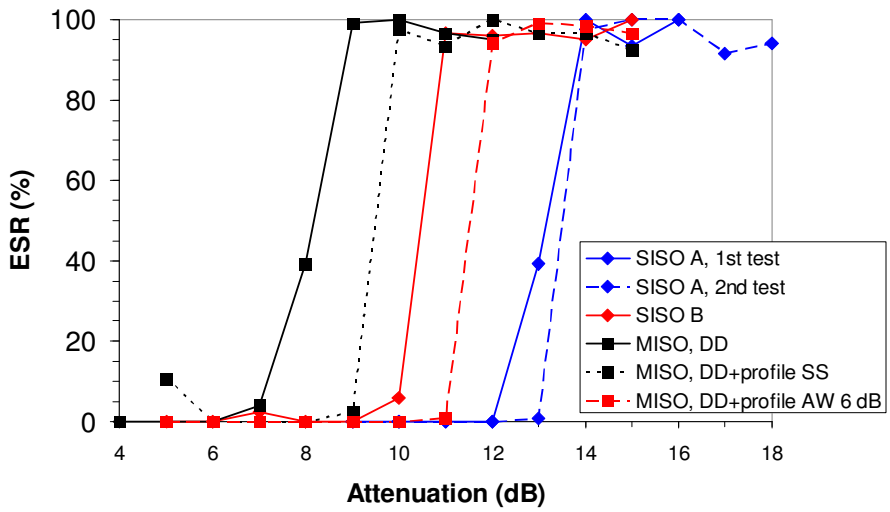

Figure 6-12: $ESR_{\%}$ vs. input attenuation for LOS Reception, for 16 QAM modulation (25th July)

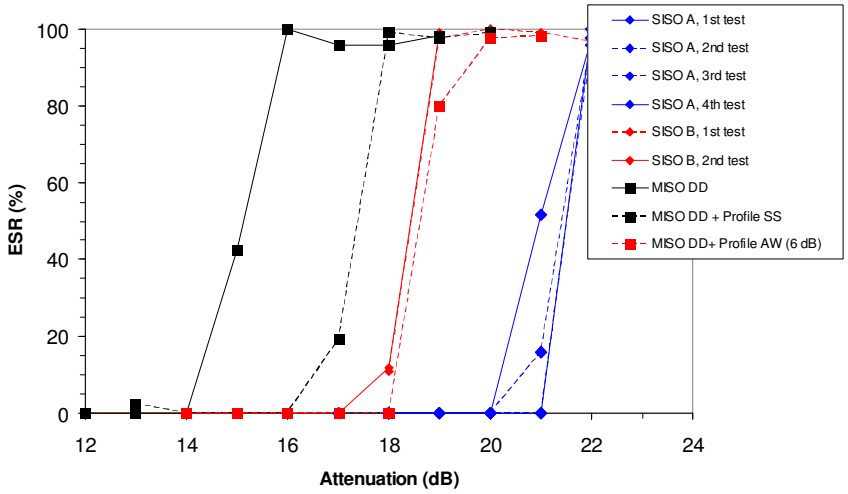

Figure 6-13: $ESR_{\%}$ vs. Input Attenuation for LOS Reception, for QPSK modulation (16th, 18th, and 21st July)

Results from the measurements performed on different days are shown in Table 6-5. Table 6-6 shows the estimated average $\tilde{M}_F$ at $ESR_{5\%}$ (e.g. $Att_{5\%}$) and the degradation relative to the best performing SISO transmitter. These measurements show that we can expect degradation in fade margin of some 5.5 dB and 6.5 dB at a relatively medium range when normal transmit diversity is applied. These results match well with the 6 dB predicted in

Figure 6-2 for channels with very high Ricean K-factor. In both modulation cases, the spectrum shaping with Profile AW reduced the LOS degradation of about 4 dB.

Table 6-5: Rooftop type measurements taken at Horsenden Hill

Broadcast Mode	Description	Date	$Att_{5\%}$ (dB)
QPSK ¾	SISO A	16th July 2008	≈ 21
	SISO A	18th July 2008	≈ 20
	SISO A	21st July 2008	≈ 20
	SISO A		≈ 21
	SISO B		≈ 17
	SISO B		≈ 17
	MISO, DD		≈ 14
	MISO, DD with Profile SS		≈ 16
	MISO, DD with Profile AW (6 dB)		≈ 18
16 QAM 3/4	SISO A	25th July 2008	≈ 13
	SISO A		≈ 12
	SISO B		≈ 10
	MISO, DD		≈ 7
	MISO, DD with Profile SS		≈ 9
	MISO, DD with Profile AW (6 dB)		≈ 11

Table 6-6: LOS degradation at Horsenden Hill for 16 QAM (a) and QPSK (b) cases

Description	16QAM, 3/4	
	Median $Att_{5\%}$ (dB)	Gain Relative to SISO A (dB)
SISO A	12.5	-
SISO B	10	-
MISO, DD	7	-5.5
MISO, DD with Profile SS	9	-3.5
MISO, DD with Profile AW (6 dB)	11	-1.5

(a)

Description	QPSK, 3/4	
	Median $Att_{5\%}$ (dB)	Gain Relative to SISO A (dB)
SISO A	20.5	-
SISO B	17	-
MISO, DD	14	-6.5
MISO, DD with Profile SS	16	-4.5
MISO, DD with Profile AW (6 dB)	18	-2.5

(b)

6.6.3 Sports Pavilion LOS Rooftop

The sports pavilion is closer to the transmitter than the Horseden Hill site and additional attenuation of 20 dB was connected to the antenna cable. Since this is a fixed location with network connectivity, we were able to conduct several sweeps over a longer period. Table 6-7 summarizes the impact on LOS performances on different transmission situations for the 16 QAM modulation. Per each transmission set-up, the number of points collected, the sample median, the sample variance, the minimum and the maximum $Att_{5\%}$ are presented. All set of data were taken from the Sport Pavilion Rooftop antenna, across different dates. Data includes both during and out of office hours, because the effect of moving people is assumed to be negligible for rooftop reception. This is confirmed by the

small variance (e.g. less than 2 dB) of $Att_{5\%}$. Although $Att_{5\%}$ for SISO A is 2.5 dB higher than $Att_{5\%}$ for SISO B at Horseden Hill test site as shown in Table 6-5, Sport Pavilion receiver shows that the $Att_{5\%}$ for SISO A is 1.8 dB lower than $Att_{5\%}$ for SISO B. These results suggest that the difference of fade margin between SISO A and B depends on the propagation channel relative to the two antennas and/or to the relative position of the receiver. Moreover, this unbalance can be due to the two transmitting antennas pointing in two slightly different directions. If the median $Att_{5\%}$ values are selected, MISO with DD produces a loss of about 3.8 dB if compared to SISO B. The loss is reduced from 2.8 dB to 1.8 dB if adopting MISO with Profile AW and SS, respectively. SISO A and SISO B have the highest variances compared to the MISO set of curves. These results suggest a low sensitivity of the MISO signals to the time channel variability. This effect was also observed in NLOS measurements.

		$Att_{5\%}$ (dB)			
Description	No. Samples	Median	Sample Variance	Minimum	Maximum
LOS, SISO A	145	34	0.54	30.1	35.07
LOS SISO B	209	35.8	1.58	31.29	37.05
LOS, MISO DD	169	32	0.19	30.5	32.84
LOS, MISO DD with Profile SS	47	34	0.02	33.4	34.02
LOS, MISO DD with Profile AW (6dB)	37	33	0.168	32	34

Table 6-7: Sport Pavilion LOS, 16 QAM ¾. Note: $Att_{5\%}$ includes the additional 20 dB attenuation

These results show that although there can be an instantaneous degradation in performance reception has not been adversely affected since there is a large fade margin in hand. In one case, MISO with amplitude imbalance of 6 dB outperforms the worst case SISO performance. Figure 6-14 and Figure 6-15 show an example of multiple $ESR_{\%}$ measurements relative to MISO DD and SISO A transmitter set-up, respectively. SISO and MISO Data are collected during different days to decorrelate the reception conditions.

The small variance suggests that the channel time variability does not affect significantly the fade margin of this set-up.

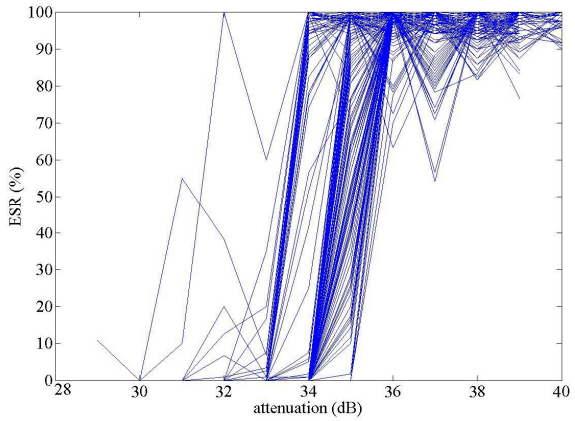

Figure 6-14: Sport Pavilion LOS $ESR_{\%}$ vs. Attenuation for SISO with 16 QAM. Note: $Att_{5\%}$ includes the additional 20 dB attenuation

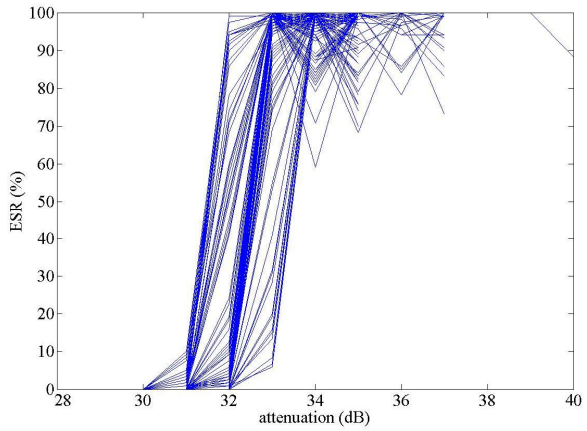

Figure 6-15: Sport Pavilion LOS $ESR_{\%}$ vs. Attenuation for MISO with 16 QAM. Note: $Att_{5\%}$ includes the additional 20 dB attenuation

6.6.4 Indoor Measurements

In indoor reception, it was observed that results produced with operator based set-up were not satisfactory. In almost all practical cases, the $ESR_{\%}$ curves passed the 5% threshold more than once making it difficult to locate the $ESR_{5\%}$ threshold and state clearly a diversity gain. Moreover, in many cases it was not possible to find the 0% condition even

with no receiver attenuation. Figure 6-16 shows a sample test at the Sports Centre office where the $ESR_{5\%}$ threshold was not clearly located and the 0% condition was not reached.

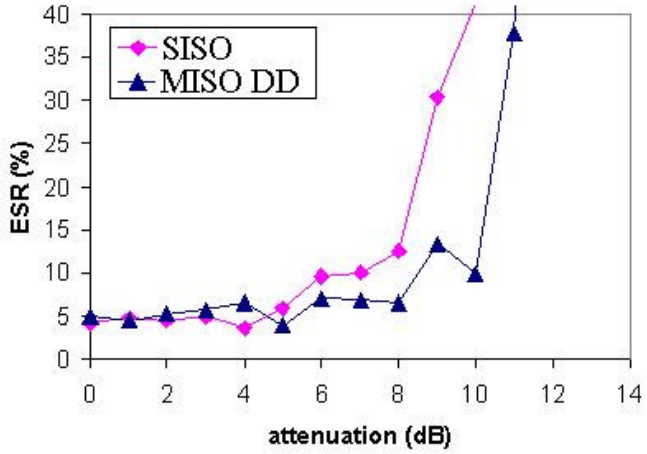

Figure 6-16: $ESR_{\%}$ vs. Attenuation at Sport Centre

This effect is probably due to presence of moving people around the receiver antenna (including the operator), momentary interference (e.g. electronic devices, neon lights, etc.), or trees. These issues made the use of $ESR_{5\%}$ criterion not practical. Increasing the integration time per each measurement point from 2 up to 5 minutes did not improve the reliability of results. Moreover, the channel's time variability made it difficult to obtain repeatability of the results over different days. Measurements were tested in other 6 test sites with no improvement of results reliability. More stable results were produced by performing multiple measurements adopting the remote controlled set up. Measurements were performed in two rooms located in two different buildings to investigate the indoor fixed reception. The diversity gain was estimated by comparing SISO and MISO tests performed during random days in different months to ensure uncorrelated fading conditions for the measurements. Data collected during office hours were purposely included in the whole data set to increase the channel variability and thus decorrelate the channel conditions while measurement sweeps with multiples $ESR_{\%}$ are removed. Table 6-8 shows the result of SISO and MISO comparison in the Sport Pavilion Office. This time, the QPSK modulation was chosen to have enough signal margin. The estimated gain is very close to 5 dB. The SISO variance is about 5.1 dB while the MISO variance reduces to 4.69 dB.

Table 6-8: NLOS Sport Pavilion, QPSK

		$Att_{5\%}$ (dB)			
Description	No. Samples	Median	Sample Variance	Minimum	Maximum
NLOS, SISO A	29	6.2	5.1	2.8	13.03
NLOS, MISO	65	11.15	4.69	4.4	15.13

Table 6-9-a shows the result of SISO and MISO comparison in the Sport Centre Office. All the MISO cases are presented. From Table 6-9 the MISO estimated gain is about 2.2 dB and 1.2 dB compared to SISO B and A, respectively. The spectrum profiling keeps the same diversity gain or in the case MISO with Profile SS, it reduces the gain of about 1 dB. The gain in this situation is much smaller than the gain measured in Table 6-8 and expected from simulations and laboratory measurements. However, Figure 6-17-a shows that the majority of SISO $Att_{5\%}$ falls outside the step attenuation range (e.g. 50 $Att_{5\%}$ values out of 70 $ESR_{\%}$ curves estimation) while Figure 6-17-b shows that the majority of MISO $Att_{5\%}$ falls within the attenuation range (e.g. 50 $Att_{5\%}$ values out of 70 $ESR_{\%}$ curves estimation). Only the $Att_{5\%}$ values falling within the attenuation range are considered for the gain estimation. Thus, the measured gain is a conservative value because it does consider the SISO $Att_{5\%}$ values occurring at a lower attenuation range that would increase the diversity gain. Subsequently, a QPSK configuration was tested in order to have all SISO $Att_{5\%}$ values falling within the attenuation range. Figure 6-17-c and Figure 6-17-d show that the majority of SISO and MISO $Att_{5\%}$ falls within the attenuation range (e.g. 61 and 157 $Att_{5\%}$ values out of 63 and 159 $ESR_{\%}$ curves estimation, respectively). The MISO variance of $Att_{5\%}$ is greatly reduced (from 5.6 dB for SISO up to 2.5 dB for MISO) and resulting in much more stable reception condition with a more predictable threshold level. Table 6-9-b summarized the QPSK results for SISO and MISO comparison. The observed 5 dB of diversity gain are very close to the gain estimated in the Sport Pavilion. While MISO DD with Profile AW maintains the same gain of MISO DD, MISO DD with Profile SS reduces it of about 1 dB.

Table 6-9: Sport Centre 16 QAM (a) and QPSK (b)

		$Att_{5\%}$ (dB)			
Description	No. Samples	Median	Sample Variance	Minimum	Maximum
NLOS, SISO B	69	1.34	1.09	0.033	5
NLOS, SISO A	20	2.05	1.6	0.29	4.12
NLOS, MISO	61	3.1	2.5	0.23	6.03
NLOS, MISO DD + Profile SS	32	2.23	1.6	0.16	5.06
NLOS, MISO DD + Profile AW	22	3.2	1.09	0.16	4.04

(a)

		$Att_{5\%}$ (dB)			
Description	No. Samples	Median	Sample Variance	Minimum	Maximum
NLOS, SISO A	59	6.3	5.6	0.23	10.599
NLOS, MISO DD	158	11.04	2.5	3.06	13.199

(b)

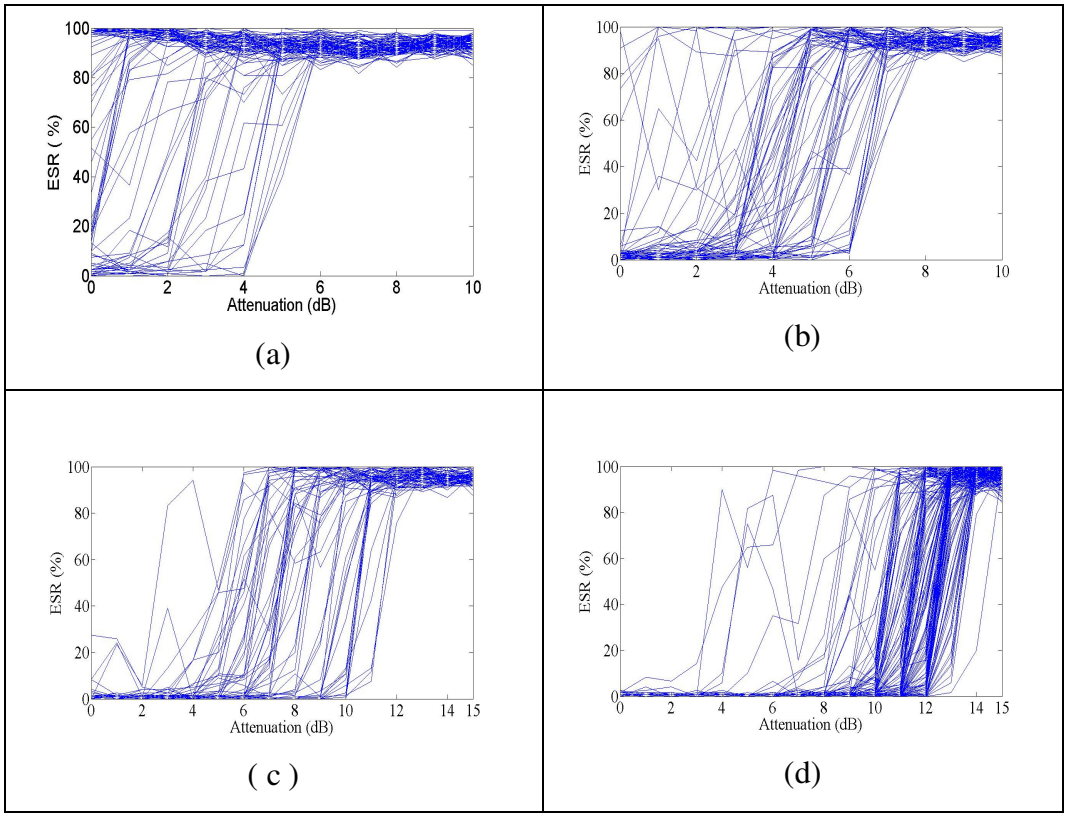

Figure 6-17: Sport Centre ESR% vs. Input attenuation for SISO 16 QAM (a), MISO 16 QAM (b) , SISO QPSK (c) , and MISO QPSK (d).

The 5.0 dB diversity gain presented in this section agrees with laboratory results of Chapter 4 presented in Fig. 10-4 where a gain of about 5.5 dB was measured for indoor office with a RMS delays spread of $0.1\mu s$, a cross correlation of about 0.25, a code delay $\delta \approx 1.1\mu s$, and a Doppler shift of 1 Hz.

6.6.5 Mobile measurements with amplitude weighting and amplitude profiling

In these tests, the $ESR_{\%}$ has been measured along the test track detailed in Chapter 5 and its effects on MISO gain measured as a function of Amplitude Weighting and Spectrum Shaping profiling. The test was repeated on two consecutive days. MISO DD is used as a reference to measure the effectiveness of Amplitude Weighting and Spectrum Shaping profiling. The modulation is QPSK. Results are summarized in Table 6-10. The results are obtained for horizontal antenna separation (e.g. 20λ H, corresponding to antenna 1 and 4) and vertical plus horizontal separation (e.g. 20λ H + 5λ V, corresponding to antenna 1 and 5. Table 6-11 shows the tests that were repeated on consecutive days to examine consistency of results.

Table 6-10: Performances vs. Antenna separation and spectrum profiling techniques, taken on 19tn June 2008

Configuration	Antenna Spacing	SISO $ESR_{\%}$	MISO $ESR_{\%}$	$\Delta_{ESR\%}$	$(\Delta^{R}_{ESR\%,})$
SISO A		60.1			
SISOA		67.2			
MISO DD	20λ H	63.6*	44.9	18.8	0.3
MISO DD with Profile SS	20λ H	63.6*	60.3	3.4	0.05
MISO DD with Profile AW (6dB)	20λ H	63.6*	55.8	7.8	0.12
MISO DD	20λ H + 5λ V	63.6*	52.1	11.5	0.18
MISO DD with Profile SS	20λ H + 5λ V	63.6*	60.8	2.9	0.044
MISO DD with Profile AW (6dB)	20λ H+ 5λ V	63.6*	55.1	8.6	0.13
*: averaged using the two SISO A values					

Table 6-11: Performances vs. Antenna separation and spectrum profiling techniques, taken on 20th June 2008

Configuration	Antenna Spacing	SISO $ESR_{\%}$	MISO $ESR_{\%}$	$\Delta_{ESR_{\%}}$	$(\Delta^{R}_{ESR\%,})$
SISO A		54.8			
SISO A		57.1			
MISO DD	20λ H	56.0*	42.0	14.0	0.25
MISO DD + Profile SS	20λ H	56.0*	52.0	4.0	0.07
MISO DD + Profile AW (6dB)	20λ H	56.0*	50.4	5.6	0.1
MISO DD	20λ H + 5λ V	56.0*	48.4	7.6	0.13
MISO DD + Profile SS	20λ H + 5λ V	56.0*	53.0	2.9	0.05
MISO DD + Profile AW (6dB)	20λ H + 5λ V	56.0*	46.8	9.2	0.16
*: values averaged using the two SISO A values					

Figure 6-18 reports the average $ESR_{\%}$ Gain vs. spectrum profiling techniques for the two antenna separations. The chart is yielded by averaging the results of data taken in the two days.

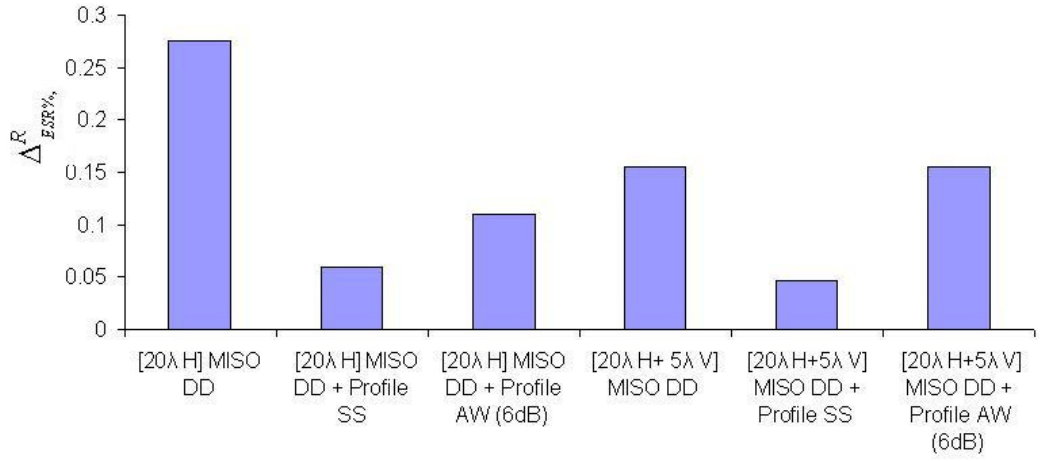

Figure 6-18: Average $ESR_{\%}$ Gain vs. Amplitude Weighting for the two antenna separations.

With 20λ horizontal separation and MISO DD applied, it was observed a good diversity gain ($\Delta^{R}_{ESR\%,} = 0.275$) since reception from these antennas exhibits a low K-factor and the receiver is possibly in a non line of sight situation during most of the drive. It can be seen that introducing MISO DD with Profile SS and MISO DD with Profile AW both significantly reduced the diversity gain. The $\Delta^{R}_{ESR\%,}$ reduces to 0.06 and 0.11 for MISO DD with Profile SS and Profile AW, respectively. A vertical plus horizontal antenna separation was tested aiming to increase the spatial separation and reduce the 2 transmit channel correlations. However, the antenna at a higher position possibly led to a higher K-factor for that channel, increasing the correlation between channels and reducing the transmit diversity gain. It was expected to observe an improvement in MISO DD performance with this high K-factor situation. However, both AW and SS profiling techniques reduce diversity gain although AW profiling is more effective than SS profiling and has only a minor degradation compared to results with MISO DD. In the MISO DD case with Profile AW, the reduction in gain is due to less power in one channel. In the case of Profile SS, the reduction is because the amplitude shapes were not the ideal 6 dB step required which would have preserved power in each channel and reduced any "LOS" interference between transmitters in high K-factor situations.

6.7 Conclusions

In this chapter a long term measurement campaign of MISO DVB-T systems has been presented for testing the DD gain in stationary conditions and for practically analyzing the spectrum profiling techniques for stationary and mobile receptions. The results show that MISO with DD provides a gain of about 5 dB for indoor propagation channel, characterized by strong NLOS components. Results are obtained by finding the median of several degradation thresholds estimations. For rooftop reception, the dominant LOS component turns the gain over into a performance loss. The maximum estimated loss is 6.5 dB. This range of degradation is confirmed by previous work based on simulation software analysis. Two spectrum profile techniques have been tested in order to reduce the loss for rooftop reception. These techniques can reduce the LOS diversity loss of a 4 dB factor while reducing the gain up to 1 dB for NLOS reception. The profiling techniques

have also been tested for mobile reception, producing a reduction up to 23% of MISO DD gain. MISO DD with Profiling AW performs as well as MISO DD only for the 20λ H + 5λ V antenna separation case. The smallest gain is yielded by MISO DD with Profile SS, significantly approaching the SISO performances for both spatial antenna spacing configurations. Thus, it is concluded that MISO DD with Profile AW is the best candidate (among the proven ones) to reduce the LOS diversity loss while aiming to maintain the MISO DD gain for NLOS situation. It is envisaged that in rooftop reception, the fade margin is typically high enough to cover this loss. This is due to the high performances aerial. On the other hand, NLOS propagation results generally in lower SNR since the receiver antenna has poor performance and electromagnetic waves are attenuated by NLOS typical effects like reflections, deflection and refraction. These poor SNR scenarios benefit from DD due to their NLOS characteristic. A maximum reduction of 2.5 dB for the LOS fade margin and a gain of 5 dB of fade margin for NLOS is considered to be fairly good trade-off for network planning purposes.

7. CONCLUSIONS

7.1 Discussions

In this thesis, the performance of transmit DD diversity technologies for DVB-T/H networks is investigated with laboratory and field trials experiments. Combined with channel coding and interleaver, DD/CDD can achieve desirable spatial diversity and coding gain for SFN network planning. Laboratory measurements confirmed that the gain predicted from previous theoretical simulations can be realized or exceeded using actual equipment in realistic propagation conditions. Diversity gains of up to 7.5 dB should be achievable for indoor scenarios with a low delay spread. For mobile reception, DD significantly improves receiver performance until the impact of Doppler on inter-symbol interference becomes unacceptably high for a particular receiver's implementation. The SISO $ESR_{5\%}$ threshold in fast fading channels strongly depends on the particular receiver implementation while the MISO is the same for both receivers tested. This would be an advantage for real world network planning, since the assumption of the same reception threshold for different implementation receivers would be realistic. Measurements have shown that scenarios with a relatively short delay spread can still deliver high diversity gain with relatively high degree of cross correlation at 50%. The results predicted by software laboratory simulations have been tested in real world situations. DVB-T experiment results showed that, when driving in a sub-urban area, the number of errored seconds observed is greatly reduced and instances of acceptable reception are significantly increased. The propagation environment has been characterized through an averaged channel model. A significantly large number of tests allowed a statistical characterization of results and a reliable 4 dB gain estimation considering the $ESR_{5\%}$ metric. The coverage was improved by about 7% and 20% for the network planning reference coverage of 95% and 70%, respectively. Several transmit antenna separations have been tested as well. The highest gain was achieved by adopting a 20λ of horizontal separation between transmit antennas while an additional 5λ of vertical separation reduced the gain as the Ricean K-factor figure increased. DVB-H experimental results have shown an approximately 1 dB of gain measured for $MFER_{5\%}$. The gain reduction is possibly due to the particular chipset implementation already optimized for high mobility reception and to the time interleaving

effects of the MPE-FEC encoding. A long term measurement campaign has shown that DD provides a gain of about 5 dB for indoor propagation channels, characterized by strong NLOS components. For rooftop-like reception, the dominant LOS component turns the gain over into a performance loss. The maximum estimated loss is 6.5 dB. Two experimental spectrum profile techniques have been tested in order to reduce the loss for rooftop reception. These techniques can reduce the LOS diversity loss of a 4 dB factor despite reducing the gain by up to 1 dB for NLOS reception. The deployment of these techniques minimized the up to 2.5 dB LOS fade margin loss due to DD while keeping a maximum gain of 5 dB for indoors. These results are considered to be a fairly good trade-off for a broadcasting network planning, targeting the indoor reception as well. The profiling techniques have also been tested for mobile NLOS reception, producing a reduction up to 23% of MISO DD gain for 20λ horizontal separation. Signal Spectrum Profiling performed as well as MISO DD in mobile NLOS only for the 20λ H + 5λ V antenna separation case, as the channel Ricean K-factor figure increased. These results show that transmit DD/CDD should be carefully considered for high elevations transmit configurations since the gain in mobile reception would be negligible while the rooftop reception results would be degraded.

7.2 Future works

Many issues still have not been solved and can be the basis for future investigations.

1. Signal Profiling Techniques for Driving Tests: although these techniques do not show a major degradation in NLOS fixed indoor reception, they exhibit a significant diversity gain reduction for driving tests. Therefore, it is important to improve and/or propose new profiling techniques for DVB-T to remove the loss in the Ricean channels systems while getting the same diversity gain in NLOS mobile reception.
2. Channel cross correlation estimation: the channel cross correlation relative to each antenna separation can be estimated from the channel impulse response and used to validate the cross correlation channel model since it is related to the performance improvements.

3. Non-adjacent and different bandwidth channel cross correlation: future broadcasting standards are targeting the distribution of the OFDM signal over l non-adjacent channel to exploit the channel frequency diversity. Moreover, future cooperative network will adopt standards supporting different licensed and unlicensed bandwidth (e.g. UHF, L band and S-band). Thus, an experimental study, targeting the cross correlation between non-adjacent and different bandwidth channels, is envisaged to be needed.
4. Application of transmit CDD to other OFDM standards: It would be beneficial to conduct a study targeting the application of transmit CDD to other OFDM based standards. In fact, it is envisaged that a 6 MHz bandwidth of Media-FLO and ISDB systems (e.g. compared with the 8 MHz relative to DVB systems) would be more susceptible to flat deep fading compared to the DVB systems based on wider 8 MHz bandwidth. Thus, the application of CDD would provide a higher gain. Moreover, the Alamouti diversity scheme chosen for DVB-T2 standard is expected to yield poor performances in fast fading channels. Thus, a DVB-T2 in mobile channel reception would take advantage from the CDD schema added on the top the existing standard.

Appendix I

The Dirac delta function is defined as:

$$D(x)=\begin{cases}1 & x=0\\ 0 & otherwise,\end{cases} \qquad \text{A.1}$$

and the sign function is defined as:

$$\operatorname{sgn}(x)=\begin{cases}1 & x>0\\ 0 & x=0\\ -1 & x<0.\end{cases} \qquad \text{A.2}$$

A.1 and A.2 are adopted to define:

$$v(x)=\frac{1+\operatorname{sgn}(x)}{2}+\frac{1}{2}D(x)=\begin{cases}1 & x\geq 0\\ 0 & x<0\end{cases} \qquad \text{A.3}$$

which represents a modification of the standard Heaviside step function, where the value for x=0 is ½. If $v(x)$ is shifted by a delay δ_i, $v(t-\delta_i)$ consequently sets zeros for $t<\delta_i$. In formula 4-1, the signal code $s_i(t)$ is shifted in the time domain at the i^{th} antenna by delay δ_i. The elements of $s_i(t-\delta_i)$ having a negative time index (i.e. $t<\delta_i$), have to be multiplied by zero to comply with the DD codeword definition [120]. This operation can be easily done by multiplying $s_i(t-\delta_i)$ by the zeroing function $v(t-\delta_i)$ as shown in formula 4-1.

Appendix II

In this appendix, the issues related to DVB-T/H receiver are presented. The objective of this section is to measure the internal noise of DVB-T/H receiver. From [63], a typical DVB-T receiver has an average noise floor of about -101.4 dBm across the integration bandwidth of 7.61 MHz. This also means an average noise floor of -170.21 dBm (or -170.21 dBm/Hz) if an integration bandwidth of 1 Hz is chosen. The HP8560E Spectrum Analyzer noise floor is about -150 dBm for the minimum Resolution Bandwidth RBW=1 Hz and minimum Input Attenuation Att=0 dB. Thus, the minimum Displayed Averaged Noise Level (DANL) is about -150 dBm/Hz. Thus, the noise floor of the DVB-T receiver is about 20 dB below the noise floor of the spectrum analyzer. Since only the signal above the noise floor can be estimated, the estimation if N_{internal} cannot be obtained directly with this spectrum analyzer but it needs indirect measurement methods. An indirect measurement approach has been developed to estimate the noise floor of the Monitor Station and the Dibcom receiver. The instruments and devices used for this measurement included:

- A DVB-T transmitter;
- Spectrum Analyzer;
- AWG Noise Generator. This device has been already described in chapter 4;
- Signal combiner with 2 inputs and 1 output;
- RF coaxial cables and connectors;

When the signal from the transmitter is directly connected through a cable to the receiver (e.g. Figure A-1), the total C/N can be approximated as:

$$\left.\frac{C}{N}\right|_{\text{INT}} \approx \frac{C}{N_{\text{internal}}} \qquad \text{A.4}$$

where N_{internal} is the internal noise of the receiver.

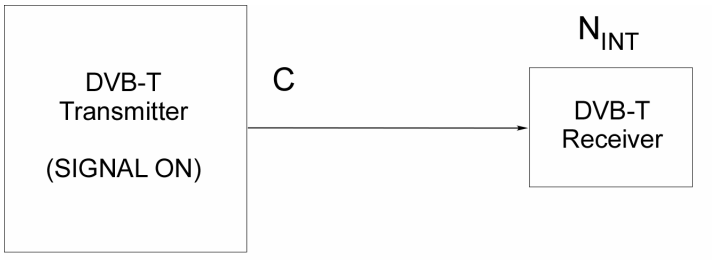

Figure A-1: Set-up for $C_{\min}$ estimation

If an external noise generator with power $N_{external} >> N_{\text{internal}}$ is inserted (e.g. Figure A-2), the total C/N is approximately equal to:

$$\left.\frac{C}{N}\right|_{EXT} = \frac{C}{N_{\text{internal}} + N_{external}} \approx \frac{C}{N_{\text{external noise}}} \qquad \text{A.5}$$

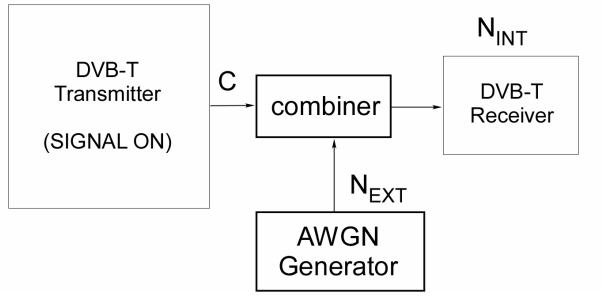

Figure A-2: Set-up for $\left.\frac{C}{N}(dB)\right|_{\text{EXT}}$ estimation

Let's define $C_{\min}$ and C_{ext} as the required signal power to achieve the QEF (e.g. after Viterbi BER=2*10^{-4}) condition without external noise and employing the external noise, respectively. It is assumed that the Quasi Error Free QEF is approximately achieved for the same C/N ratio. Thus,

$$\frac{C_{\min}}{N_{\text{internal}}} \approx \left.\frac{C_{ext}}{N_{\text{ext}}}\right|_{QEF} \qquad \text{A.6}$$

From this, it follows that N_{internal} expressed in dBm is equal to:

$$N_{\text{internal}}(dBm) = C_{\min}(dBm) - \frac{C_{ext}}{N_{\text{ext}}}(dB) \qquad \text{A.7}$$

The values $C_{\min}$ and $\frac{C_{ext}}{N_{\text{ext}}}(dB)$ needs to be estimated to evaluate N_{internal}.To measure the signal and noise power the spectrum analyzer was used. After checking that the signal spectrum is flat across the B_{DVB} bandwidth, a value of *10Log(B_{DVB}/RBW)* has to be added to the DANL to compute the total power, where B_{DVB} is a 7.61 MHz bandwidth and RBW is the selected spectrum analyzer resolution bandwidth. The noise level is measured using the same spectrum analyzer configuration in order to cancel measuring errors. The noise spectrum is also flat across the B_{DVB} bandwidth. The measurement process consisted of:

1. Connecting the transmitter to the receiver with signal on (see Figure A-1), regulating the signal level until the QEF point is reached, and measuring the correspondent signal level C_{min}.
2. Connecting the AWGN generator through the combiner to the system (see Figure A-2), increasing the signal power at the transmitter by 20 dB and adjusting the noise power until the QEF point is achieved. Finally, the $\frac{C_{ext}}{N_{\text{ext}}}(dB)$ value was measured by estimating the signal and the noise power at the combiner input ports. Once that $C_{\min}$ and $\frac{C_{ext}}{N_{\text{ext}}}(dB)$ are estimated, N_{internal} can be derived by using A.7.

Table A-1 shows the Sensitivity, the Noise floor and the C/N for minimum performance. The sensitivity corresponds to $C_{\min}$. Transmitted signal Centre Frequency was 498 MHz, the FFT size was 2K, the code rate=3/4 and the modulation were QPSK and 16 QAM, respectively. Both Monitor Station and Dibcom receiver were tested, measuring the power in the bandwidth of the channel used for DVB-T/H broadcasting in Europe that is 7.61 MHz. Results are benchmarked with the calibrations presented in MBRAI documentation [63].

Table A-1: MBRAI and calibration results benchmark

Receiver and Modulation	Sensitivity (dBm)		Noise Floor (dBm)		C/N for minimum performance (e.g. at QEF)	
	MBRAI	Calibration	MBRAI [63]	Calibration	MBRAI	Calibration
MS, 16 QAM, CR=3/4	-87.2*	-88.4	-101.2	-101.4	14	13
Dibcom, 16 QAM, CR=3/4		-89		-101		12
MS, QPSK, CR=3/4	-93.8*	-93.4		-101.4	7.4	8
Dibcom, QPSK, CR=3/4		-94		-101		7
*=estimated as -101.2 dBm + C/N db as specified in the document						

The Noise Figure F , characterizing the C/N degradation of actual receiver compared to an ideal on, is estimated. The noise floor of an ideal receiver (e.g. with no C/N degradation caused by components in the RF signal chain) is given by:

$$N = KTB \qquad \text{A.8}$$

where $K = 1.38 \cdot 10^{-23}$ $[J \cdot K^{-1}]$ is the Boltzmann constant, T=290 [K] is the reference temperature for noise calculation, and B=7.61 MHz is the system noise bandwidth. F is given by:

$$F(dB) = N_{\text{internal}}(dBm) - 10 \cdot \log[K \cdot T \cdot b(Hz)] + 30 = N_{\text{internal}}(dBm) + 105.16\,\text{dBm} \qquad \text{A.9}$$

Finally, from A.8 and the values provided in Table A-1, the Noise figure can be estimated. A noise figure of 3.76 dB and 4.16 dB was estimated for the Monitor Station and the Dibcom receiver, respectively.

References

[1] Yue Zhang, Kok-Keong Loo, John Cosmas and Yong-Hua Song, 2008, "Digital Video Broadcast: Systems and Implementations" in "Mobile Multimedia Broadcasting Standards Technology and Practice", Springer US
[2] European Telecommunications Standard Institute ETSI, Digital Video Broadcasting (DVB); Framing structure, channel coding and modulation for digital terrestrial television, July 1999, EN 300 744 V1.2.1.
[3] Kavitha Ramakrishna, "DVB-H layers 1 and 2 , Project Report". Available at: http://itpcourses.colorado.edu/borsuk/current/tlen5380/present/su08/Ramakrishna_DVB-H.doc
[4] Digital Video Broadcasting (DVB); DVB-H Implementation guidelines, TR 102 377 V1.2.1. European Telecommunications Standard Institute ETSI York, Nov. 2005
[5] European Telecommunications Standard Institute ETSI , DVB-SH Implementation Guidelines:http://www.dvb-h.org/PDF/a120.tm3731r5.ssp252r9f.DVB-SH_implementation_guide.pdf
[6] IST Project PLUTO, Available at: http://www.ist-pluto.org
[7]H. Parviainen, P. Kyosti, X. Zhao, H. Himmanen, P.H.K. Talmola, and J. Rinne, "Novel Radio Channel Models for Evaluation of DVB-H Broadcast Systems", presented at IEEE 17th Int. Symp. on Personal, Indoor and Mobile Radio Communications, Sept. 2006.
[8] A. Dammann and S. Kaiser, "Standard conformable antenna diversity techniques for OFDM systems and its application to the DVB-T system," in Proceedings IEEE Global Communication Conference (GLOBECOM 2001), San Antonio, TX, USA, pp. 3100–3105, Nov. 2001.
[9] A. Wittneben. "A new bandwidth efficient transmit antenna modulation diversity scheme for linear digital modulation". In Proceedings IEEE International Conference on Communications (ICC 1993), pages 1630-1634, May 1993.
[10] R. Raulefs, J. Cosmas, K.-K. Loo, M. Bard, G. Pousset, D. Bradshaw, Y. Lostanlen, I. Defee, P. Kasser, and S. Kalli, "Physical layer DVB transmission optimisation (PLUTO)," in Proceedings 15th IST Mobile Summit 2006, Mykonos, Greece, June 2006.
[11] Kaiser, S. "Spatial transmit diversity techniques for broadband OFDM systems" in: Global Telecommunications Conference, 2000. GLOBECOM '00. IEEE, On page(s): 1824-1828 vol.3
[12] A. Dammann and R. Raulefs. "Increasing time domain diversity in OFDM systems". In Proceedings IEEE Global Telecommunications Conference (GLOBECOM 2004), Dallas, TX, USA, Nov.-Dec. 2004.
[13] A. Dammann and S. Kaiser. "Transmit/receive antenna diversity techniques for OFDM systems". In European Transactions on Telecommunications, 13(5):531-538, Sept.-Oct. 2002.

[14] A. Hübner, F. Schülein, M. Bossert, E. Costa, and H. Haas. “On space-frequency coding using cyclic delay diversity for OFDM based transmission systems”. In European Transactions on Telecommunications, 14(6):491-500, Nov.-Dec. 2003.
[15] R. Raulefs, A. Dammann, S. Kaiser, and G. Auer. “The Doppler spread - gaining diversity for future mobile radio systems“ In Proceedings IEEE Global Telecommunications Conference (GLOBECOM 2003), San Francisco, CA, USA, volume 3, pages 1301-1305, Dec. 2003.
[16] S. Alamouti, “A simple transmitter diversity scheme for wireless communications,” IEEE J. Select. Areas Commun., vol. 16, pp. 1451–1458, Oct. 1998.
[17] Vahid Tarokh, Hamid Jafarkhani, and A. R. Calderbank (July 1999). "Space–time block codes from orthogonal designs". IEEE Transactions on Information Theory 45 (5): 744–765
[18] V. Tarokh, N. Seshadri, and A. Calderbank, “Space-time codes for high data rate wireless communications: Performance criterion and code construction,” IEEE Trans. Inform. Theory, vol. 44, pp. 744–765, Mar. 1998.
[19] Vahid Tarokh, Ayman Naguib, Nambi Seshadri and A. Robert Calderbank, "Space–time codes for high data rate wireless communication: performance criteria in the presence of channel estimation errors, mobility, and multiple paths". IEEE Transactions on Communications, Publication Date: Feb 1999, Volume: 47, Issue: 2 On page(s): 199-207
[20] A. Dammann, R. Raulefs, G. Auer, and G. Bauch. “Comparison of space-time block coding and cyclic delay diversity for a broadband mobile radio air interface”. In Proceedings 6th International Symposium on Wireless Personal Multimedia Communications (WPMC 2003), Yokosuka, Japan, volume 2, pages 411-415, Oct. 2003.
[21] A. Dammann, P. Lusina, and M. Bossert. “On the equivalence of space-time block coding with multipath propagation and/or cyclic delay diversity in OFDM”. In Proceedings European Wireless 2002, Florence, Italy, volume 2, pages 847-851, Feb. 2002.
[22] R. Raulefs, A. Dammann, and S. Kaiser. “Beamforming in combination with space-time diversity for broadband OFDM systems”. In Proceedings IEEE International Conference on Communications (ICC 2002), New York, USA, volume 1, pages 165-171, Apr.-May 2002.
[23] G. Bauch and J. Hagenauer. “Smart versus dumb antennas - capacities and FEC performance”. In IEEE Communications Letters, 6(2):55-57, Feb. 2002.
[24] Y. Zhang, J Cosmas, M. Bard, Y.H Song, “Obtain Diversity Gain for DVB-H by Using Transmitter/Receiver Cyclic Delay Diversity”, to appear in IEEE Trans. on Broadcasting, Dec. 2006.
[25] Yue Zhang, Cosmas, J.; Kok-Keong Loo; Bard, M.; Bari, R. “Analysis of cyclic delay diversity on DVB-H systems over spatially correlated channel” IEEE Transactions on Broadcasting, v 53, n 1, pt.2, March 2007, p 247-55
[26] A. Dammann, R. Raulefs, and S. Plass. “Performance of cyclic delay diversity in Riceanan channels”. In Multi-Carrier Spread Spectrum 2007, Kluwer Academic Publishers, May 2007
[27] A. Dammann, and R. Raulefs, “PLUTO Deliverable 4.1, Simulation Lab Facility and Test Report”. Available at: http://dea.brunel.ac.uk/pluto/publications/del4-1.pdf
[28] D. Masse, G. Pousset, “PLUTO Deliverable 7.2, Report on Simulated Performance

Analysis" Avilable: on application to the authors.
[29] D. Masse, G. Pousset, "PLUTO Deliverable 7.3, Report on Dibcom Rx Pilot Trial Performance Analysis" Avilable: on application to the authors.
[30] Oksanen, M. & Defee, I. " DVB-H transmit diversity: evaluation in environments and results", Proceedings of ISCE 2008, IEEE International Symposium on Consumer Electronics 2008, Algarve, Portugal, 14-16 April 2008
[31] E. B. Hogenauer. An economical class of digital _lters for decimation and interpolation. IEEE Transactions on Acoustics, Speech and Signal Processing, ASSP-29(2):155{162, 1981.
[32] Philips web' page, TDA10046HT DVB-T Receiver Data Sheet: Available at http://www.nxp.com/acrobat_download/literature/9397/75009522.pdf
[33] S. H. Müller-Weinfurtner, J. F. Rößler, and J. B. Huber, "Analysis of a frame and frequency synchronizer for (Bursty) OFDM," in Proc. Globecom'98 Commun. Theory Mini-Conf., pp. 344–349.
[34] Echavarri, J. Woodward, M.E. Barton, S.K., "A comparison of time and frequency synchronization algorithms for the European DVB-T system" in: Vehicular Technology Conference, 1999. VTC 1999 - Fall. IEEE VTS 50th, Publication Date: 1999 Volume: 2, On page(s): 678-682 vol.2 Amsterdam. Netherlands,
[35] J.-J. van de Beek, O. Edfors, M. Sandell, S. K. Wilson and P. O. Börjesson, "On channel estimation in OFDM systems," in *Proc. IEEE 45th Vehicular Technology Conf.,* Chicago, IL, Jul. 1995, pp. 815-819.
[36] M. Morelli and U. Mengali, "A comparison of pilot-aided channel estimation methods for OFDM systems," IEEE Trans. Signal Process., vol. 49, no. 12, pp. 3065-3073, Dec. 2001.
[37] M. Hsieh, C. Wei, "Channel estimation for OFDM systems based on comb-type pilot arrangement in frequency selective fading channels", IEEE Transactions on Consumer Electronics, Vol. 44, No. 1, Feb.1998,pp.217-225.
[38] Fritsh, R.Carlson, "Monotone piecewise cubic interpolation," SIAM J. Numerical Analysis, Vol.17, No.2, 1980, pp.238-246
[39] H. Sarbazi-Azad, L. M. Mackenzie, M. Ould-Khaoua, and G. Min, "An efficient parallel algorithm for Lagrange interpolation and its performance", in Proc. 4th High Performance computing in the Aisa-Pacific Region, Vol.2, May.2000, pp. 593-598.
[40] Ingo Gaspard, "Mobile reception of the terrestrial DVB- systems", in Proc. Veh. Technol. Conf., May 1999, pp. 151–155 vol.1.
[41] Ana García Armada, "Understanding the Effects of Phase Noise in Orthogonal Frequency Division Multiplexing", IEEE Trans. Broadcasting., vol. 47, no. 2, pp. 153-159, June. 2001.
[42] Michael Speth, 'OFDM Receivers for Broadband-Transmission'. Available at: http://www.iss.rwth-aachen.de/Projekte/Theo/OFDM/node1.html
[43] Xiaodong Xu, Ya Jing, Xiaohu Yu, "Subspace-Based Noise Variance and SNR Estimation for OFDM Systems", This paper appears in: Wireless Communications and Networking Conference, 2005 IEEE Publication Date: 13-17 March 2005 Volume: 1, On page(s): 23- 26 Vol.
[44] Tevfik Yücek, Hüseyin Arslan, "MMSE Noise Power and SNR Estimation for OFDM Systems".

[45] Min-Young Park and Weon-Cheol Lee, “A demapping Method Using the Pilots in COFDM systems,” IEEE Trans. On Consumer Electronics, Vol.44. No.3, Aug. 1998, pp.1150-1153.
[46] Weon-cheol Lee, Hyung-Mo Park, Kyung-jin Kang, Kuen-bae Kim, “Performance Analysis of Viterbi Decoder Using Channel State Information in COFDM System”, IEEE Transaction on Broadcasting, Vol. 44, No. 4, December 1998
[47] Dao, H.Q. Zeydel, B.R. Oklobdzija, V.G. “Energy-Efficient Optimization of the Viterbi ACS Unit Architecture”, Asian Solid-State Circuits Conference, 2005, Publication Date: Nov. 2005, pag.: 233-236
[48] Yue Zhang (2008), “Optimal Transmitter and Receiver Diversity Technologies in DVBT/H Networks”, Doctoral thesis, School of School of Engineering and Design, Brunel University, Brunel University, Uxbridge, London.
[49] “Planning parameters for hand held reception. Concerning the use of DVB-H and T-DMB in Bands III, IV, V and the 1.5 GHz band”. Available at: http://www.ebu.ch/CMSimages/en/tec_doc_t3317-2007_tcm6-48865.pdf
[50] European Telecommunications Standard Institute ETSI, “Digital Video Broadcasting Digital Video Broadcasting (DVB); Specification for Service Information (SI) in DVB systems ETSI EN 300 468 V1.4.1 (2000-11)”. Available at: http://www.turbosight.com/data/pdf/en300468.pdf
[51] Available at: http://www.bit-tech.net/news/industry/2009/07/10/dibcom-s-chipset-is-ready-to-welcome-mobile/1
[52] J.-C. Guey, M.R. Bell, M.P. Fitz, and W.-Y. Kuo, “Signal design for transmitter diversity wireless communication systems over Rayleigh fading channels,” in IEEE Vehicular Technology Conf., pp. 136-140, Atlanta, 1996.
[53] Hamid Jafarkhani, “Space-Time coding. Theory and practice”, Cambr5idge University Press, 200
[54] P. Hoeher, “A Statistical Discrete-Time Model for the WSSUS Multipath Channel,” IEEE Trans. on Veh. Technol, vol. 41, no. 4, pp. 461–468, 1992.
[55] Proakis J. G., Salehi M. “Digital Communications”, McGraw Hill, Fifth Edition, 2008, pag. 832-833
[56] P. Soma, D.S. Baum, V. Erceg, R. Krishnamoorthy, and A.J. Paulraj, “ Analysis and modeling of multiple-input multiple-output (MIMO) radio channel based on outdoor measurements conducted at 2.5 GHz for fixed BWA applications,” in *Proc.IEEE ICC Conf., New York, April 2002.*
[57] Clarke R. H., A statistical theory of mobile radio reception, “Bell System Tech. J.”, 1989, vol 47, pp.957-1000.
[58] Mengali U., Morelli M., “Transmissione numerica”, McGraw-Hill, 2001, pp. 149
[59] Dmitry Chizhik, Jonathan Ling, Peter W. Wolniansky, Reinaldo A. Valenzuela, Nelson Costa, and Kris Huber (April 2003). "Multiple-Input–Multiple-Output Measurements and Modeling in Manhattan". *IEEE Journal on Selected Areas in Communications* 21 (3): 321–331. doi:10.1109/ JSAC.2003.809457.
[60] Rappaport, Wireless Communications, Prentice Hall, 2002
[61] Lee, W. C. Y., Mobile Cellular Telecommunications systems, McGraw Hill Publications, New York, 1989

[62] COST 207, “Digital land mobile radiocommunications,” Office for Official Publications of the European Communities. Abschlussbericht, Lussemburg, 1989.
[63] EICTA MBRAI 2.0 “Mobile and Portable DVB-T/H Radio Access. Part 1: Interface Specifications”. Available at: www.eicta.org/web/news/telecharger.php?iddoc=587
[64] Wing TV Reference Receiver, Celtic Wing-TV WP3 Deliverable D3, 2007. Avilable: http://projects.celtic-initiative.org/WING-TV/
[65] D. M. J. Devasirvatham, “The delay spread measurements of wideband radio signals within a building,” Electron. Lett., vol. 20, no. 23, pp. 950-951, Nov. 8, 1984.
[66] T. S. Rappaport, “Characterization of UHF multipath radio channels in factory buildings” IEEE Transactions on Antennas and Propagation, v 37, n 8, Aug, 1989, pp.1058-1069
[67] A. A. M. Saleh, and R. A. Valenzuela, “A statistical model for indoor multipath propagation,” IEEE J. Selected Areas. Commun., vol. SAC-5, no. 2, pp. 138-146, Feb. 1987.
[68] J. Medbo and P. Schramm, “Channel models for HIPERLAN/2,” ETSI/BRAN document no. 3ERI085B.
[69] J. Medbo and J-E. Berg, “Measured radiowave propagation characteristics at 5 GHz for typical HIPERLAN/2 scenarios,” ETSI/BRAN document no. 3ERI084A.
[70] Joint Technical Committee on Wireless Access, Final Report on RF Channel Characterization, September 1993, JTC(AIR)/93.09.23-238R2.
[71] AC 318 Motivate: Deliverable 06: Reference Receiver Conditions for Mobile Reception, January 2000
[72] Web page avilable at: http://www.eicta.org/index.php?id=1
[73] J. D. Parsons, “The Mobile Radio Propagation Channel”, 2nd ed. Chichester, New York: J. Wiley, 2000.
[74] Saunders S. R., Aragon-Zavala A., “Antennas and propagation for wireless communication Systems”, Wiley, 2nd edition, 2007.
[75] A. Abdi, M. Kaveh, “A space-time correlation model for multielement antenna systems in mobile fading channels,” IEEE J. Selected Areas in Commun., Vol. 20, No. 3, Apr. 2002, p 550-60
[76] Oestges C. and Clerckx B., “MIMO Wireless Communications”, First Editcion, Elsevier, 2007
[77] V. Erceg and others, “IEEE P802.11Wireless Lan(s), Tgn Channel Models”. Available at: www.ece.arizona.edu/~yanli/files/11-03-0940-04-000n-tgn-channel-models.doc
[78] Space Time Block Code, from Wikipedia web page. Available at: http://en.wikipedia.org/wiki/Space%E2%80%93time_block_code
[79] Gerard J. Foschini and Michael. J. Gans (January 1998). "On limits of wireless communications in a fading environment when using multiple antennas". *Wireless Personal Communications* 6 (3): 311–335.
[80] J.-C. Belfiore, G. Rekaya, E. Viterbo: "The Golden Code: A 2 x 2 Full-Rate Space-Time Code with Non-Vanishing Determinants," IEEE Transactions on Information Theory, vol. 51, n. 4, pp. 1432-1436, Apr. 2005.

[81] K.F.Lee, D.B.Williams, "A space-time coded transmitter diversity technique for frequency selective fading channels", Sensor Array and Multichannel Signal Processing Workshop, 2000, pp. 149-152.
[82] COST 207, “Digital land mobile radio communications”, Office for Official Publications of the European Communities. Abschlussbericht, Lemburg, 1989.
[83] M.I. Rahman, K. Witrisal, S.S. Das, F.H.P. Fitzek, O. Olsen, R. Prasad, “Optimum pre-DFT combining with cyclic delay diversity for OFDM based
[84] S. B. Weinstein and P. M. Ebert, “Data transmission by frequency division multiplexing using the discrete Fourier transform,” IEEE Transactions on Commun. Vol. 19, No. 15, pp 628–634, Oct. 1971.
[85] Damman A. & Kaiser S., “Performance of Low Complex Antenna Diversity Techniques for Mobile OFDM Systems”, Proc. 3rd International Workshop on Multi-Carrier Spread-Spectrum, Oberpfaffenhofen, Germany, September 2001.
[86] Ronald Raulefs, Armin Dammann, S Kaiser, Gunther Auer, “The Doppler spread-gaining diversity for future mobile radio systems”, IEEE Globecom 2003 pp 1301-1306
[87] Armin Dammann, “On the Influence of Cyclic Delay Diversity and Doppler Diversity on the Channel Characteristics in OFDM Systems” IEEE International Conference on Communications, 24-28 June 2007 Page(s):4179 – 4184
[88] Sanchez, M. “Analysis of polarization diversity at digital TV indoor receivers” IEEE Transactions on Broadcasting, v 46, n 4, Dec. 2000, p 233-9
[89] A dual Polarization MIMO broadcast TV service, BBC R&D White Paper. Available at: http://www.bbc.co.uk/rd/pubs/whp/whp-pdf-files/WHP144.pdf
[90] Mirko Oksanen, Irek Defee, “DVB-H transmit diversity: Evaluation in environments and results”, Consumer Electronics, 2008. ISCE 2008. IEEE International Symposium on Volume , Issue , 14-16 April 2008 Page(s):1 - 4
[91] K. Krishnapillai, R. Di Bari, H. Shirazi, J. Cosmas, M. Bard, D. Masse, M. Oksanen, C. Raynal, I. Defee, P. Kasser, “PLUTO Deliverable 3.3, Pilot Trial Facilities including Service Creation System”. Available at: http://dea.brunel.ac.uk/pluto/publications/del3-3.pdf
[92] R. Di Bari, D. Masse, M. Oksanen, M. Bard, J. Cosmas, “PLUTO Deliverable 3.4, Final Test Report”. Available at: http://dea.brunel.ac.uk/pluto/publications/del3-4.pdf
[93] A. Auer, “Channel estimation for OFDM with cyclic delay diversity,” in Proc. of PIMRC'04, pp. 1792-1796, September 2004.
[94] Jing Lei and Tung-Sang Ng, “A consistent OFDM carrier frequency offset estimator based on distinctively spaced pilot tones,” IEEE Trans. Wireless Commun., vol. 3, no. 2, pp. 588- 599, March 2004.
[95] Spirent’s web page support. Available at: http://www.spirentcom.com/analysis/technology.cfm?SS=156&WS=68
[96] R&S ETX-T DTV Monitoring Receiver Data Sheet page. Avilable: http://www2.rohde-schwarz.com/product/ETX-T.html
[97] Dibcom product and application web page. Available at: http://www.dibcom.info/Website/site/eng_accueil_applicationsproducts_products_chipset.htm
[98] Broadreach Monitor Station Product Detail Webpage. Available at: http://www.broadreachsystems.com/

[99] IST PLUTO PROJECTS– Del 3.2 Backwards Compatibility Testing. Available at: http://www.ist-pluto.org
[100] Digital Video Broadcasting (DVB); Transmission to Handheld Terminals (DVB-H); Validation Task Force Report, TR 102 401 V1.1.1 European Telecommunications Standard Institute ETSI York, 2005
[101] European Telecommunications Standard Institute ETSI York: Digital Video Broadcasting (DVB); Digital Video Broadcasting (DVB); Measurement guidelines for DVB systems, May 1997, ETR 290.
[102] R. Di Bari, Y. Zhang, K. Nasr, K. Krishnapillai, M. Bard, J. Cosmas "IST PLUTO PROJECTS– Del 3.1a Simulation Lab Facility and Test Report." Available at: http://www.ist-pluto.org
[103]A. Bertella, M. Rossini, P. Sunna, L. Vignaroli, "Mobile DVB-T reception: quality of streaming over IP of audiovisual services". Available at: http://www.broadcastchapters.com/whitechapters/
[104] Broadreach Diversity Unit Product Detail Webpage. Available at: http://www.broadreachsystems.com/
[105] R. Di Bari, M. Bard, J. Cosmas, R. Nilavalan, K.K. Loo, H. Shirazi, K. Krishnapillai., "Measurement results from transmit delay diversity for DVB-T networks", presented at the IEEE International Symposium on Broadband Multimedia Systems and Broadcasting, Las Vegas, NV, March 28-29, 2008.
[106] H. Parviainen, P. Kyosti, X. Zhao, H. Himmanen, P.H.K. Talmola, and J. Rinne, "*Novel Radio Channel Models for Evaluation of DVB-H Broadcast Systems*", presented at IEEE 17th Int. Symp. on Personal, Indoor and Mobile Radio Communications, Sept. 2006.
[107] M. Abramowitz, and I.A. Stegun. Handbook of Mathematical Functions with Formulas, Graphs, and Mathematical Table. 10th edition, Dec. 1972. Available at: http://www.math.sfu.ca/~cbm/aands/intro.htm#001
[108] D. Plets, W. Joseph, L. Verloock, E. Tanghe, L. Martens, E. Deventer, and H. Gauderis, "Influence of Reception Condition, PE-FEC Rate and Modulation Scheme on Performance of DVB-H," IEEE Trans. on Broadcasting, vol. 54(3), Part 2, pp. 590-598, Sept. 2008
[109] Y. Zhang, J. Cosmas, K. K. Loo and M. Bard, "Performance Analysis of Combined CDD and Discontinuous Doppler Diversity in Riceanan and Rayleigh Channels," presented at the Global Mobile Congress, Shangai, Oct. 10-12, 2007.
[110] W. C.-Y. Lee, and Y. S. Yeh. Polarization Diversity System for Mobile Radio,. IEEE Transactions on Communications, vol. COM-20, no. 5, pp. 912-923, October 1972.
[111] Goldhirsh, J. Vogel, W. "Roadside tree attenuation measurements at UHF for land mobile satellite systems", IEEE Transactions on Antennas and Propagation, Vol.: 35, May 1987, Issue: 5, on page(s): 589- 596
[112] Benoit Ledoux, Yiyan Wu, Sébastien Laflèche, Charles Nadeau, Robert Gagnon, "Field test evaluation of the a-vsb digital television system for terrestrial broadcasting, field test proposal", version 12.0, march 21, 2007.
[113] 12 Element Super Yagi UHF TV Aerial datasheet. Available at: http://cpc.farnell.com/jsp/level5/module.jsp?moduleId=cpc/467345.xml

[114] Radio Mobile software website. Avilable at:
http://www.cplus.org/rmw/english1.html
[115] Georges A. Hufford, Anita G. Longley and William A. Kissick. A Guide to the Use of the ITS Irregular Terrain Model in the Area Prediction Mode, National Telecommunications and Information Administration (NTIA) Report 82-100, US Department of Commerce, April 1982
[116] Anita G. Longley. Radio Propagation in Urban Area, Institute of Telecommunication Sciences, Office of Telecommunications, Boulder, Colorado 80302
[117] Terrain database for radio mobile. Available at:
http://www.cplus.org/rmw/dataen.html
[118] WiMAX's technology for LOS and NLOS environments. Available at:
http://www.wimaxforum.org/technology/downloads/WiMAXNLOSgeneral-versionaug04.pdf
[119] "Wireless Point−to−Point Quick Reference Sheet" website. Available at:
http://www.cisco.com/warp/public/102/wwan/quick-ref.pdf
[120] Claude Oestges and Bruno Clerckx, *MIMO Wireless Communications*, 1st ed. Elsevier/Academic Press, Jan. 2007.